

Department of the Navy
Bureau of Ships
Contract Nonr-220(12)

Water Tunnel Tests of
NACA 4412 AND WALCHNER PROFILE 7 HYDROFOILS IN
NONCAVITATING AND CAVITATING FLOWS

by

Robert W. Kermene

This research was carried out under the Bureau of Ships
Fundamental Hydromechanics Research Program
Project NS 715-102, David Taylor Model Basin

Reproduction in whole or in part is permitted for any
purpose of the United States Government

Hydrodynamics Laboratory
California Institute of Technology
Pasadena, California

Report No. 47-5
February, 1956

Approved:
M. S. Plesset

TABLE OF CONTENTS

	<u>Page</u>
ABSTRACT	
INTRODUCTION	1
HYDROFOILS	1
APPARATUS AND TEST PROCEDURE	2
1. Apparatus	2
2. Test Procedure	14
3. Data Reduction	15
RESULTS	18
DISCUSSION OF RESULTS	18
1. NACA 4412 Hydrofoil	18
2. Walchner Profile 7	36
CONCLUSIONS	52
ACKNOWLEDGMENTS	53
REFERENCES	54
APPENDIX A - Working Section Flow Calibration Tests	55
APPENDIX B - Hydrofoil End Gap Experiments	61
APPENDIX C - Data Corrections	65
APPENDIX D - Data Tables	

ABSTRACT

The results of force and cavitation tests on two-dimensional flow are presented. The hydrofoils are the NACA 4412 profile and a modified circular arc, flat plate, hydrofoil designated as a Walchner profile 7. The results of experiments performed in wind tunnels and in other water tunnels are presented for comparison. The experiments described in this report are the first tests using the High Speed Water Tunnel two-dimensional working section and the new force balance; therefore, the experimental setup, procedure and methods of data reduction have been described in detail.

The results of the tests on the NACA 4412 hydrofoil are in good agreement with those obtained for this profile in the Langley two-dimensional low-turbulence wind tunnel. The results of the tests on the circular arc, flat plate hydrofoil are not in good agreement with the results obtained by Walchner for cavitating flow. The differences in the forces on the hydrofoils can be accounted for with a difference in cavitation number of approximately 0.1.

The tests indicate that accurate force measurements can be made with the new water tunnel force balance and that the methods developed during these tests provide a satisfactory means of obtaining the section characteristics of hydrofoils in cavitating and noncavitating flow.

INTRODUCTION

The hydrofoil research program at the Hydrodynamics Laboratory, California Institute of Technology, which was begun on March 1, 1953, has as its purpose a theoretical and experimental study of the forces on hydrofoils in noncavitating and cavitating flow.

The experimental program can be divided into several phases. The first phase of the work was the modification of the High Speed Water Tunnel working section and force balance. The modification of the circular cylinder working section to provide a two-dimensional channel for the hydrofoil experiments is described in the section on Apparatus and Test Procedure. The modifications to the water tunnel force balance system are described in Ref. 1.

The second phase of the experimental program was a series of proofing tests to determine the accuracy and reliability of the new force balance and to develop testing techniques for measuring the forces and moments on hydrofoils in cavitating and noncavitating flow. The results of this second phase of the experimental program are presented in this report. Proofing tests require some standard for comparison of results. For this reason the hydrofoil models selected for these initial experiments were ones for which many of the hydrodynamic and aerodynamic characteristics were known.

Other phases of the present experimental program include the measurement of forces on other hydrofoil shapes, pressure distribution studies, and an investigation of the effects of a free water surface or submergence on hydrofoil performance.

HYDROFOILS

Two hydrofoils were selected for the initial proofing experiments. The first was an NACA 4412 profile and the second a shape tested by Walchner in 1934 and designated as a Walchner profile 7. The NACA 4412 hydrofoil was selected for several reasons. First, there is a wealth of wind tunnel

data available on this shape for a wide range of Reynolds numbers from tests in several facilities. Second, the NACA 4412 profile was tested in the old California Institute of Technology water tunnel in 1944 for noncavitating flow.² Third, the hydrofoil model could be made by shortening the 7-inch span model used in 1944 so that tests could be made on a shape that was identical to the one previously tested. Water tunnel lift and drag data in both fully wetted and cavitating flow are available for the Walchner profile 7.³

The NACA 4412 hydrofoil model has a 3.00-inch chord, a 2.90-inch span, is 12% thick and has a 4% camber. The Walchner profile 7 has a 3.30-inch chord and a 2.90-inch span. This profile is 11% thick, has a circular arc upper surface and a flat lower surface with modified, or rounded, leading and trailing edges. Both models were made of stainless steel. These hydrofoil models are shown in Fig. 1 and their ordinates are presented in Tables I and II, Appendix A.

APPARATUS AND TEST PROCEDURE

1. Apparatus

The experimental investigation of the hydrodynamic characteristics of deeply submerged hydrofoils was conducted in the High Speed Water Tunnel.⁴ The tunnel has a 14-inch diameter closed jet working section. For the hydrofoil tests it was necessary to modify the working section to obtain two-dimensional flow. This was done by inserting nozzle castings, flat plates, and short diffuser castings inside the circular working section to provide a channel which is 3 in. wide by 14 in. high. The channel is not quite rectangular since portions of the wall of the circular working section form the top and bottom of the two-dimensional section.

The nozzle castings have a 20-inch radius circular arc profile hand-faired at the downstream juncture with the flat plates to eliminate the sudden discontinuity in curvature. The two-dimensional nozzle section gives a 3:1 area reduction from the circular section. Except for fairing the downstream end and turning the outside to fit the circular working section, the two-dimensional nozzle was installed as cast. There is no fairing at the upstream end or around the juncture of the castings and the water

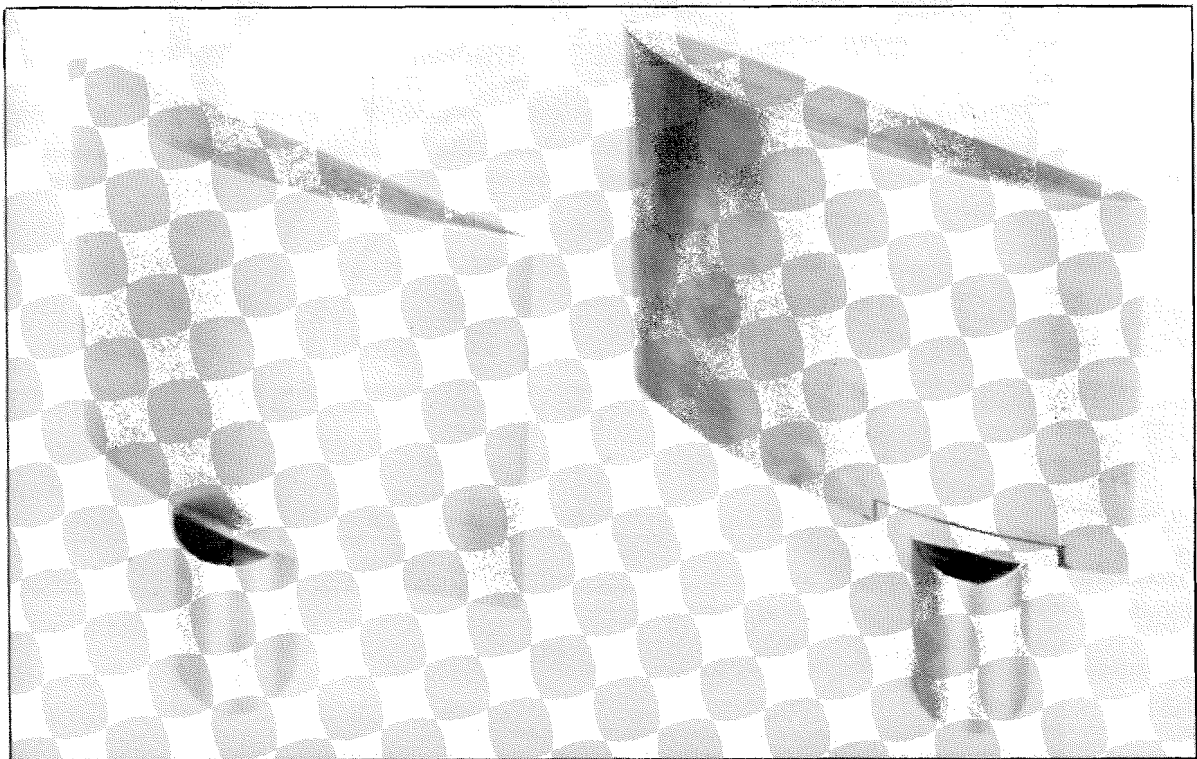


Fig. 1 - NACA 4412 hydrofoil (left) and Walchner Profile 7, (right).

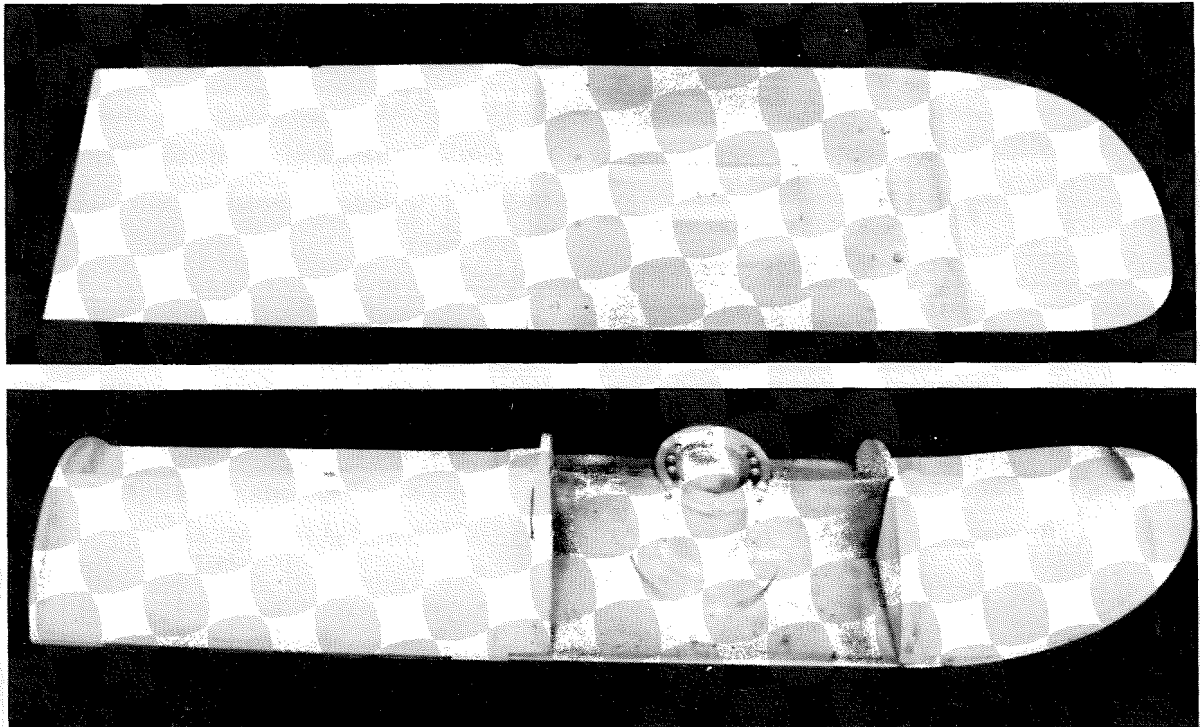


Fig. 2 - The two-dimensional channel nozzle and diffuser castings and flat plate walls assembled for installation. The sealed spindle shield can be seen in the lower photograph. The lucite window can be seen in the upper photograph.

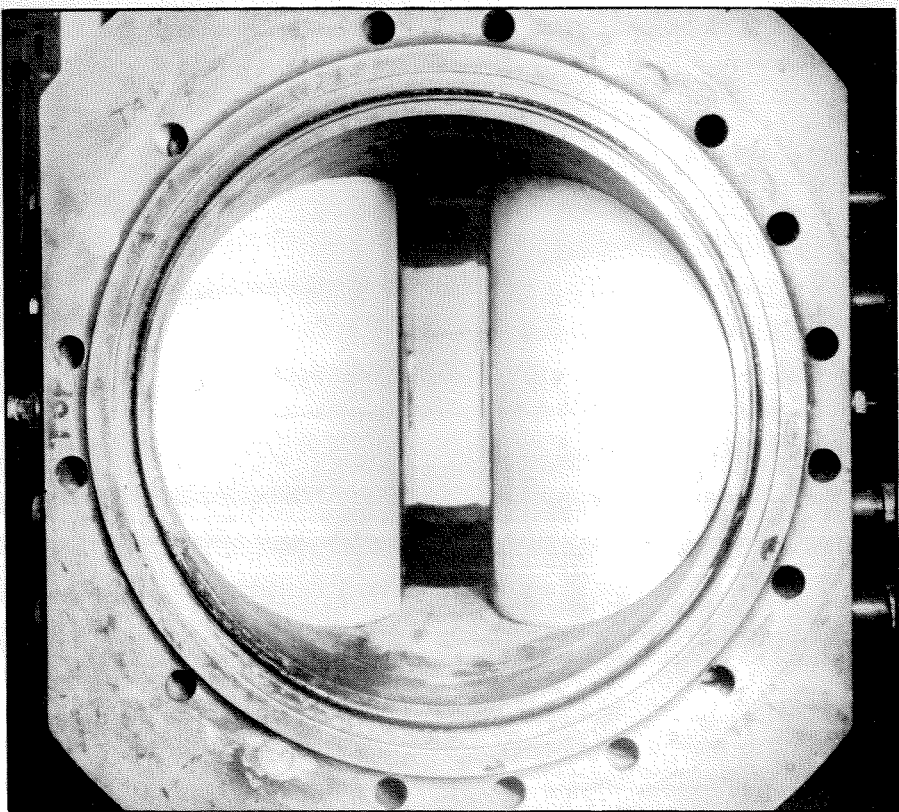


Fig. 3 - View looking downstream of the two-dimensional channel assembly in the water tunnel working section.

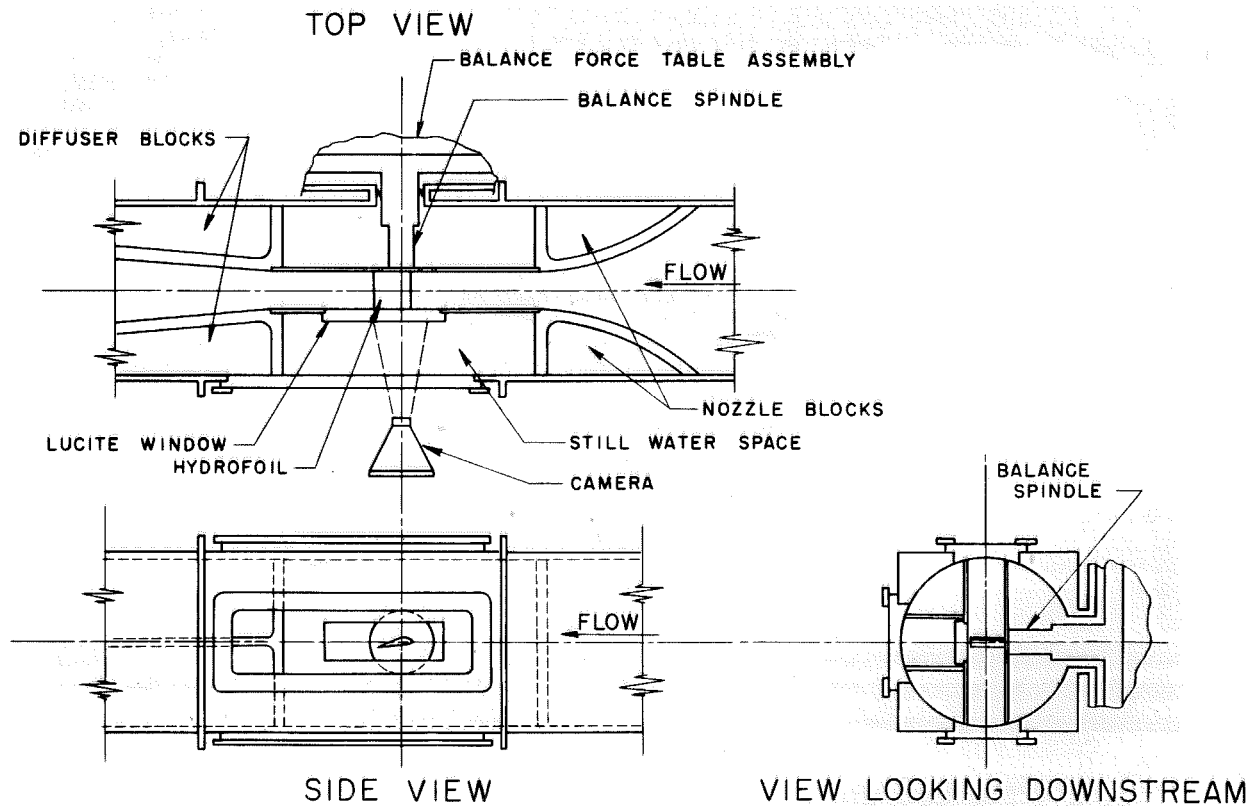


Fig. 4 - Sketch showing the two-dimensional working section setup for hydrofoil force tests.

tunnel walls. The nozzle and diffuser castings are aluminum painted with zinc chromate. After three months of use there was very little evidence of corrosion or electrolytic action.

Flat, parallel, vertical brass plates extend 20-7/8 inches downstream from the tangent line with the two-dimensional nozzle to the intersection with the diffuser section. These plates extend 11 inches upstream from the balance spindle centerline. There is a flat lucite window 3 inches high by 10 inches long in the flat plate opposite the spindle position. The space between the flat two-dimensional channel walls and the circular working section walls is filled with water though there is no flow through this region. Struts are provided in this space to prevent deflection of the flat plates caused by high pressure in the dead water space. For the latest tests the dead water space on the window side and the balance spindle shield was sealed from the high pressure water coming from either end of the two-dimensional channel and was vented to the same pressure as in the hydrofoil channel. The lucite circular working section windows extend 20-5/8 inches along the two-dimensional channel, giving windows on three sides for lighting and photographing the model.

Flat diffuser castings extend 22-1/2 inches downstream from the parallel channel walls. This two-dimensional diffuser has a 7 degree total angle and ends abruptly in the transition section of the circular diffuser. In order to completely diffuse the water in the two-dimensional channel by extending the diffuser section until it intersected the walls of the 7.6 degree circular water tunnel diffuser would have required long and expensive castings and a much higher diffuser angle. Because of installation difficulties and the fact that unsteady flow separation would probably result from such a large angle diffuser, it was decided to end the two-dimensional diffuser abruptly with separation at a known and stable position.

Figure 2 shows the assembled plates and castings ready for installation. Figure 3 shows the two-dimensional channel in place in the circular working section. Sketches of the hydrofoil channel are shown in Fig. 4.

Velocity and pressure calibration experiments were made at several positions in the two-dimensional channel. The velocity profile is uniform throughout the entire section except for the boundary layers on the plates and tunnel walls. The boundary layer on the flat plate is approximately 0.22 in.

thick at the hydrofoil position. A description of the flow calibration tests and the results are presented in Appendix A.

The hydrofoils shown in Fig. 1 were machined with a short 3/4-in. diameter stub spindle on one end. The hydrofoils were positioned between the flat two-dimensional working section walls with small end clearances. The end of the 3/4-in. stub spindle was made flush with the wall with a radial clearance gap to allow for spindle and balance deflection under load. The stub spindle was fastened to the balance spindle which in turn was bolted to the top of the new force table. The spindle used in most of these tests has a diamond-shaped cross section, which permitted it to be rotated through ± 22 degrees in a rectangular space inside the spindle shield.

Because of radial interferences caused by spindle deflection, spanwise interferences caused by deflection of the two-dimensional channel walls, and jetting of water through the stub spindle clearance gap from the high pressure dead water region, the spindle shield assembly was modified. A new cylindrical spindle, 3-5/16 in. in diameter and 6 in. in length, has reduced spindle deflection and reduced the size of the radial clearance needed between the channel walls and the spindle. Both the old and new spindles with the NACA 4412 hydrofoil attached are shown in Fig. 5. The spindle shield was modified to provide space for the larger spindle and was sealed from the high pressure water. The sealed spindle shield which is soldered to the flat channel wall and has an "O" ring seal at the outside working section wall can be seen in the lower photograph, Fig. 2. With this new shield the pressure around the spindle is the same as in the two-dimensional channels.

With the new spindle shield assembly the angle of attack of the hydrofoil can be set at any value through 360 degrees to within one minute of arc. The angle of attack can be changed during a test without stopping the tunnel or interrupting the run in any way.

The hydrofoil end gap at the spindle end of the hydrofoils has been eliminated by attaching the hydrofoils to the spindle through a 5.00-in. diameter disk set flush with the channel wall. There is a 0.027-in. vertical and 0.012-in. horizontal clearance gap between the disk and the channel wall. Figure 6 shows the NACA 4412 hydrofoil mounted on the new disk-spindle assembly in the working section. The viscous drag forces on the

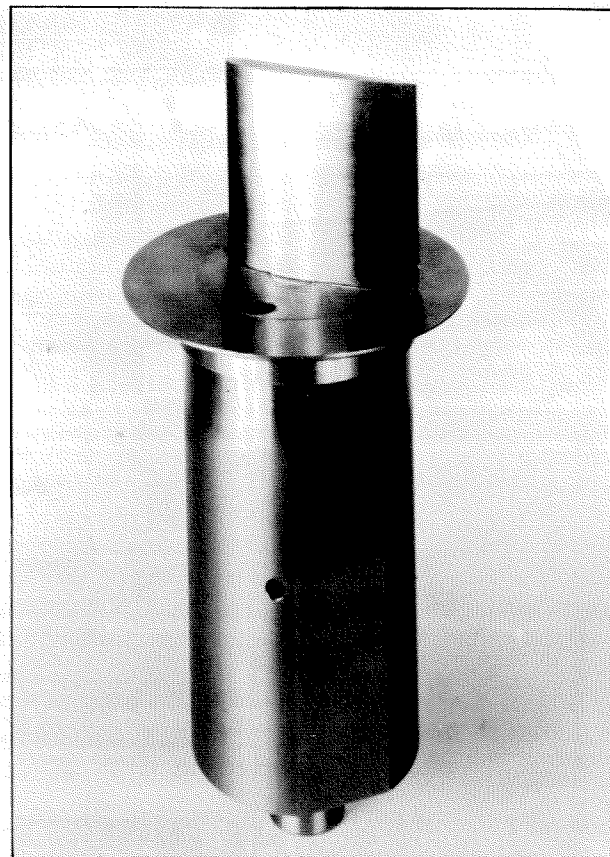
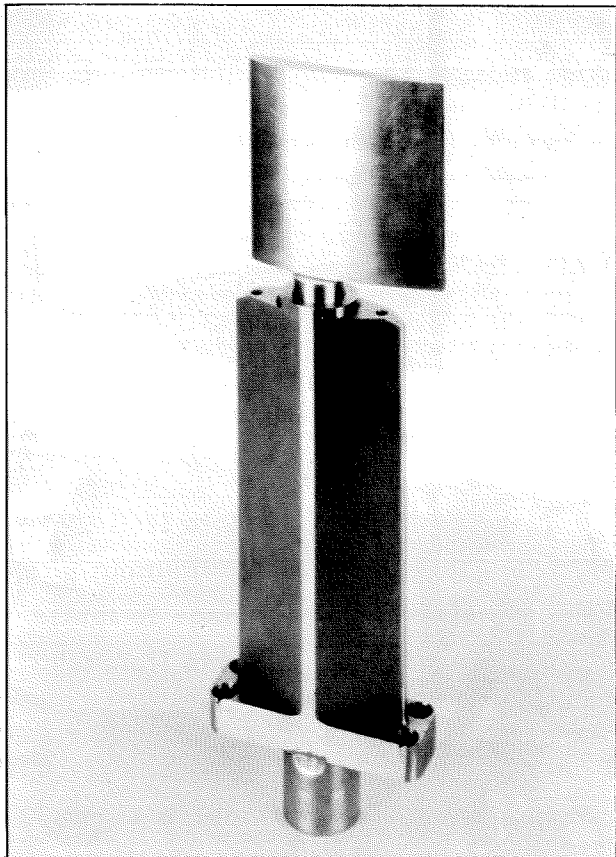


Fig. 5 - The NACA 4412 hydrofoil attached to the balance spindles. The original spindle is on the left; the new spindle-disk assembly is on the right.

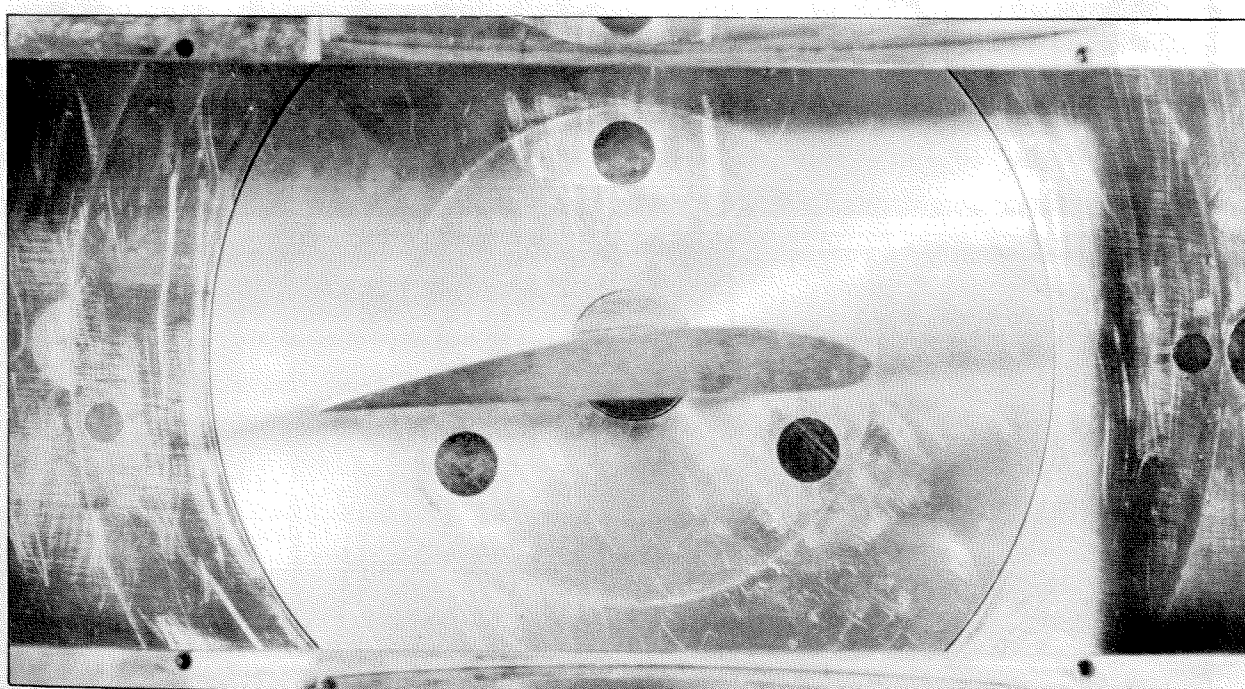


Fig. 6 - The NACA 4412 hydrofoil mounted on the spindle-disk assembly in the two-dimensional working section.

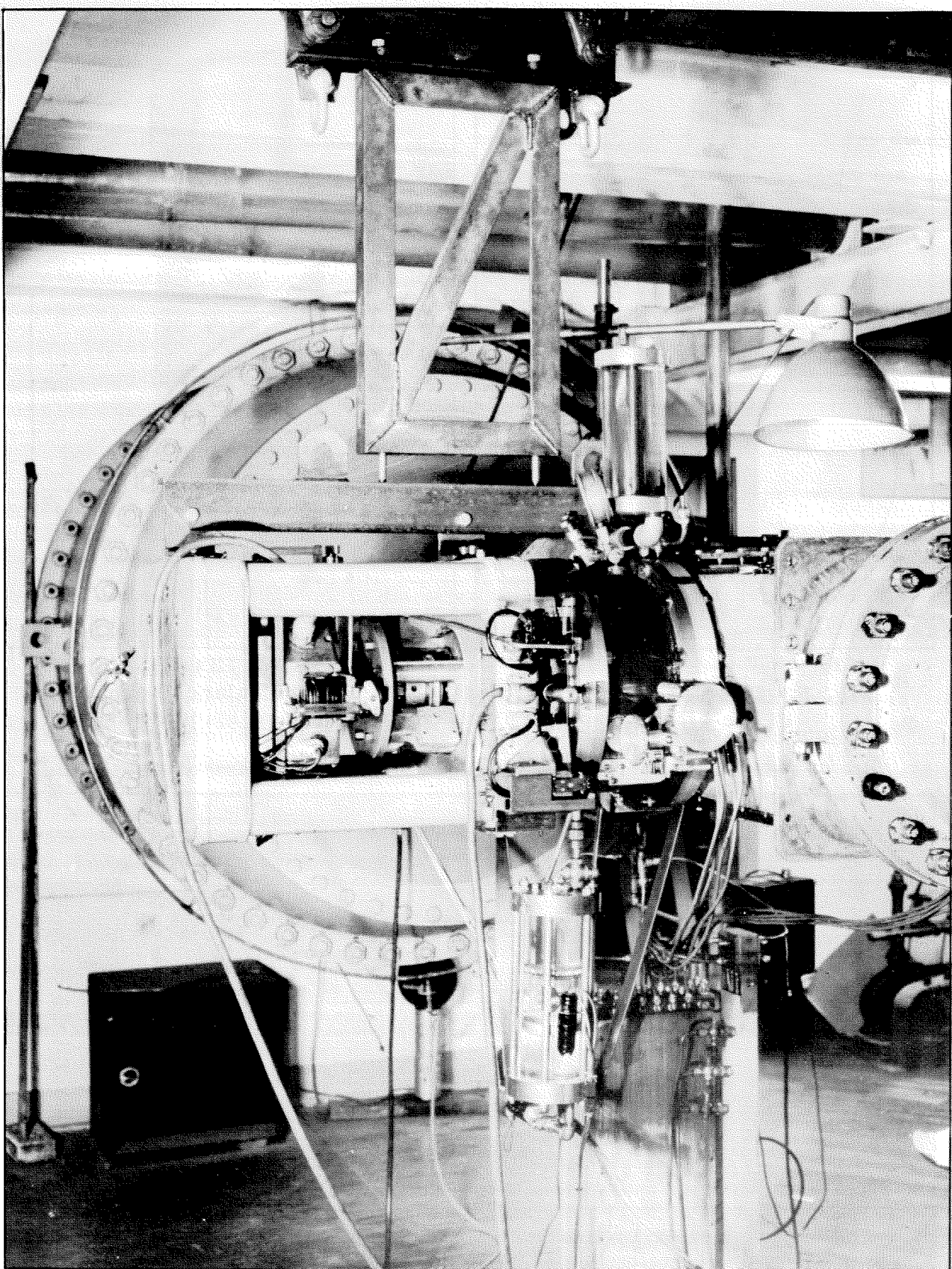


Fig. 7 - Balance installed on the High Speed Water Tunnel for hydrofoil force measurements.

hydrofoil mounting disk were calibrated by supporting the hydrofoil from the opposite side of the two-dimensional channel at the viewing window with a small end gap between the hydrofoil and the disk. The forces were then measured on the disk alone and corrections applied to the hydrofoil force data. The details of the method of obtaining these corrections are given in Appendix C.

For regular force runs the gap between the end of the hydrofoil and the lucite viewing window in the channel wall was held at approximately 0.002 in. The effect of end gap was investigated by changing the gap from 0.001 to 0.032 in. Over this range there was an increase in drag on the NACA 4412 hydrofoil of 25% and a decrease in lift of 8%. There was no change in pitching moment over this range of end gap width. Experiments to determine the effect of spanwise gap between the working section wall and the end of the hydrofoil are described in Appendix B.

The force balance,¹ supported on a monorail carriage, is mounted horizontally on the working section, Fig. 7. The horizontal hydrofoil and balance orientation was used in order to avoid spanwise variations in the cavitation caused by the vertical gravity pressure gradient in the working section. The force balance measures lift, drag, and pitching moment. The design loads for the modified balance are 150 lbs lift, 150 lbs drag, and 560-in/lbs of pitching moment. The design load for the hydrofoils reported here is 150 lbs of lift. This corresponds to $C_L \text{max}$ for conventional airfoil shapes at 45 ft per second tunnel velocity. Tests can be run at higher velocities at smaller attack angles.

The forces and moments on the hydrofoil models are balanced by pressure in hydraulic cylinders attached to the frame of the force balance. This pressure is measured on automatic hydraulic weighing gages. Figure 8 shows the four pressure gages on the force gage console. The drag gage is shown alone in Fig. 9. In this photograph the beam with the automatic rider which is geared to the readout counter, the Schaevitz linear variable differential transformer for sensing the balance of the beam, and the chain-driven selsyn generator for transmitting the readout of the gage to remote reading counters, can be seen.

Counters on the gages read directly in pounds of lift and drag and inch-pounds of moment. When making force measurements on a model in the tunnel, the gages do not in general give a steady force reading but hunt slightly around an average value. This gage hunting, which is primarily due to small velocity fluctuations in the tunnel, can be controlled by a rheostat in the gage balancing circuit. The data is taken by stopping the gage counters at random intervals when the gages are at balance and recording the readings. A small sample of ten readings are taken and averaged for each data point. Tests using a much larger number of counter readings show that this small sample method gives very satisfactory results.

Several methods of force data recording were used in these hydrofoil experiments. In the first method which was standard in the past, the gage operator copied all gage readings on data sheets. The second method of data readout was developed during the hydrofoil tests. With this system the data was recorded with a camera mounted above the gage console which photographed the entire gage console. After a run, the film was developed and the gage counters read on a microfilm enlarger. The third system which is in use at the present time is a refinement of the second method above. With this system the gage readout is displayed on a duplicate set of selsyn-operated counters. The remote reading counters are photographed on 35 mm film and the data read with a small desk film viewer. Figure 10 shows the counter box and camera setup for the force gage readout system. Figure 11 shows a section of data film giving the force and velocity information for one data point. The use of this new data recording method has reduced readout time by a factor of five.

The balance cylinders and the three force gages are constructed so that one psi of hydraulic pressure is equivalent to one pound of force or one inch/pound of pitching moment. The pressure is read out on the gage counters with a least count of 0.01 psi.

Before beginning the hydrofoil experiments complete calibration tests were made of the force balance and gages. The force gages were tested with an Ashcroft hydraulic dead weight tester for pressures from 5 to 150 psi. The gages showed an accuracy of 0.2% of the applied pressure at 5 psi increasing to an accuracy of 0.002% at 100 psi. The force balance was

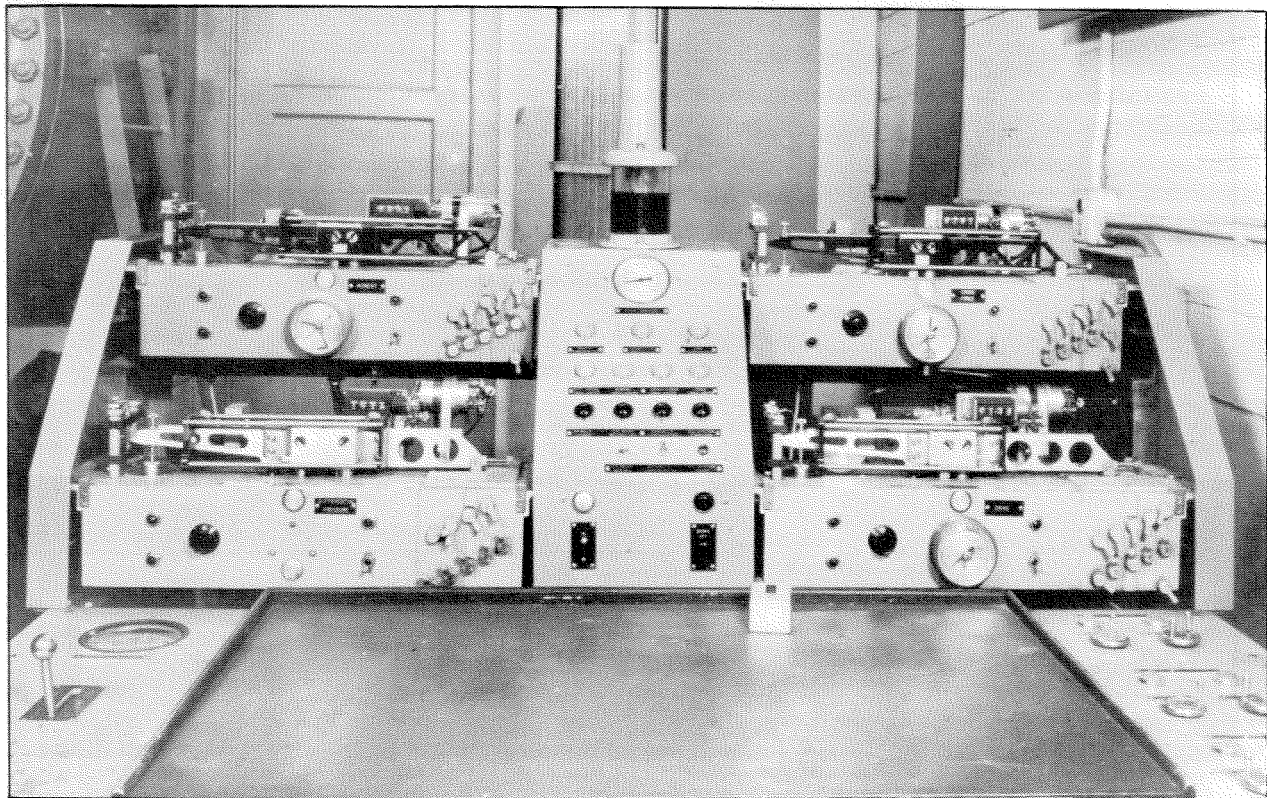


Fig. 8 - The High Speed Water Tunnel force gage console showing the three forces gages and the differential pressure gage.

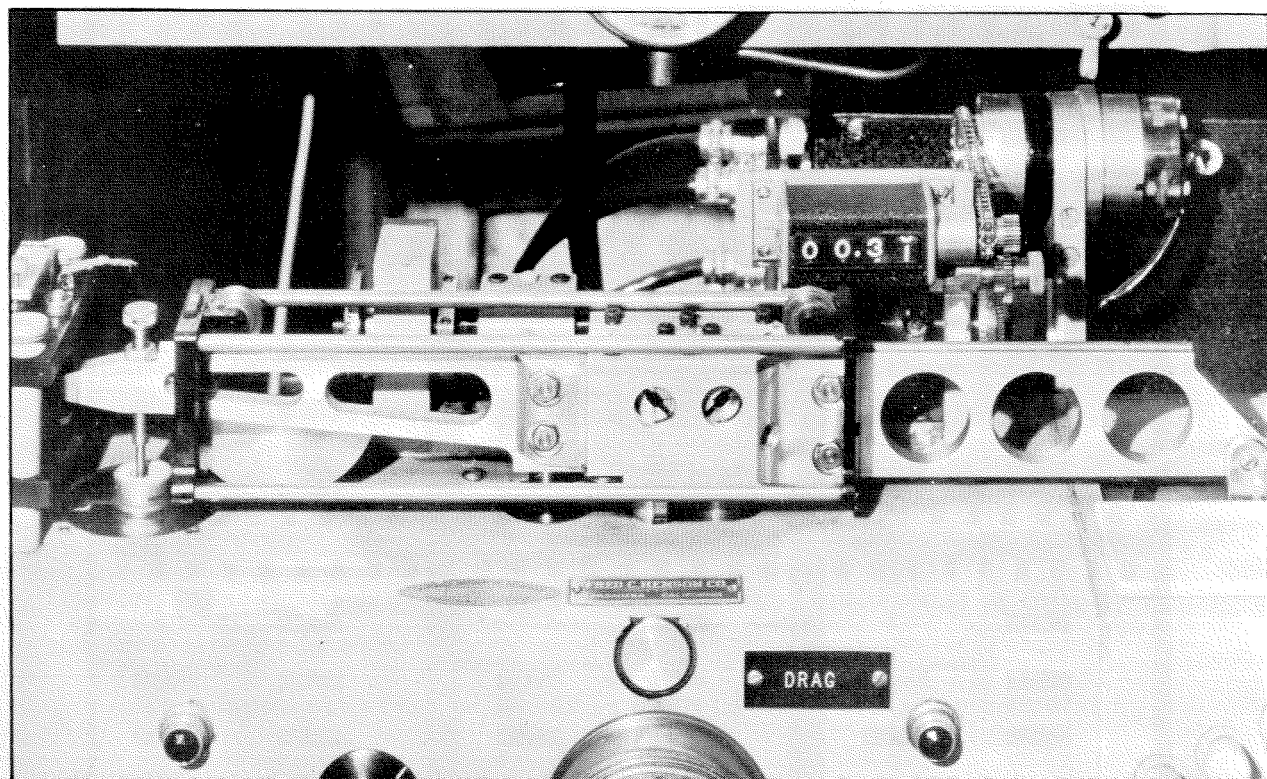


Fig. 9 - The High Speed Water Tunnel drag gage showing the chain-driven selsyn generator for remote readout.

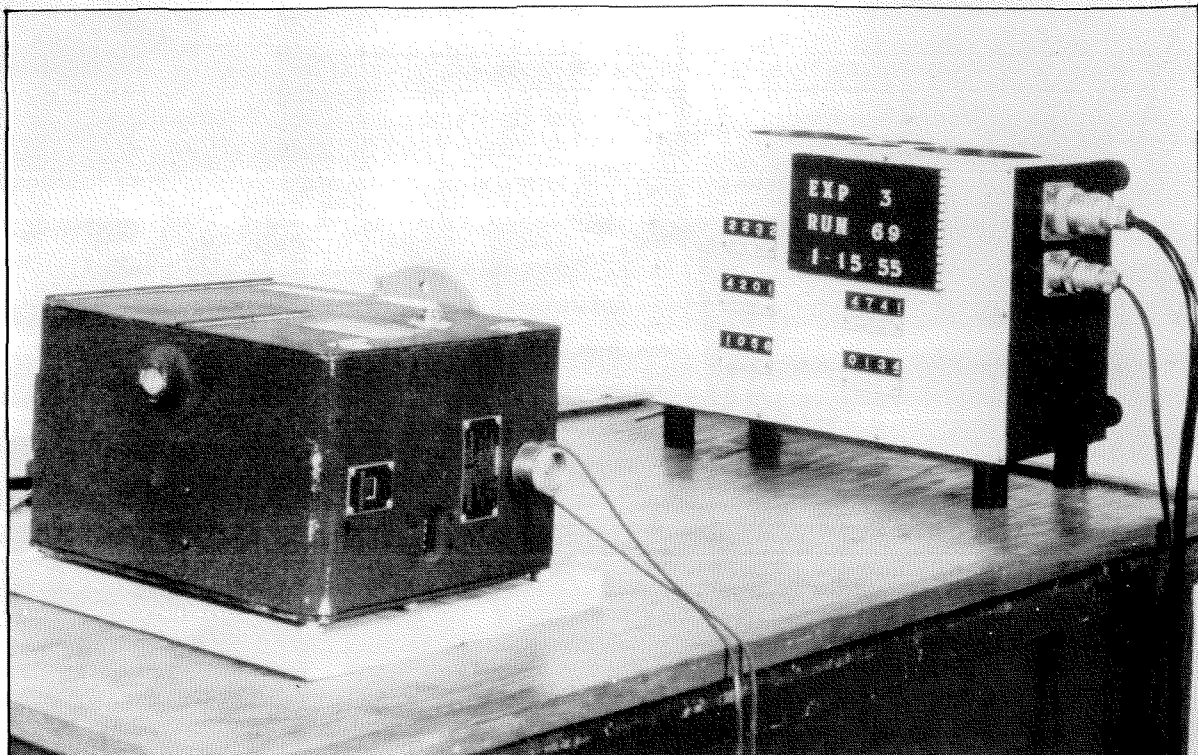


Fig. 10 - Force and differential pressure gage remote readout system showing the force counters and the microfilm camera for recording the data.

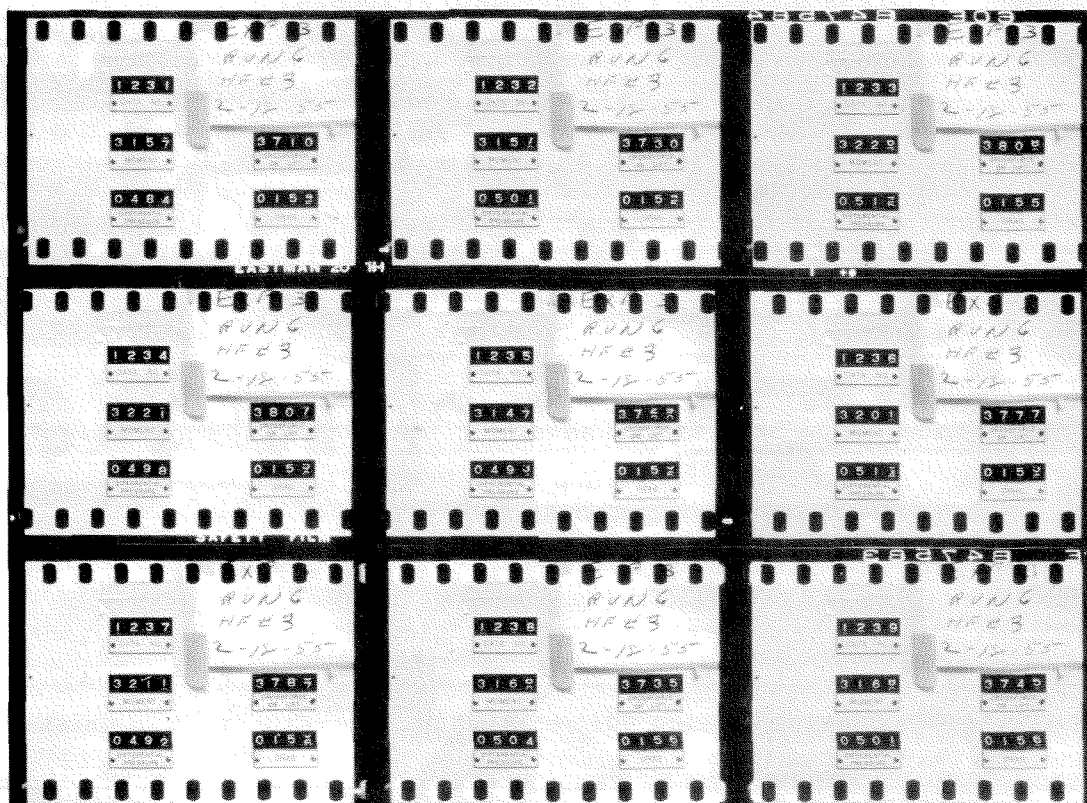


Fig. 11 - A portion of the data film from a hydrofoil force test. Ten frames are obtained for each data point.

tested for accuracy and force and moment interactions. For small forces on the order of five pounds or less the balance system showed an accuracy of 0.4% of the applied force. For forces on the order of 50 pounds or larger, the percentage accuracy was increased to the order of 0.03%. Over the full range of forces tested the lift and drag interactions were 0.2%, and the moment interaction indicates a misalignment of the balance moment center of 0.012 in. Since the force gages were used for readout of the balance calibration, the gage errors are included with the balance system calibration. The calibration runs are described more completely in Ref. 1.

A fourth hydraulic weighing gage is used for measuring a pressure differential. This gage is connected across the tunnel nozzle for measuring flow velocity. The least count of this gage is 0.001 psi. At 5 psi static pressure difference the gage reads to an accuracy of 0.06% and better than 0.005% for pressure differences greater than 10 psi.

Piezometer rings are attached at each end of the water tunnel nozzle for velocity and static pressure measurements. For the hydrofoil tests the pressure drop across the three-dimensional nozzle is measured and the velocity in the two-dimensional channel is calculated from continuity considerations. The velocity head is measured on the differential pressure gage for noncavitating runs and on U-tube manometers for cavitation tests. A carbon tetrachloride-water manometer is used at low velocity and a mercury-water manometer at high velocity.

The static pressure, p_0 , is obtained from measurements of the static pressure made upstream of the two-dimensional channel nozzle. The pressure at the hydrofoil position was calibrated relative to the upstream pressure reference point for the clear working section without the hydrofoil. Because the two-dimensional working section is short, the static pressure throughout this section is affected by the pressure field of the hydrofoil and therefore the free stream static pressure cannot be measured in this region. By using the measured upstream pressure and the calibrated correction for the pressure drop across the two-dimensional nozzle and the friction losses, the free stream pressure which would exist at infinity in the free stream is obtained.

The vapor pressure of water is used in most tests for calculating

cavitation number. However, with fully cavitating hydrofoils the cavity pressure can be measured, and should be measured whenever possible. A pressure tap on the model or a single pressure tap which protrudes from the channel wall into the region behind the hydrofoil was connected to a mercury U-tube manometer. A water trap was used in the manometer line to the tunnel and the line cleared of water before each measurement. The other side of the manometer is open to atmospheric pressure.

Electrically operated 35 mm microfilm cameras, mounted above and below the working section are used to record the amount of cavitation on the model at each test point during the runs.

2. Test Procedure

Some of the details of the test procedure were described in the preceding section on test apparatus. In this section the experimental procedure for each type of test is briefly described.

The hydrofoil force characteristics for noncavitating flow are obtained over a wide range of hydrofoil attack angles and at several Reynolds numbers. In each run the tunnel velocity is held constant, the working section pressure is held at a constant value sufficient to suppress all cavitation on the model, and the angle of attack of the hydrofoil is varied. In these runs the lift, drag, pitching moment and velocity data are photographically recorded. The runs are repeated at several Reynolds numbers. The Reynolds number range for the tests reported here is 0.55×10^6 to 1.49×10^6 for the NACA 4412 hydrofoil, based on a chord length of 3.00 in. The tests of the 3.3 in. chord Walchner profile 7 were made at Reynolds numbers from 0.53×10^6 to 1.05×10^6 .

For the NACA 4412 hydrofoil the cavitation number for incipient cavitation was determined as a function of tunnel velocity and hydrofoil attack angle. In each run the tunnel velocity was held constant and the angle of attack and cavitation number were varied. At each hydrofoil angle of attack the working section pressure was reduced until cavitation occurred on the model. The pressure was then slowly increased until the cavitation just disappeared. The disappearance of cavitation was used as a measure of the incipient cavitation number to avoid cavitation hysteresis effects. These runs were repeated over a wide range of velocities. The model was

mounted on the force balance to facilitate changes in angle of attack. The only data recorded were the working section pressure and velocity manometer readings.

In another series of runs the force characteristics of the hydrofoil in cavitating flow were determined. The principal controlled variables in these tests were velocity, cavitation number, and hydrofoil angle of attack. The complete set of cavitation force characteristics were compiled from the results of many test runs in which velocity and angle of attack were held constant and the cavitation number varied from completely wetted flow to full cavity flow. The cavitation number was varied in steps by changing working section pressure. At each test point the lift, drag, and pitching moment gage readings were photographically recorded, the velocity and working section pressure were read on manometers and photographs were taken of the cavitation on the hydrofoil. The runs were repeated at a constant velocity for a wide range of angles of attack and at several velocities for selected attack angles.

3. Data Reduction

The force and cavitation data are reduced to dimensionless coefficients as follows:

$$\text{Lift coefficient, } C_L = \frac{\text{Lift}}{\frac{\rho}{2} V^2 A}$$

$$\text{Drag coefficient, } C_D = \frac{\text{Drag}}{\frac{\rho}{2} V^2 A}$$

$$\text{Pitching moment coefficient (about 1/4 chord point), } C_M = \frac{\text{Pitching Moment}}{\frac{\rho}{2} V^2 A_c}$$

$$\text{Cavitation number, } K_v = \frac{p - p_v}{\frac{\rho}{2} V^2}, \quad K_k = \frac{p - p_k}{\frac{\rho}{2} V^2}$$

$$\text{Reynolds number, } R_e = \frac{V c}{\nu}$$

where

V = velocity of undisturbed flow, ft/sec

ρ = density of water at temperature of the run, slugs/ft³

A = plan area of hydrofoil (chord x span), ft²

c = chord of hydrofoil, ft

p = pressure of undisturbed flow, lb/ft²

p_v = vapor pressure of fresh water at the temperature of the run, lb/ft²

p_k = measured cavity pressure, lb/ft²

ν = kinematic viscosity of fresh water at the temperature of the run, ft²/sec

In calculating the force and cavitation coefficients a number of corrections are applied to the tunnel data. The lift, drag, and pitching moment gage readings are corrected for balance pressure sensitivity, balance and force gage temperature drift and spindle disk tare forces.

During a cavitation run the balance and seal may be subjected to pressure changes from 40 psig down to vapor pressure of water. The change of drag and pitching moment with working section pressure are approximately linear over this range and amount to 0.0058 lb per psi for drag and 0.045 in./lb per psi for moment. The change of lift with working section pressure is small over the range of pressures used in these tests and was therefore neglected. Curves of balance pressure sensitivity are given in Ref. 1. The balance pressure sensitivity may be caused by tare forces introduced by non-uniformity in material, fabrication or eccentricity of alignment of the old balance seal, or by deflection or nonuniform preloading of the old balance spindle support wires. The balance pressure sensitivity is independent of the force and moment loading of the balance.

The balance and force gages are sensitive to changes in temperature due to the warm-up of the equipment and changes in ambient temperature. Small restoring springs on the force gage weighing beam and the preload springs on the force table are the principal sources of temperature drift. Heat from the gage electronic equipment and motors gives a gage warm-up

period of several hours. Since it is impractical to wait for the gages and balance to reach temperature equilibrium, a linear correction based on the pre-run and post-run zero readings is applied to the gage readings. Calibrations have shown the corrections to be as great as 0.08 lb of drag for the first run of the day, requiring approximately 1.5 hours. The temperature correction of course becomes less for subsequent runs during the day. The single springs in the force gages were replaced by two identical opposing springs for the final tests reported here, thus providing temperature compensation and essentially eliminating the gage temperature sensitivity.

The force gage readings are also corrected for the forces on the spindle disk. To calibrate these tare forces the hydrofoils were mounted on a brass plate in the window opening in the flat plate opposite the spindle. The hydrofoil is adjusted to give a very small gap between the end of the hydrofoil and the spindle disk and the force runs repeated at the same conditions of velocity, angle of attack, and cavitation number. For these runs, only the forces and moments on the spindle disk are measured and the results are applied as corrections to the hydrofoil test data. This correction for the viscous drag on the plate was approximately 28% of the total measured drag on the NACA 4412 hydrofoil at a velocity of 30 fps and an angle of attack of 4 degrees. The lift and pitching moment on the disk were approximately 0.5% of the total measured on the hydrofoil for the same test conditions. Some of the results of the spindle disk tare force tests are given in Appendix C.

The force data from the fully wetted flow runs were corrected for the errors in the measured forces due to the flow constraints imposed by the closed jet working section. The corrections have been applied only to the data of Figs. 12, 13, 30, 31, 32, and 33, and to the corresponding data in Appendix D. These corrections for solid and wake blockage, lift effect and working section pressure gradient were based on two-dimensional wind tunnel techniques.⁵ Calculations and curves of these corrections are given in Appendix C. Since tunnel interference corrections were not applied for fully cavitating flow, or the intermediate region of partially cavitating flow, the corrections for fully wetted flow have been omitted on all curves such as the polar diagrams, which include cavitating and noncavitating data.

RESULTS

Because of the basic differences in the shapes of the two hydrofoils tested, the results are presented separately. The results of the tests on the NACA 4412 hydrofoil are presented in Figs. 12 to 29 and discussed on pages 12 to 20. The results of the tests on Walchner profile 7 are given in Figs. 30 to 43 and discussed on pages 20 to 25. The results of experiments on these same shapes in other facilities are included with the High Speed Water Tunnel data for comparison.

DISCUSSION OF RESULTS

1. NACA 4412 Hydrofoil

A. Noncavitating flow

The results of the tests of the NACA 4412 hydrofoil in fully-wetted flow are shown in Figs. 12 and 13. The tests were run at tunnel velocities of 20, 30, 40, 50, and 60 fps, giving Reynolds numbers from 0.55×10^6 to 1.49×10^6 . Lift coefficients and moment coefficients about the quarter chord point are shown in Fig. 12. A polar diagram of lift coefficient vs drag coefficient is shown in Fig. 13. Results of tests from several sources at comparable Reynolds numbers are included in these figures. Curves A and B are the results of tests in the Langley Two-Dimensional Low Turbulence Wind Tunnel, 1949.⁶ Curves marked C are the results of tests on a larger span of the same hydrofoil in the old water tunnel at the Hydrodynamics Laboratory by J. W. Daily, 1944.² Curves D and E are from tests on a finite rectangular span section in the NACA Variable-Density Wind Tunnel, 1937.⁷

The water tunnel lift and drag data for fully-wetted flow has been corrected for tunnel wall and blockage effects. No corrections have been applied to the pitching moment. The corrections for solid and wake blockage, lift effect and working section pressure gradient are based on two-dimensional wind tunnel techniques. Calculations and curves of these corrections are given in Appendix C. The corrections are functions of attack angle, and for lift they vary between 2 and 3 per cent for attack angles

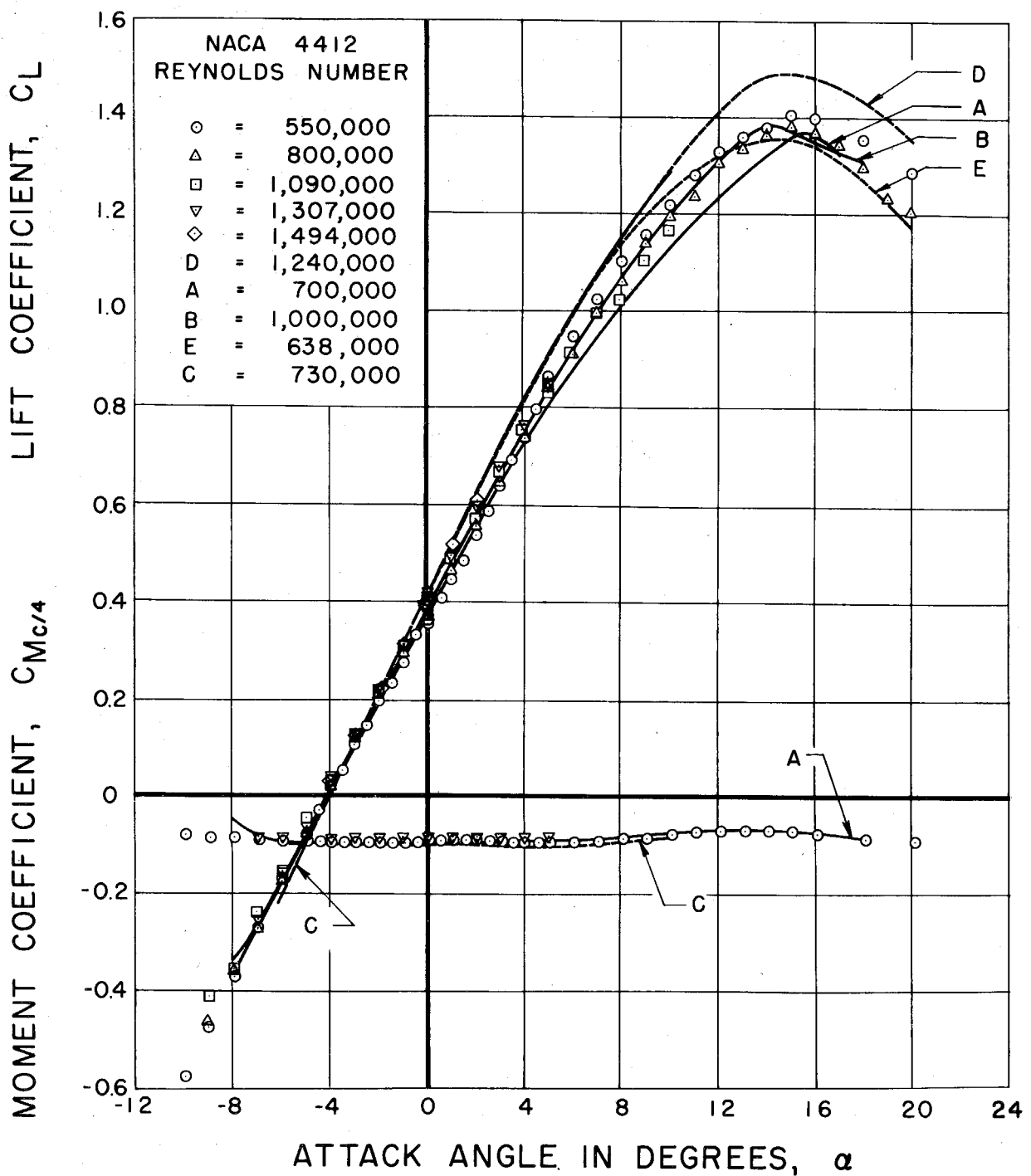


Fig. 12 - Lift coefficient and moment coefficient about the quarter chord point as functions of angle of attack for the NACA 4412 hydrofoil for noncavitating flow. The data points in this figure are the results of the present tests. The curves are from the following sources:

A and B. Langley Two-Dimensional, Low Turbulence Wind Tunnel, 1949.

C. J. W. Daily, Hydrodynamics Laboratory,
C. I. T., 1944.

D and E. NACA Variable Density Wind Tunnel, 1937.

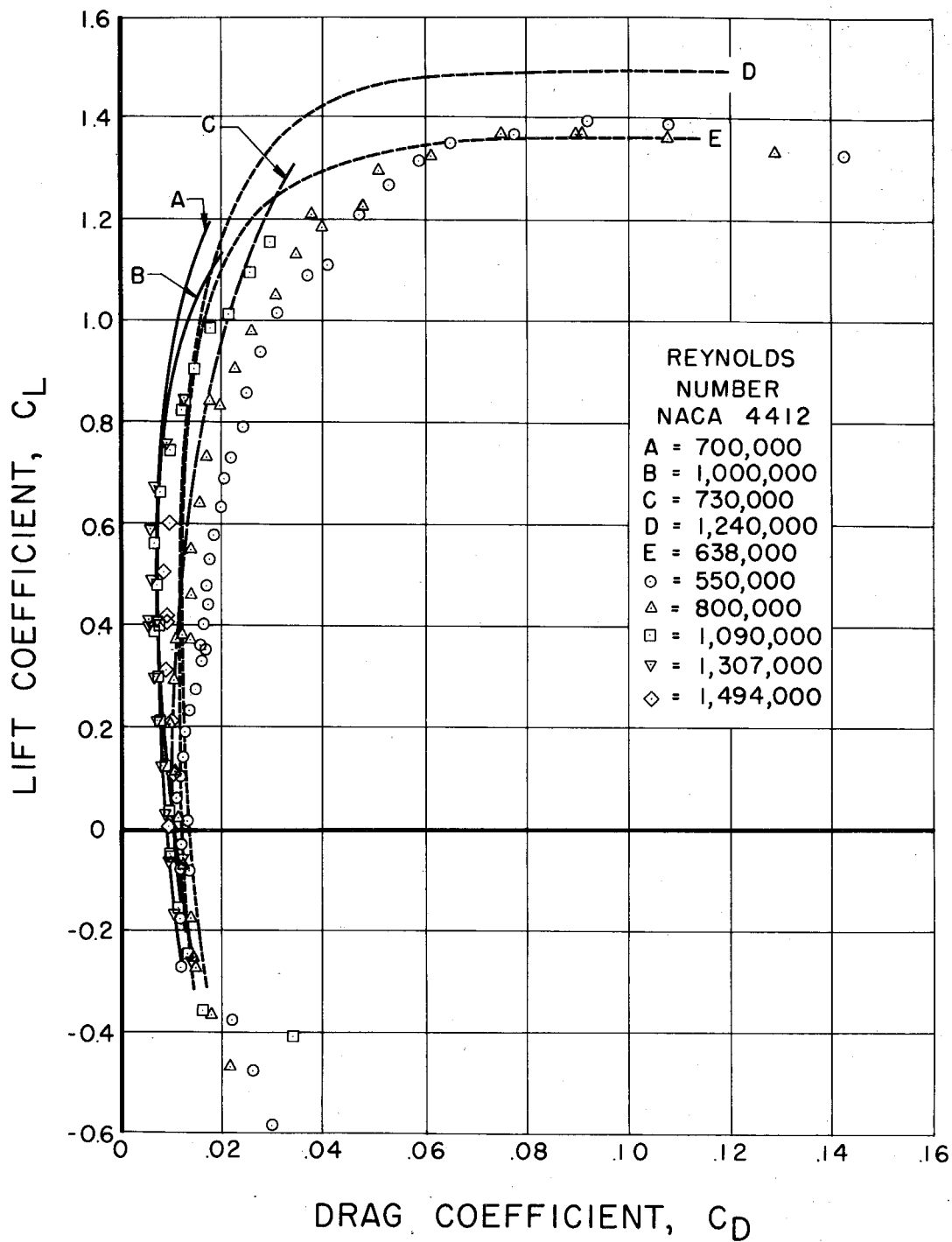


Fig. 13 - Polar diagram for the NACA 4412 hydrofoil in noncavitating flow. The data points are from the present tests. The curves are from the following sources:

A and B. Langley Two-Dimensional, Low Turbulence Wind Tunnel, 1949

C. J. W. Daily, Hydrodynamics Laboratory, C.I.T., 1944.

D and E. NACA Variable Density Wind Tunnel, 1937.

from 0 to 10 degrees. The corrections for drag are in general somewhat larger. The corrections to pitching moment, though given in the appendix, have not been applied to the data of Fig. 12. The moment corrections are of the same order as the lift corrections but they are negligibly small when plotted to the C_M scale of Fig. 12. No wall corrections were applied to the curves from Daily's water tunnel tests, Ref. 2.

The hydrofoil angle of attack range for the higher velocities was limited in the present tests by load limitations of the force balance. At 50 fps tunnel velocity, for instance, the lift was 134.0 lbs and the drag 2.58 lbs at an angle of attack of 5 degrees. However, even at 60 fps, force measurements could be made over the attack angle range of primary interest for hydrofoil applications.

The runs made at Reynolds numbers of 0.55 and 0.80×10^6 were made with the model supported with clearance gaps at each end of its span which provided a leakage passage for flow around the stub spindle supporting the hydrofoil. The later tests at higher Reynolds numbers were made with the hydrofoil mounted solidly on the large spindle disk set flush with the channel wall. For these reasons the tests at higher Reynolds numbers are believed to be more accurate. Except for the runs at the two lowest velocities the results showed the expected slight increase in slope of the lift coefficient vs attack angle curves with Reynolds number. Since there was no appreciable change in moment coefficient with Reynolds number, only the data taken at 20 and 50 fps are included in Fig. 12. The polar diagram, Fig. 13, shows the expected decrease in drag coefficient with increasing Reynolds number.

The lift and moment coefficient data are in excellent agreement with the more recent of the NACA wind tunnel data.⁶ The drag coefficient curves from the two NACA tests differ considerably. This may be due to differences in the turbulence of the two wind tunnels and the fact that the older tests⁷ were made on a finite span model. The present water tunnel drag coefficients agree very well with the 1949 NACA results over the low drag range up to attack angles of approximately 5 degrees. At higher attack angles the water tunnel tests show somewhat higher drag.

B. Incipient cavitation

The cavitation numbers for incipient cavitation on the upper surface of the NACA 4412 hydrofoil are shown as functions of velocity and attack angle in Fig. 14, and for the lower side in Fig. 15. The data of Figs. 14 and 15 show an increase in incipient cavitation number with increased velocity. The change in incipient cavitation number increases as the angle of attack is increased. Taking average values of the cavitation number from Fig. 14 gives an increase in K of 0.46 to 0.54 or 17% at zero degree attack angle for a velocity change from 28 to 48 fps and from 1.72 to 2.30 or 34% at an angle of attack of 8 degrees for the same velocity range.

Figure 16 shows incipient cavitation number as a function of attack angle for velocities of 25, 40, and 60 fps. The flagged symbols in this figure are for cavitation on the lower surface of the hydrofoil. The solid line in Fig. 16 gives incipient cavitation number obtained on the same model by Daily in 1944.² The tests by Daily were made in the old California Institute of Technology water tunnel at a velocity of 40 to 45 fps. The dashed line in Fig. 16 shows incipient cavitation as predicted from pressure distribution measurements made on an NACA 4412 airfoil in the NACA Variable Density Wind Tunnel.⁸ It is well known from the definition of the cavitation number and pressure coefficient that when the local minimum pressure is equal to vapor pressure, the cavitation number is equal to the negative of the pressure coefficient at that point. Therefore the dashed curve represents the negative of the minimum pressure coefficient on the airfoil measured over a wide range of attack angles. The pressure distribution tests were made at a Reynolds number of approximately 3.0×10^6 .

The incipient cavitation number for the upper surface at the higher velocities agrees very well with that predicted from the pressure distribution measurements for attack angles up to 5 degrees and also for attack angles greater than 10 degrees. From 5 to 10 degrees the measured values of incipient cavitation number are higher than the predicted values. The measured incipient cavitation numbers are much smaller than the predicted values for the lower surface for all attack angles. On the lower surface and on the upper surface at higher attack angles, the pressure coefficient has a very sharp peak near the leading edge. Also the minimum pressure coefficient changes very rapidly with attack angle. Small differences in the

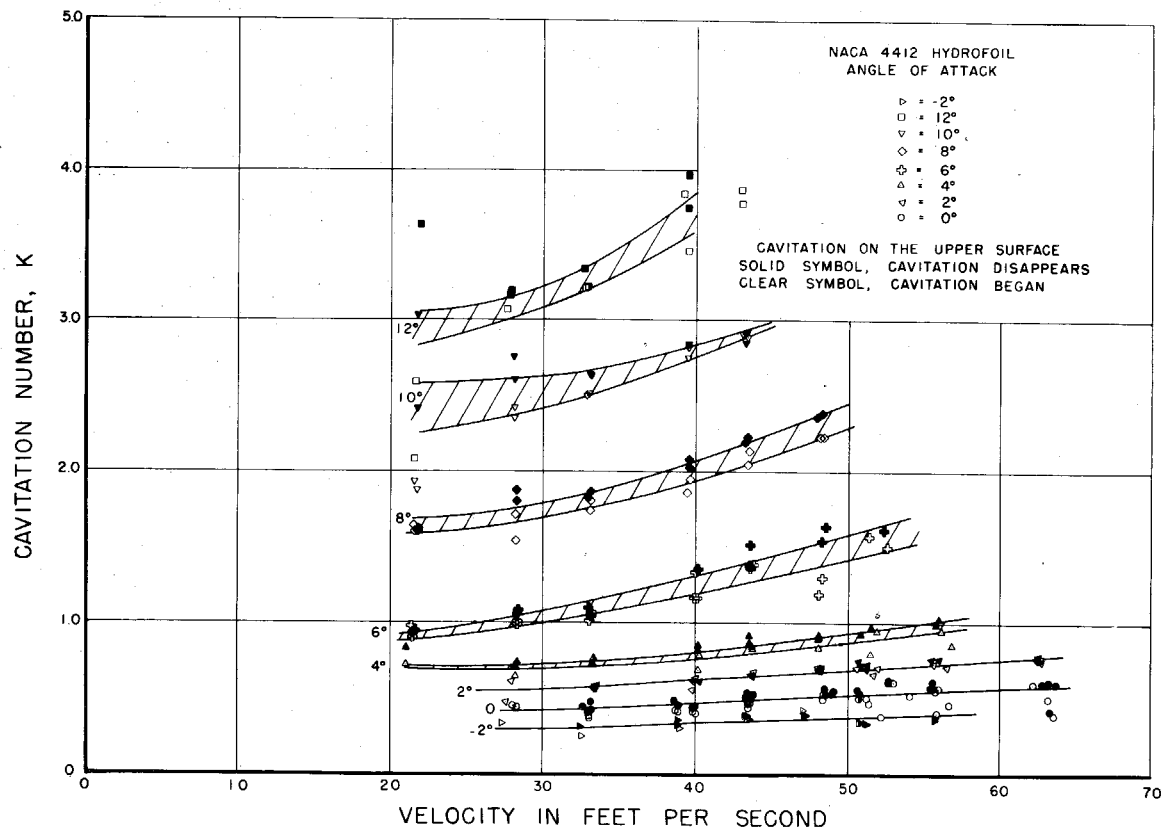


Fig. 14 - Cavitation number for incipient cavitation on the upper or suction surface as a function of velocity and angle of attack for the NACA 4412 hydrofoil.

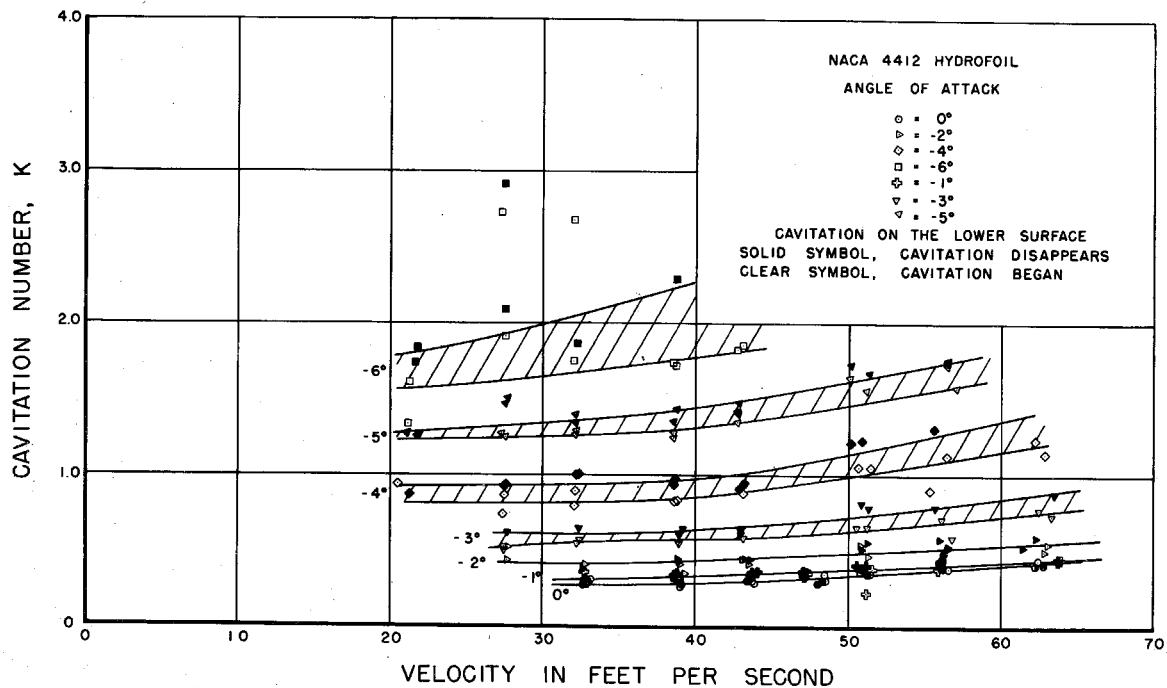


Fig. 15 - Cavitation number for incipient cavitation on the lower or pressure surface as a function of velocity and angle of attack for the NACA 4412 hydrofoil.

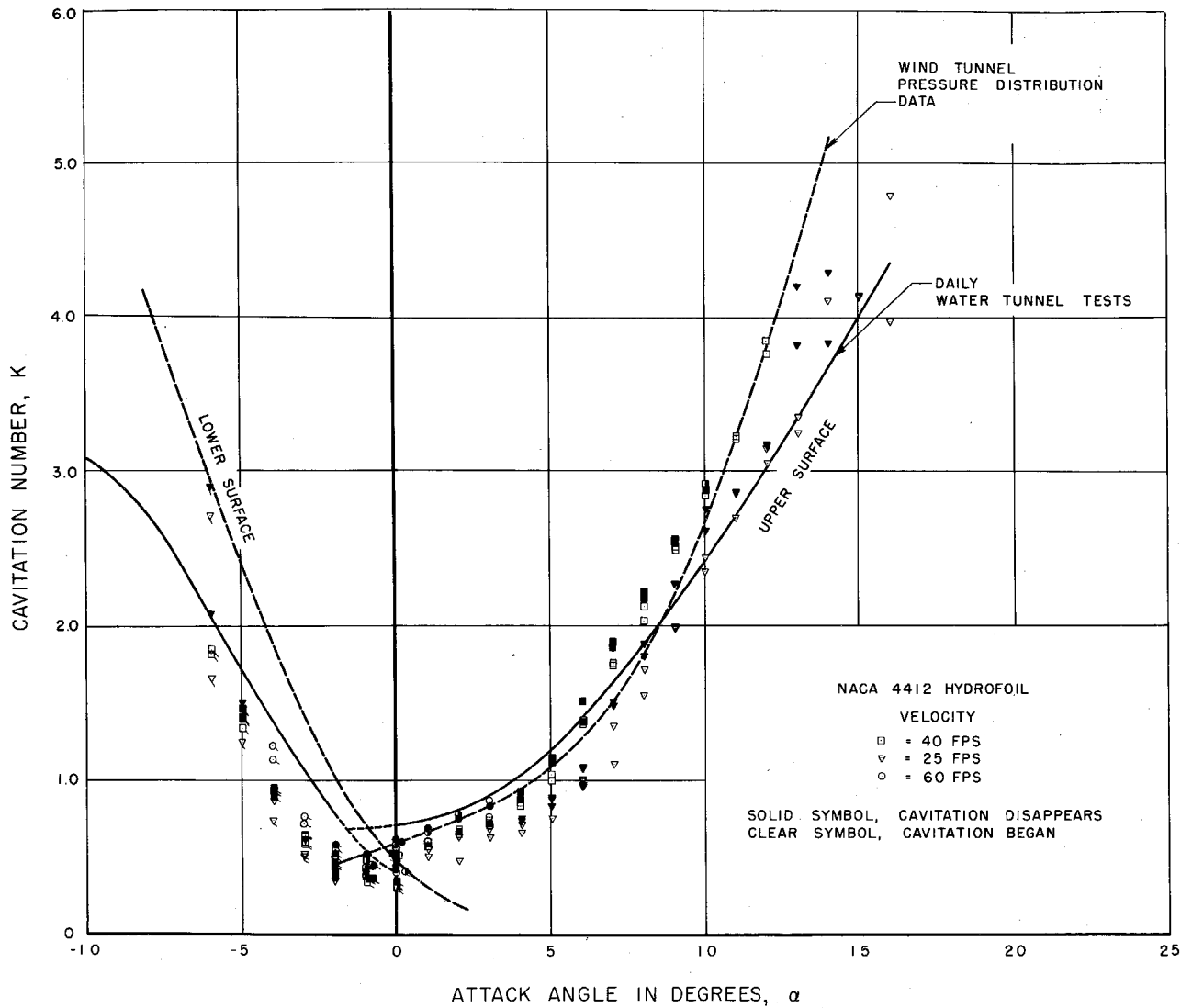


Fig. 16 - Incipient cavitation number as a function of angle of attack for the NACA 4412 hydrofoil at velocities of 25, 40 and 60 fps. The incipient cavitation number predicted from wind tunnel pressure distribution measurements on this profile are included for comparison. The flagged symbols on the left are for cavitation on the lower surface of the hydrofoil.

nose contour of the models could easily account for the differences between the observed and predicted values of cavitation number.

The data for incipient cavitation was taken in two ways; first by lowering the pressure slowly at constant water velocity until cavitation began and measuring the velocity and pressure, and second, by raising the pressure slowly at constant velocity after cavitation had been established on the model until the cavitation just disappeared. In general, these two methods gave different values of the incipient cavitation number. The difference in the cavitation numbers obtained by these two methods is referred to in the literature as cavitation hysteresis. In Figs. 14, 15, and 16, the clear symbol indicates the incipient cavitation number obtained by lowering the pressure, and the solid black symbol, the cavitation number at which cavitation disappeared. The shaded areas show roughly the limits of the start and disappearance of cavitation. The points which are partially clear indicate that there was no hysteresis and cavitation would begin and then disappear repeatedly at constant cavitation number. There is some overlapping of the data obtained by the two methods, but in general, cavitation hysteresis was observed over the full test range and became greater at higher attack angles. The air content of the water in the tunnel was between 12.4 and 13.3 moles of air per million moles of water throughout the incipient cavitation tests. The saturation value for the tunnel water at the temperature of the tests is approximately 15 parts per million.

C. Cavitating flow

Lift, drag and pitching moment were measured for the NACA 4412 hydrofoil for a range of cavitation numbers from fully wetted flow to full cavity flow at angles of attack of -8 to +16 degrees. These tests were made at a tunnel velocity of 30 fps corresponding to a Reynolds number of 0.8×10^6 . At 4 degrees attack angle, cavitation force runs were made at velocities of 25, 30, 35 and 40 fps. Except for changes in drag coefficient in fully wetted flow and at incipient cavitation, the force coefficients for the hydrofoil did not change with velocity.

The forces and moments on the hydrofoil for fully wetted and cavitating flow are given in Figs. 17 through 20. The curves are compiled from the results of twenty runs at different attack angles in which the velocity and angle of attack of the hydrofoil were held constant and the cavitation number

varied from completely wetted to full cavity flow. Curves were faired through the data for each run and coefficients were taken from these faired curves at particular cavitation numbers. By this means the curves of constant cavitation number in Figs. 17, 18, and 20 could be obtained. Since the curves shown here do not give measured data points, the measured coefficients are presented in Table IC, Appendix D. As explained in the section on experimental procedure, no wall corrections were applied to the coefficients measured in the cavitation force runs.

Lift coefficient as a function of angle of attack is shown in Fig. 17. Each curve in this figure represents a different cavitation number. We can see from these curves that once a cavity has been established on the hydrofoil, the lift coefficient becomes relatively insensitive to changes in attack angle. We can also note that at high attack angles near stall, small amounts of cavitation, beginning near the leading edge, delay stalling and give an increase in lift coefficient.

Figure 18 shows the moment coefficient about the quarter chord point as a function of angle of attack for various cavitation numbers. It should be noted that the scale of moment coefficient has been greatly expanded relative to the scale for fully wetted flow in Fig. 12 in order to show the changes more clearly. We can see from these curves that at higher positive attack angles the beginning of cavitation results in a more negative or downward pitching moment, and as the cavitation number is reduced and the cavitation covers more of the model, the moment coefficient returns to its fully-wetted value and then to less negative values. The same is true at negative angles, except the directions of the trends are reversed due to the fact that the cavitation originates on the lower surface of the hydrofoil. The region near zero attack angle where the curves converge is the region of no cavitation.

The polar diagram, Fig. 19, gives lift and drag coefficients as functions of angle of attack and cavitation number. In Fig. 19 the solid lines are curves of constant cavitation number and the dashed lines curves of constant angle of attack. It should be noted that the drag coefficient has been plotted to a scale ten times as large as the lift coefficient.

In order to correlate the force and moment coefficients of Figs. 17, 18 and 19 with the extent of cavitation on the hydrofoil, it is necessary to study these curves in conjunction with the cavitation diagram for the hydrofoil, Fig. 20.

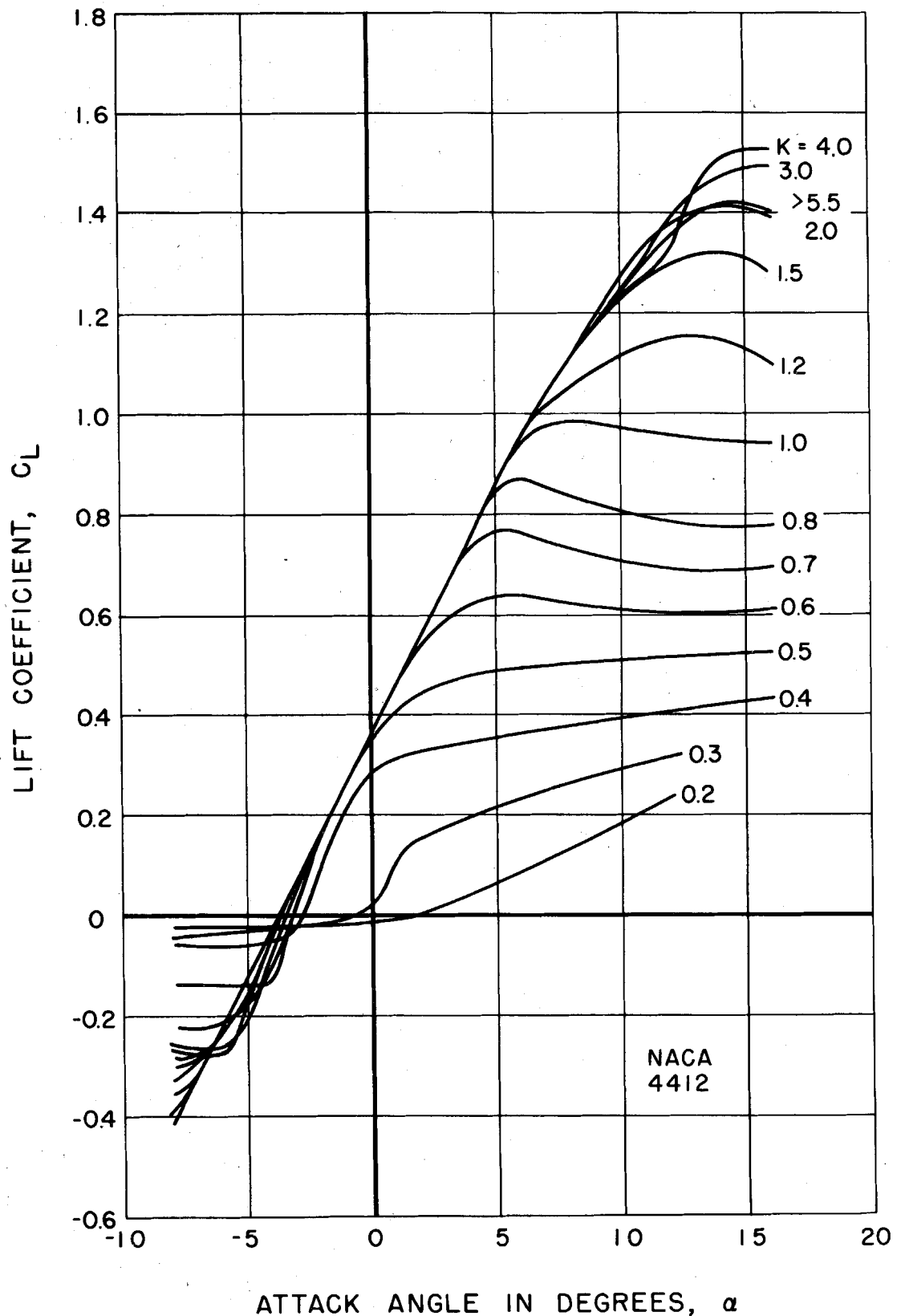


Fig. 17 - Lift coefficient as a function of angle of attack and cavitation number for the NACA 4412 hydrofoil.

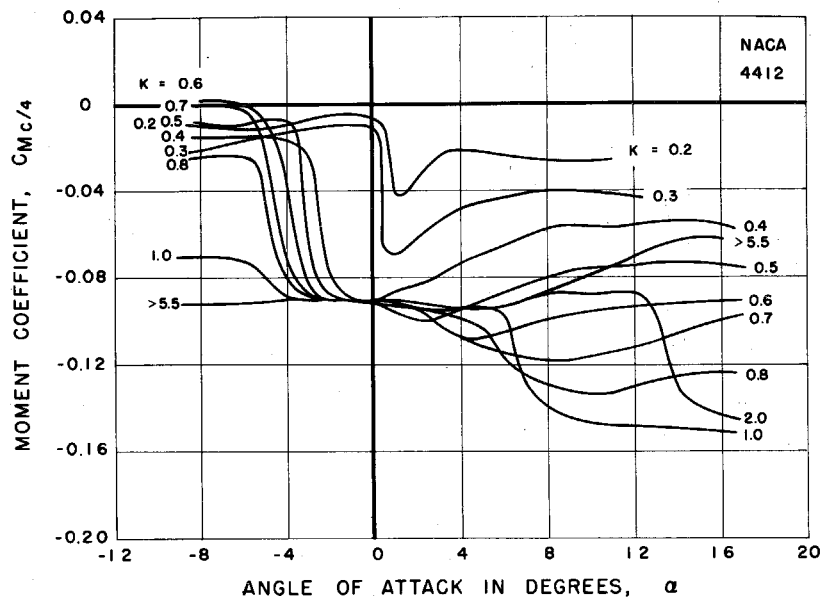


Fig. 18 - Moment coefficient about the quarter chord point as a function of angle of attack and cavitation number for the NACA 4412 hydrofoil.

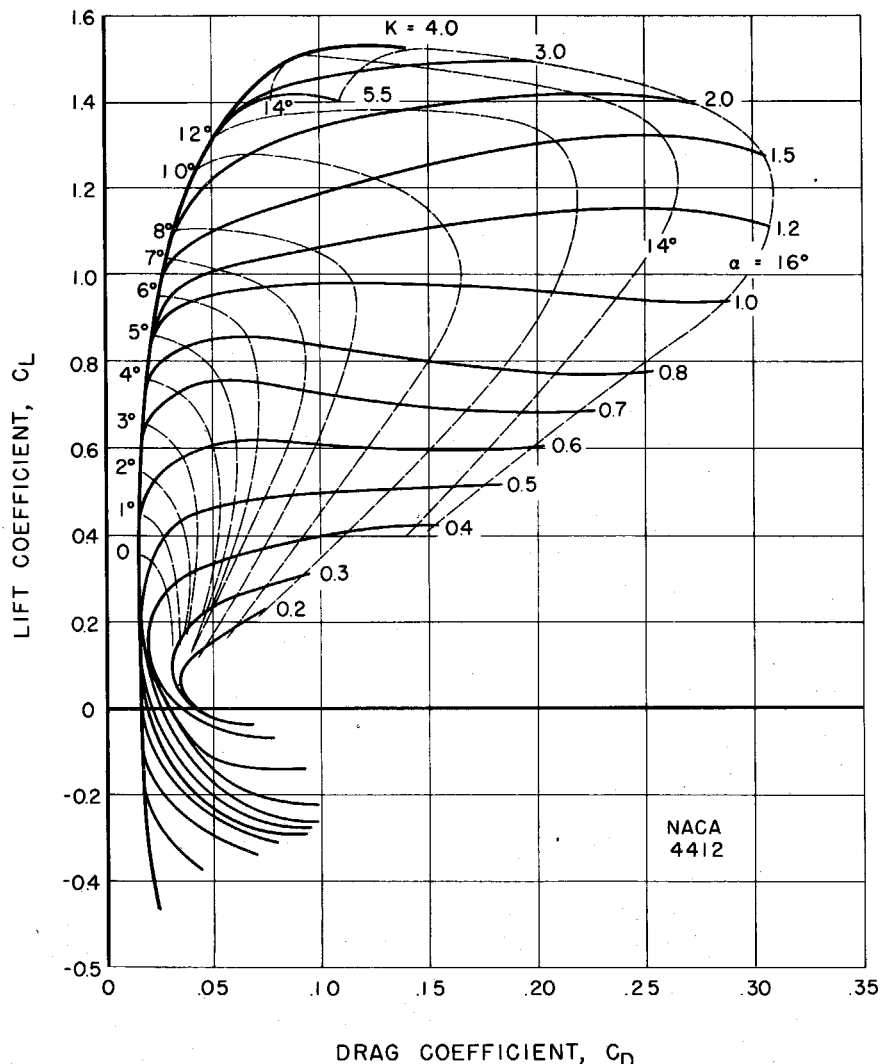


Fig. 19 - Polar diagram for cavitating and noncavitating flow for the NACA 4412 hydrofoil.

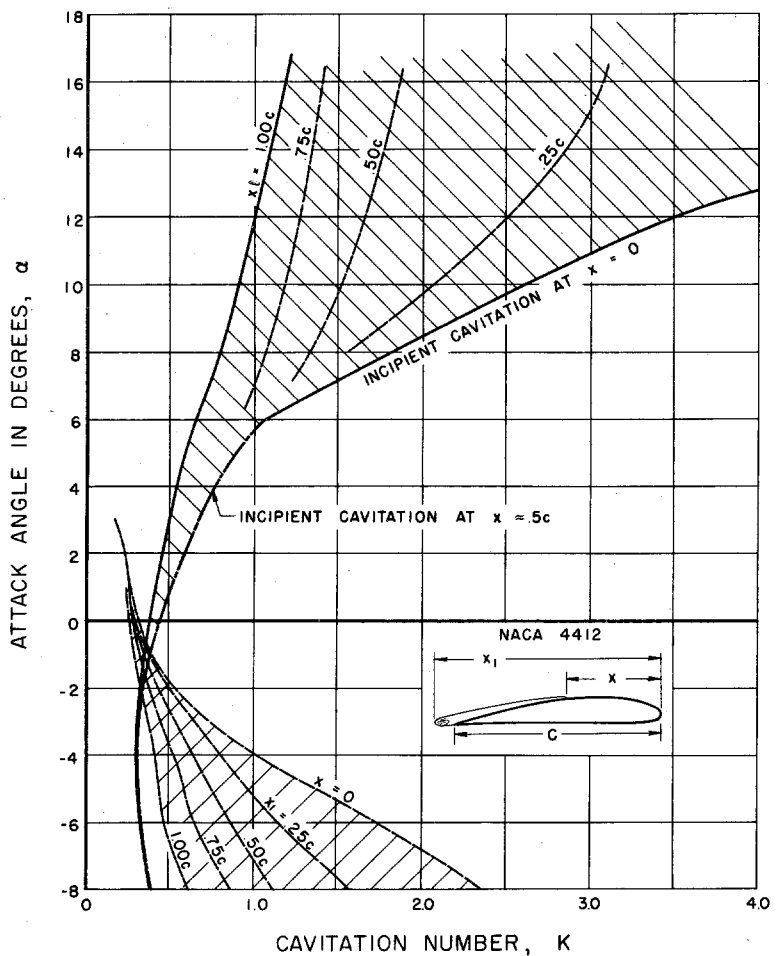


Fig. 20 - Cavitation diagram for the NACA 4412 hydrofoil. The shaded areas are regions of cavitation number and attack angle wherein the cavitation collapses on the hydrofoil.

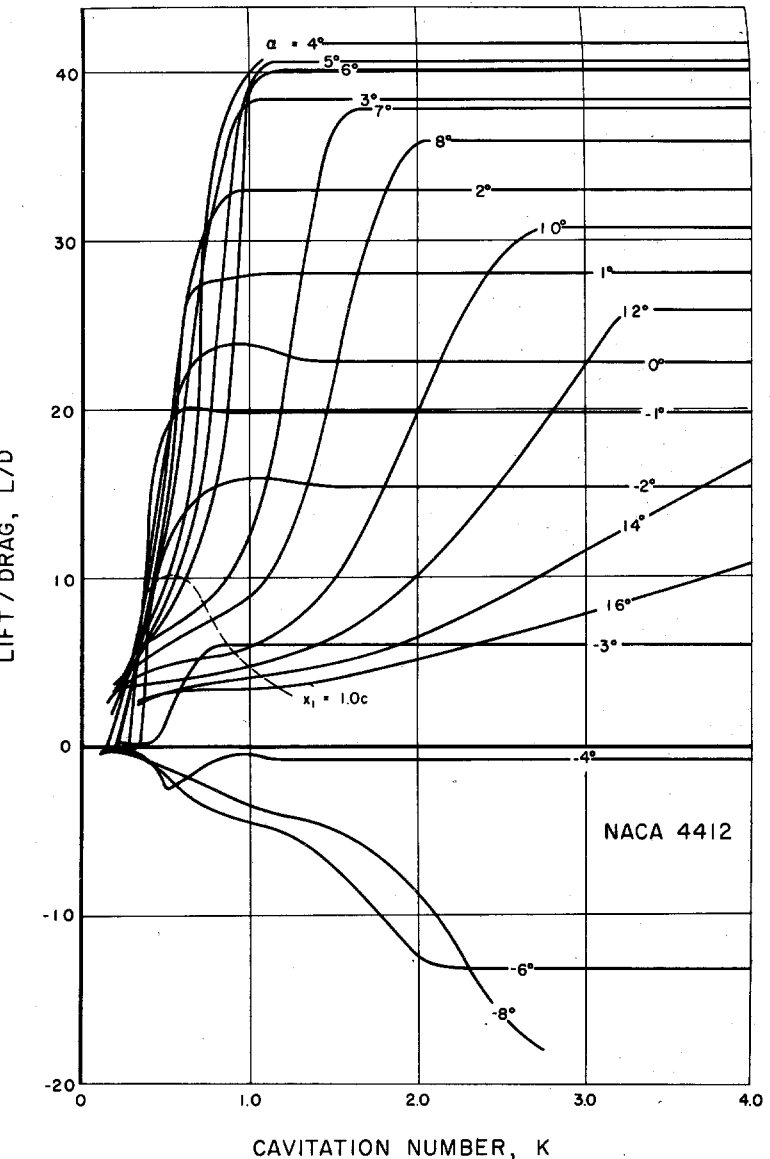


Fig. 21 - Lift/drag ratio as a function of cavitation number and angle of attack for the NACA 4412 hydrofoil. The dashed line at the lower left indicates the cavitation number at which the cavitation extends downstream to the trailing edge of the hydrofoil.

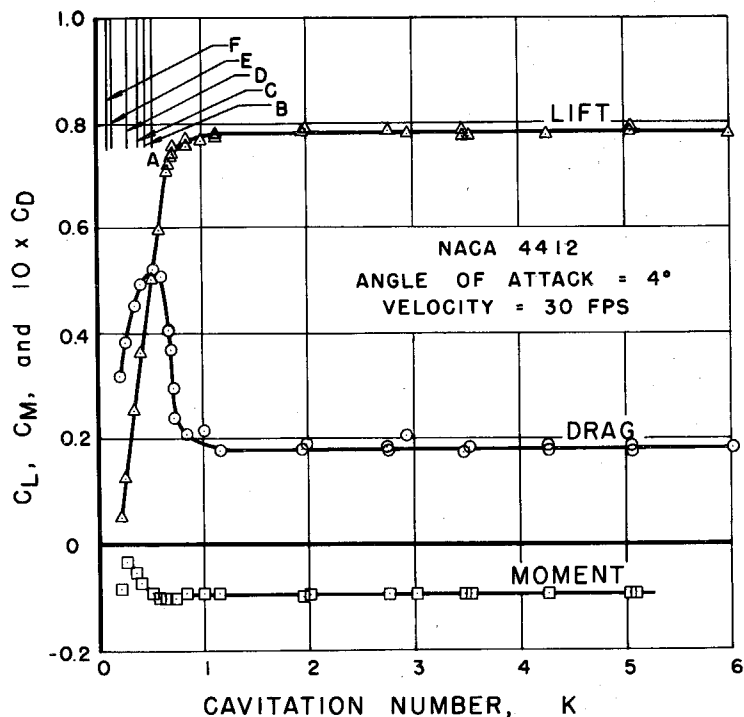


Fig. 22 - Lift, drag and pitching moment coefficients as functions of cavitation number for the NACA 4412 hydrofoil at an angle of attack of 4 degrees. The drag coefficient is plotted to a scale 10 times that of the lift and moment coefficients. The cavitation numbers noted A through F correspond to the photographs of Fig. 24.

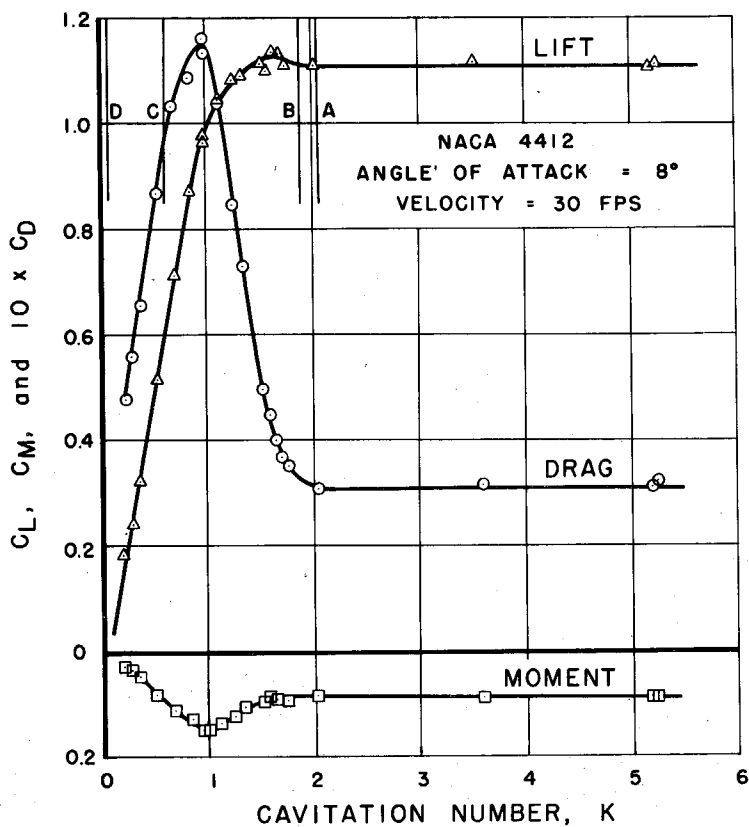


Fig. 23 - Lift, drag and pitching moment coefficients as functions of cavitation number for the NACA 4412 hydrofoil at an angle of attack of 8 degrees. The drag coefficient is plotted to a scale 10 times that of the lift and moment coefficients. The cavitation numbers noted A through D correspond to the photographs of Fig. 25.

This figure shows the extent of cavitation on the model as a function of angle of attack and cavitation number. The broken line marked $X \approx .50 c$ indicates the cavitation number at which cavitation began at approximately mid-chord on the upper surface of the hydrofoil. The position of the leading edge of the cavitation varied from approximately $0.2 c$ to $0.6 c$ with angle of attack in this region. The upper, solid curve, marked $X = 0$, above 6 degrees attack angle indicates the beginning of cavitation on the upper surface, originating near the leading edge. The solid line to the left in the figure, marked $X_1 = 1.00 c$ indicates the cavitation number at which the downstream end of the cavitation zone reaches the trailing edge of the hydrofoil. Therefore the shaded region indicates that the cavitation collapses on the hydrofoil. The dashed lines in the shaded area give the portion of the hydrofoil covered by cavitation. The region to the left of the $X_1 = 1.00 c$ line is in full cavity flow with the cavity closing downstream from the hydrofoil. The $X \approx .50 c$ and $X_1 = 1.00 c$ lines for cavitation on the upper surface converge for negative attack angles. This is due to the fact that as the angle of attack decreases the leading edge of the cavitation moves farther back along the upper surface and even at incipient cavitation the downstream end of the cavitation reaches the trailing edge of the hydrofoil. The lines and shaded region in the lower portion of Fig. 20 give the extent of cavitation on the lower surface. Cavitation on the lower surface always began near the leading edge.

The cavitation diagram was obtained from photographs made at each test point during the runs. The cavitation numbers in the cavitation diagram and in the force coefficient curves are based on vapor pressure.

Figure 21 shows the lift/drag ratio as a function of angle of attack and cavitation number. Each curve in this figure is drawn for a constant angle of attack. The straight horizontal portions of the curves are regions of zero cavitation. When cavitation begins there is a rapid decrease in the lift/drag ratio. This is due both to a decrease in lift and an increase in drag; however, the increase in drag is proportionately much greater than the decrease in lift with small amounts of cavitation. The rapid increase in drag coefficient causes a decrease in the lift/drag ratio even for the flow regime at high attack angles where there is an increase in lift when cavitation begins.

The greatest reduction in the lift/drag ratio occurs between incipient

cavitation and when the downstream end of the cavitation zone reaches the trailing edge of the hydrofoil. The dashed curve marked $X_1 = 1.00 c$, in Fig. 21, shows the cavitation number at which the cavitation reaches the trailing edge for positive attack angles. The region between this line and the knees of the curves of lift/drag ratio is the region of partial cavitation between incipient and full cavity flow. In the region under the dashed, full cavity line, the reduction in lift/drag ratio with cavitation number becomes less steep particularly at higher attack angles. This is due primarily to the fact that with full cavity flow there is a decrease in drag coefficient as cavitation number is reduced.

If the curves of Fig. 21 are compared with the cavitation diagram, it appears that there is a reduction in the lift/drag ratio before cavitation begins. The knees of the curves for lower attack angles occur at cavitation numbers higher than the incipient cavitation numbers indicated by the cavitation diagram. This is due to spurious cavitation occurring on the stub spindle supporting the hydrofoil. Flow through the clearance gap around the stub spindle causes cavitation which covers a portion of the hydrofoil near the wall before cavitation begins on the hydrofoil itself. The effect of this spurious cavitation is to cause a slight loss of lift and increase in drag and a rounding off of the knee of the lift/drag ratio curves. The lift/drag ratio curves should drop more sharply when cavitation begins than is indicated by Fig. 21. The experimental setup employing the stub spindle was used in all the cavitation force runs described in this report. Some of the runs with the NACA 4412 hydrofoil for noncavitating flow and later runs on a different profile used the spindle disk mounting setup described in the section on apparatus and test procedure. With the flush disk mount, the spindle and hydrofoil end gap clearance and the spurious spindle cavitation have been eliminated.

Curves of lift, drag and pitching moment coefficient as functions of cavitation number for representative runs are given in Fig. 22 for an angle of attack of 4 degrees and in Fig. 23 for an angle of attack of 8 degrees. The points in these figures are the coefficients calculated from the measured data. It should be noted that the drag coefficient has been plotted to a scale ten times that of the lift and moment coefficient. Photographs of the cavitating hydrofoil at 4 degrees angle of attack are shown in Fig. 24. Figure 25 shows simultaneous top and side view photographs of cavitation on the hydrofoil at

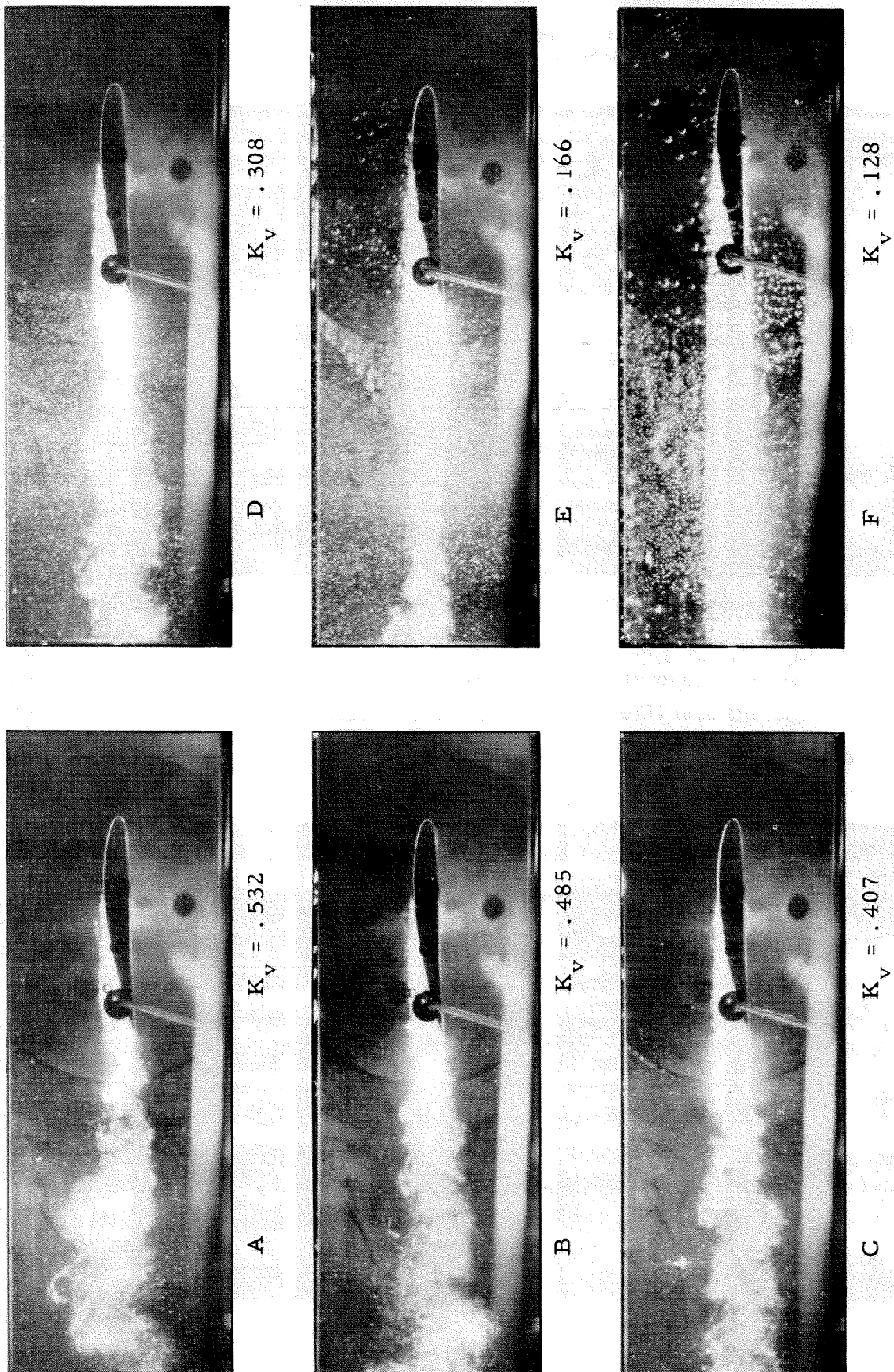
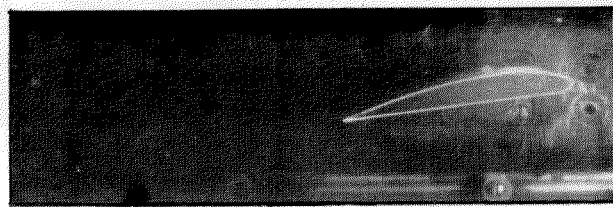
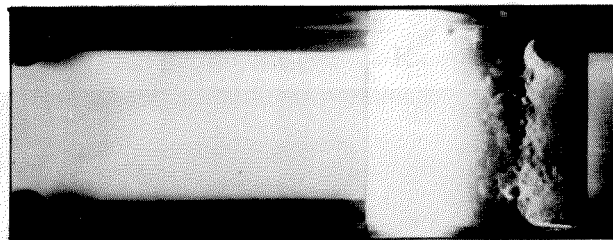
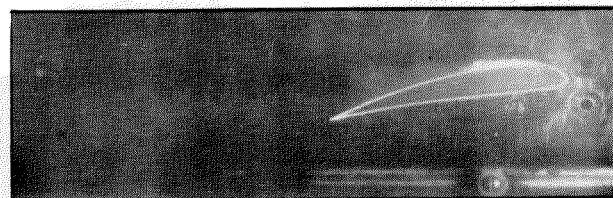
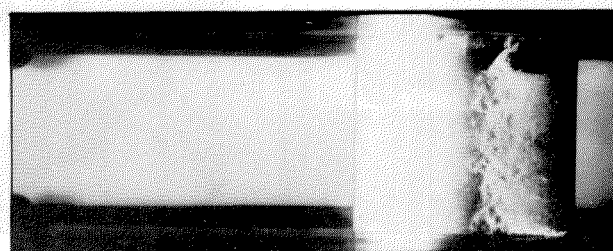


Fig. 24 - Cavitation on the NACA 4412 hydrofoil at an angle of attack of 4 degrees. The force coefficients corresponding to these conditions of cavitation are shown in Fig. 22.



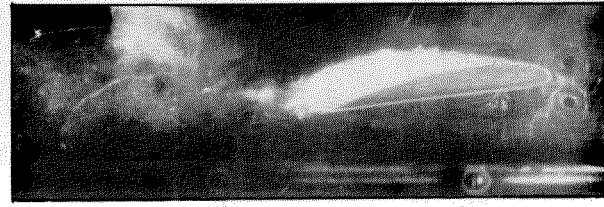
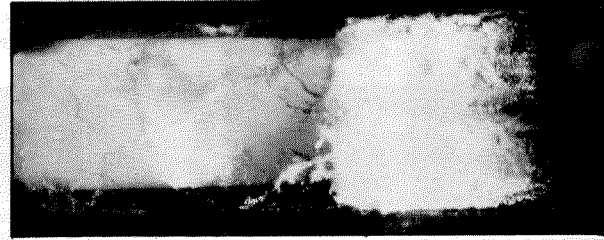
A

$$K_v = 2.048$$



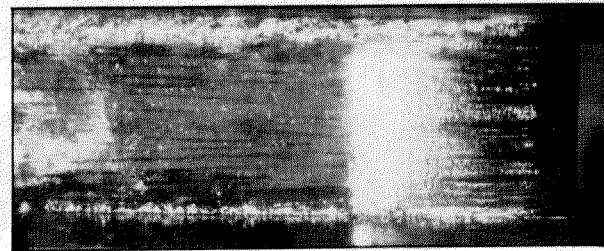
B

$$K_v = 1.873$$



C

$$K_v = 0.610$$



D

$$K_v = 0.064$$

Fig. 25 - Simultaneous top and side views of cavitation on the NACA 4412 hydrofoil at an angle of attack of 8 degrees. Force coefficients corresponding to these photographs are shown in Fig. 23.

an angle of attack of 8 degrees corresponding to the force run of Fig. 23. The cavitation numbers corresponding to the photographs of Figs. 24 and 25 have been indicated on the force coefficient curves of Figs. 22 and 23.

When the cavitation area is on the order of one-half to one chord in length, severe buffeting forces may be encountered particularly at higher attack angles. The buffeting is caused by violent fluctuations in the cavitation which may cause the hydrofoil to change from nearly fully wetted to full cavity flow very rapidly. Figure 26 shows cavitation on the hydrofoil under conditions of severe buffeting at an angle of attack of 12 degrees. Buffeting may occur at all attack angles, but its severity increases with attack angle. When the cavitation number is reduced so that the cavity closes downstream of the hydrofoil, the buffeting ceases and the forces are steady, Fig. 26.

The cavitation numbers given in the incipient cavitation plots, the cavitation force curves and in the data tables in the appendix, are based on vapor pressure. A series of cavitation runs was made with the NACA 4412 hydrofoil in which the pressure in the cavity was measured, thus permitting a comparison between the cavitation numbers based on vapor pressure and on measured cavity pressure. In these runs the cavity pressure was measured by means of a probe protruding from the channel wall into the cavity. The runs could be made only over the range of cavitation numbers which gave a cavity sufficiently long to cover the pressure probe. The line leading to the pressure probe and the position of the probe can be seen in Fig. 26. Because of the location of the probe, the minimum attack angle of the runs was +4 degrees. Figure 27 shows a comparison between the cavitation numbers based on vapor pressure and the measured cavity pressure for these runs. At low cavitation number the difference is small, however as the cavitation number is increased, the cavitation number based on vapor pressure becomes increasingly greater than that based on the measured cavity pressure. Figure 28 shows the measured cavity pressure as a function of the free stream absolute pressure. From this figure we see that as the free stream pressure increases the cavity pressure increases to several times the vapor pressure. In the region of high cavity pressure, the cavity on the hydrofoil is short and fluctuates because the cavity collapses on the model and forms a strong reentrant jet. The measured cavity pressure in this region then probably includes both the average of the dynamic pressure of the rapidly

fluctuating flow and the gas pressure in the cavitating region. It should be noted that the measurements of pressure by means of a static pressure probe gives doubtful results in a region of a water-gas mixture. Therefore, the points at the extreme right in Figs. 27 and 28 give only approximate values.

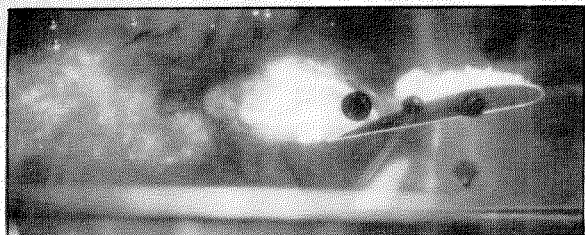
In the region of full cavity flow where the cavitation becomes a clear steady cavity, the measurements of the cavity pressure are accurate. Figure 29 shows the measured cavity pressure as a function of free stream static pressure for this region of full cavity flow for several hydrofoil attack angles and at two velocities. From this figure we see that the cavity pressure is constant over a range of free stream pressures. The solid lines in Figs. 28 and 29 give the range of vapor pressures corresponding to the water temperature range of these tests. The air content of the water during these runs was very nearly constant at 11.2 moles of air per million moles of water. The measured cavity pressure in Fig. 29 is 28% greater than vapor pressure. This gives a partial pressure of air in the cavity which is 22% of the total cavity pressure. No experiments were made in which the air content of the water was varied, however the cavity pressure may vary with the amount of dissolved or entrained air in the flow.

If the cavitation force results obtained in different facilities are to be compared, they should be compared on the basis of the cavitation number calculated from the measured cavity pressure whenever possible. The measurement of the cavity pressure, however, becomes extremely difficult for high cavitation numbers because of the turbulent mixture of water and gas and because the position of the cavitation on the hydrofoil changes with attack angle. Therefore in the range where there are large differences between the two cavitation numbers it becomes nearly impossible to compare results based on a measured cavity pressure.

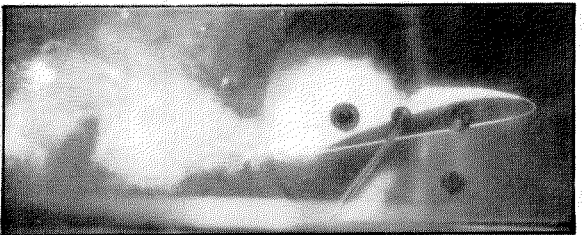
2. Walchner Profile 7

A. Noncavitating flow

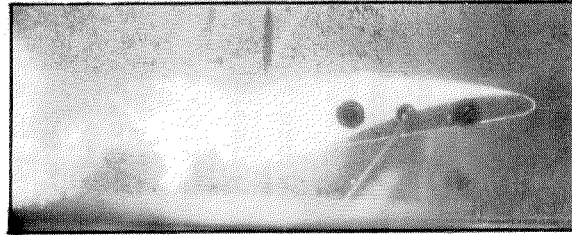
Two series of experiments were run to determine the section characteristics of the Walchner profile 7 hydrofoil in noncavitating flow. The hydrofoil was first tested in fully wetted and in cavitating flow and then the leading edge of the model was reworked and the tests repeated for noncavitating flow. Figures 30 and 31 show the section characteristics obtained on the original



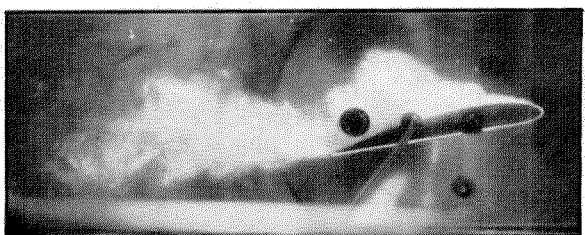
$$K_v = 1.614$$



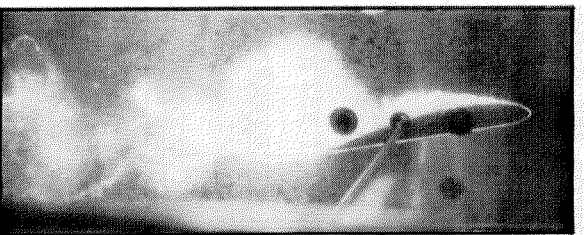
$$K_v = 0.925$$



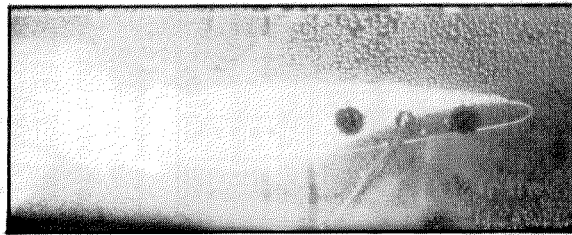
$$K_v = 0.428$$



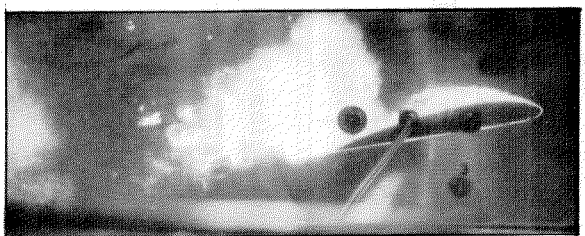
$$K_v = 1.780$$



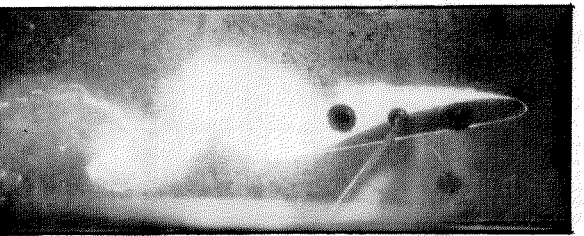
$$K_v = 1.152$$



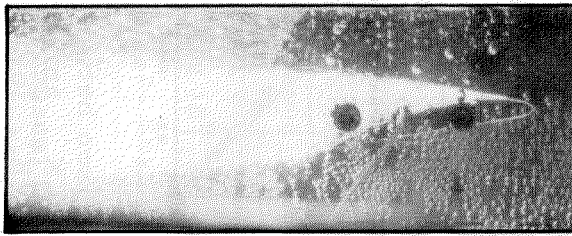
$$K_v = 0.623$$



$$K_v = 1.331$$



$$K_v = 0.833$$



$$K_v = 0.289$$

Fig. 26 - Cavitation on the NACA 4412 hydrofoil at an angle of attack of 12 degrees. The large fluctuations in the cavitation cause severe buffeting forces on the hydrofoil.

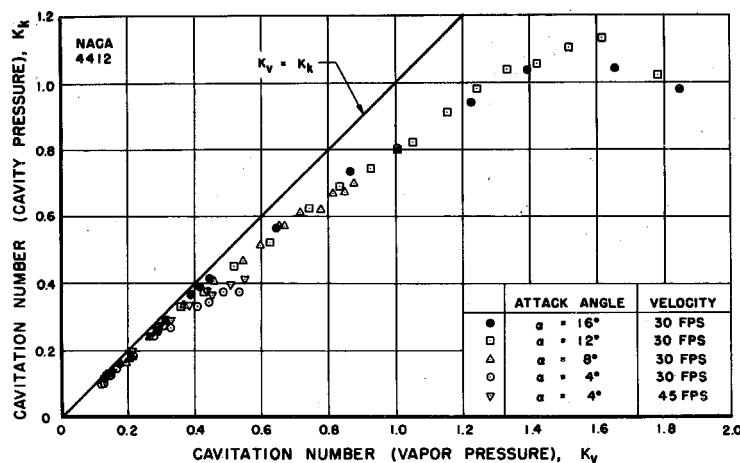


Fig. 27 - A comparison between the cavitation number based on vapor pressure, K_v , and cavitation number based on the measured cavity pressure, K_k , for the NACA 4412 hydrofoil. The data of this figure is for well-developed cavitation on the hydrofoil.

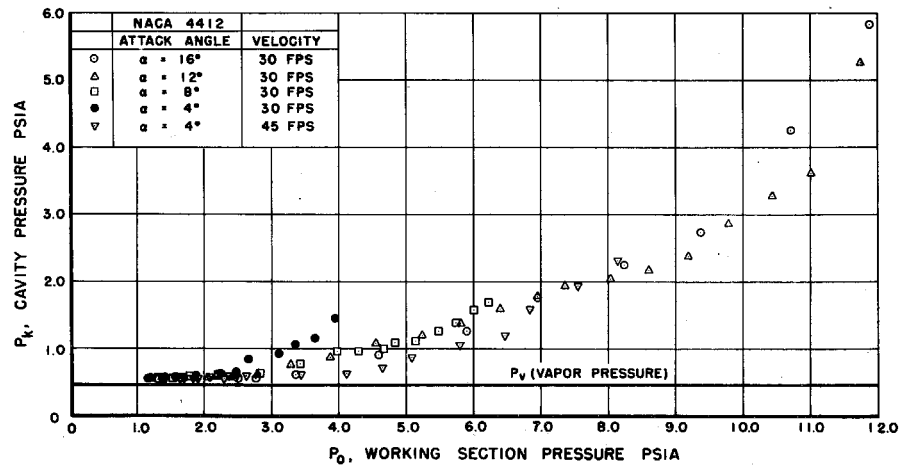


Fig. 28 - Measured cavity pressure as a function of free stream pressure at several attack angles for the NACA 4412 hydrofoil. The solid line shows the vapor pressure of water at the temperature of these tests.

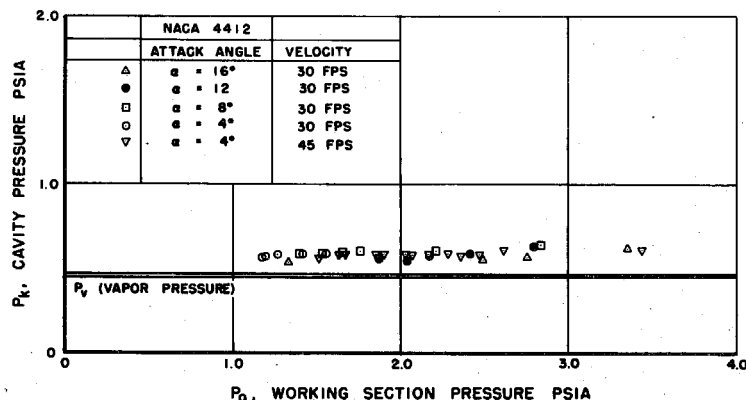


Fig. 29 - Measured cavity pressure for full cavity flow as a function of free stream pressure at several attack angles for the NACA 4412 hydrofoil. The double, solid lines show the vapor pressure range corresponding to the water temperature range of these tests.

unmodified model in noncavitating flow. The data for fully wetted flow has been corrected for wall and blockage effects. These corrections are described in Appendix C. The lift and moment coefficients as functions of attack angle are shown in Fig. 30, and the polar diagram giving lift and drag coefficients is shown in Fig. 31. The solid lines in these figures are the results obtained on this profile by Walchner.³ Walchner does not report any pitching moment coefficients. The CIT water tunnel tests were made at velocities from 20 to 35 fps corresponding to Reynolds numbers of 0.53×10^6 to 1.05×10^6 based on the 3.30 inch chord. Walchner tests were made at Reynolds numbers from 0.3×10^6 to 0.5×10^6 .

The lift coefficient data of Fig. 30 shows an unusual inflection at approximately zero degree attack angle. In addition to the inflection in the curves, the slope of the lift coefficient curve is greater for positive attack angles than it is for negative attack angles. An inflection in the lift coefficient curve at small attack angles is characteristic of airfoils with rather sharply rounded leading edges at low Reynolds numbers. However, in the instances cited in the literature, the sign of the inflection is opposite to that obtained in these hydrofoil tests. The kink in the lift coefficient curves of airfoils is ascribed to laminar boundary layer separation and reattachment near the leading edge.⁹ This produces a highly turbulent "bubble" under the detached boundary layer. It seems possible that this same condition which occurs when there is a sharp suction peak near the leading edge could occur on the lower surface of a profile as well as on the upper surface. Such laminar "bubble" separation from the lower surface would occur near zero or small negative attack angles and would result in an inflection in the lift coefficient curve in the same direction as was obtained with this hydrofoil.

Close examination of the hydrofoil revealed a very slight discontinuity in the curvature of the rounded leading edge of the profile. Instead of a smoothly rounded surface the leading edge was somewhat more sharply rounded on the lower portion followed by a very short, nearly flat, region. After it was determined that the kink in the lift coefficient curve was not due to experimental technique or errors, the hydrofoil leading edge was reworked to eliminate the rather abrupt change in curvature and the hydrofoil was tested again in fully wetted flow. The results of the tests on the reworked model are shown in Figs. 32 and 33. We can see from the curves of lift and

moment coefficient vs attack angle in Fig. 32 that the inflection was greatly reduced. The most striking result of smoothing the contour of the leading edge, however, was the sizable reduction in drag coefficient, Fig. 33. The hydrofoil was mounted on the flush spindle disk in the second series of experiments which eliminated one end gap and the stub spindle clearance gap. The difference in experimental setup may account for part of the change in drag coefficient; however it cannot account for the smoothing out of the kink in the lift coefficient curves. In the second set of tests, the drag coefficient for a Reynolds number of 0.53×10^6 agrees very well with the results obtained by Walchner.

The experience with this hydrofoil points out very clearly the extreme care which must be taken to produce an accurate contour. The forces are particularly sensitive to differences in the leading edge contour. In reworking this hydrofoil, a maximum of about 0.002 inch of material was removed to smooth the contour. This increased the nose radius to approximately 0.94% c compared with the design radius of 0.74% c. Contours drawn from magnified photographs of the leading edge near the center of the hydrofoil span are shown in Fig. 34. These before and after photographs made by carefully sectioning castings of the leading edge of the model show how small the differences in the nose contour were for the two sets of experiments.

B. Cavitating flow

The cavitation force experiments were made with the hydrofoil before the leading edge was modified. The cavitation tests were not repeated with the reworked model. Curves of lift coefficient as a function of angle of attack and cavitation number shown in Fig. 35 are from the High Speed Water Tunnel experiments and in Fig. 36 from the experiments by Walchner. The curves obtained in the CIT experiments in general show decreasing lift coefficient for attack angles greater than 4 degrees while Walchner's curves show increasing values over the range of his tests. The curves are similar, however Walchner's curves show a greater lift for all curves of constant cavitation number. This difference amounts to a change in cavitation number of approximately 0.1.

Walchner gives force data for zero cavitation number but does not indicate how such low cavitation numbers were obtained. Low cavitation numbers are often obtained by injecting air into the cavity and using the

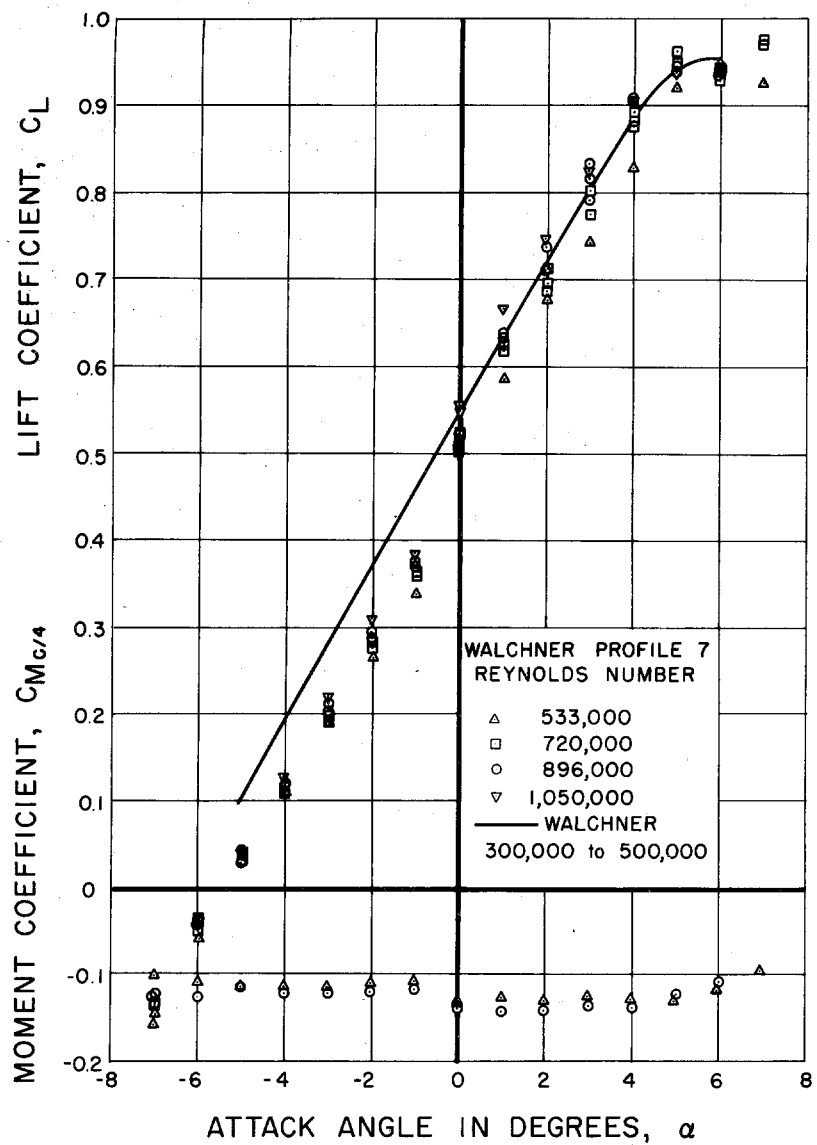


Fig. 30 - Lift coefficient and moment coefficient about the quarter chord point as functions of angle of attack for the Walchner profile 7 hydrofoil in noncavitating flow. The data are for the hydrofoil before modification of the leading edge.

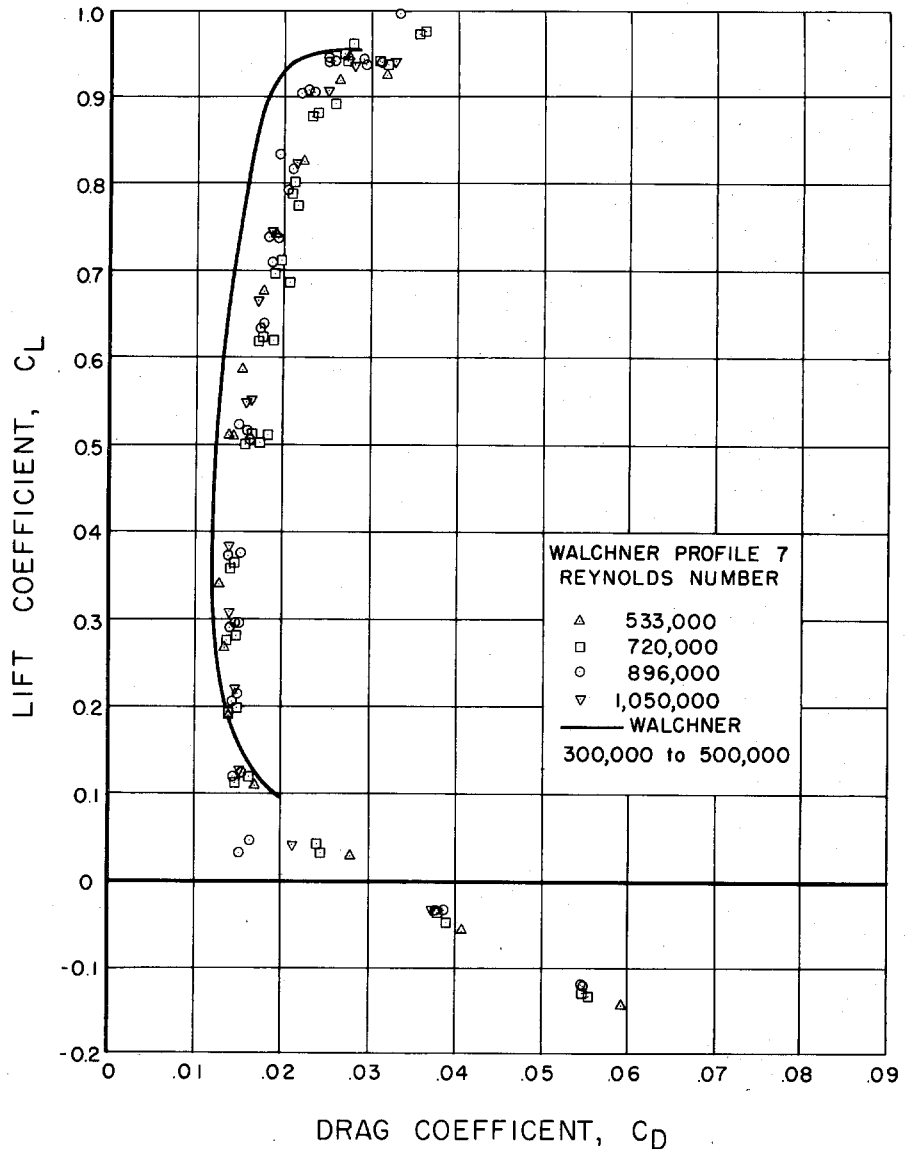


Fig. 31 - Polar diagram for the Walchner profile 7 hydrofoil in noncavitating flow. The data are for the hydrofoil before modification of the leading edge.

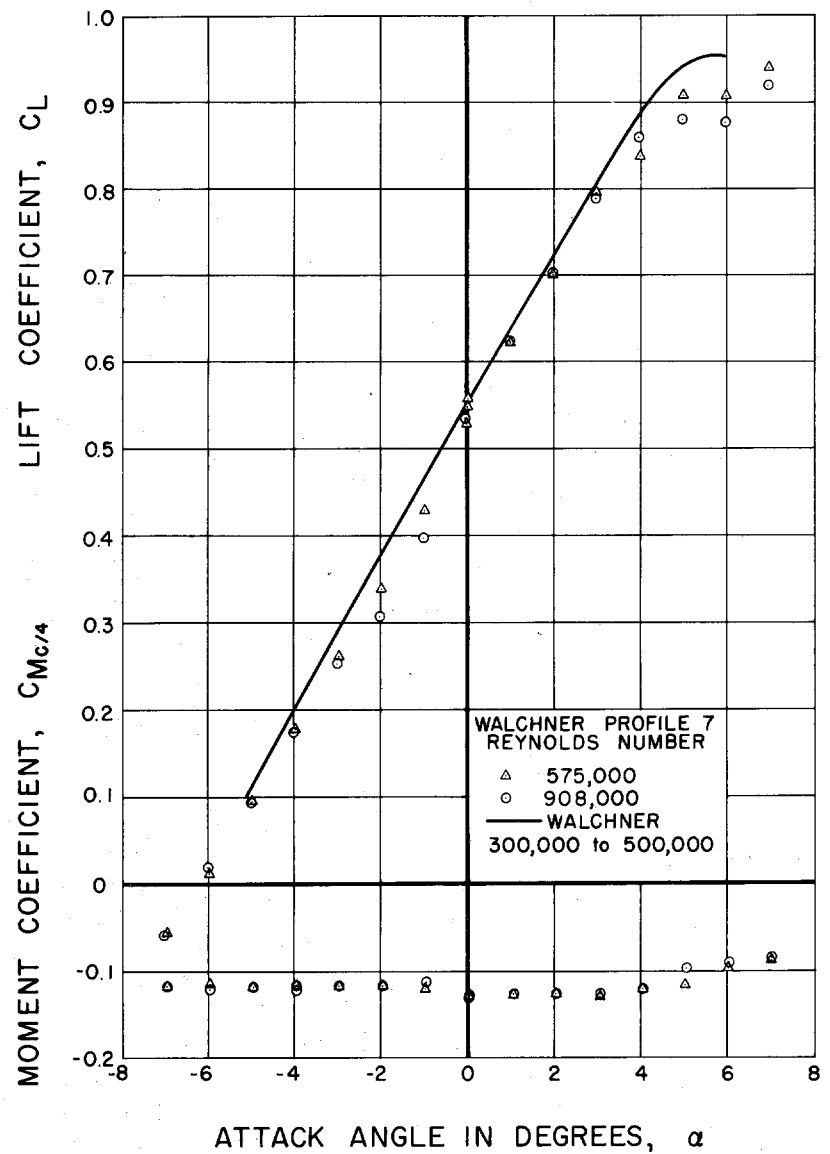


Fig. 32 - Lift coefficient and moment coefficient about the quarter chord point as functions of angle of attack for the Walchner profile 7 hydrofoil in noncavitating flow. The data are for the hydrofoil after modification of the leading edge.

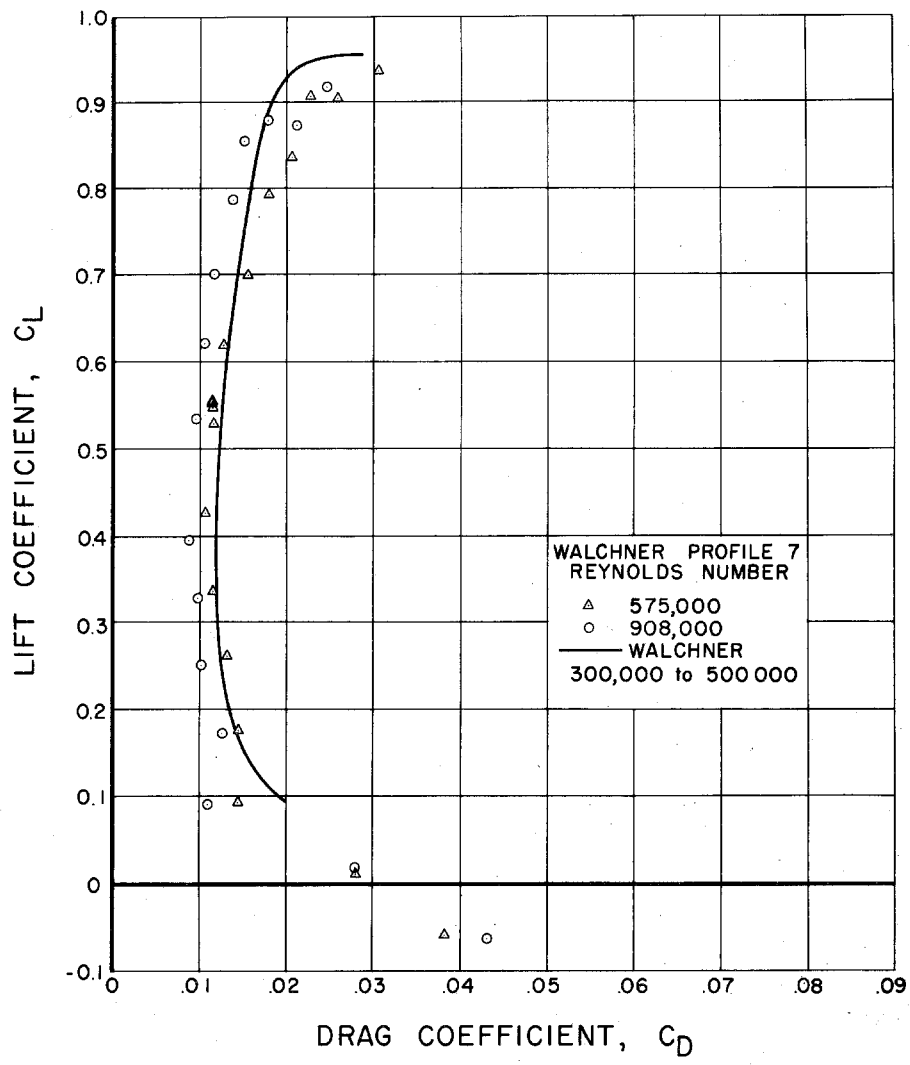


Fig. 33 - Polar diagram for the Walchner profile 7 hydrofoil in noncavitating flow. The data are for the hydrofoil after modification of the leading edge.

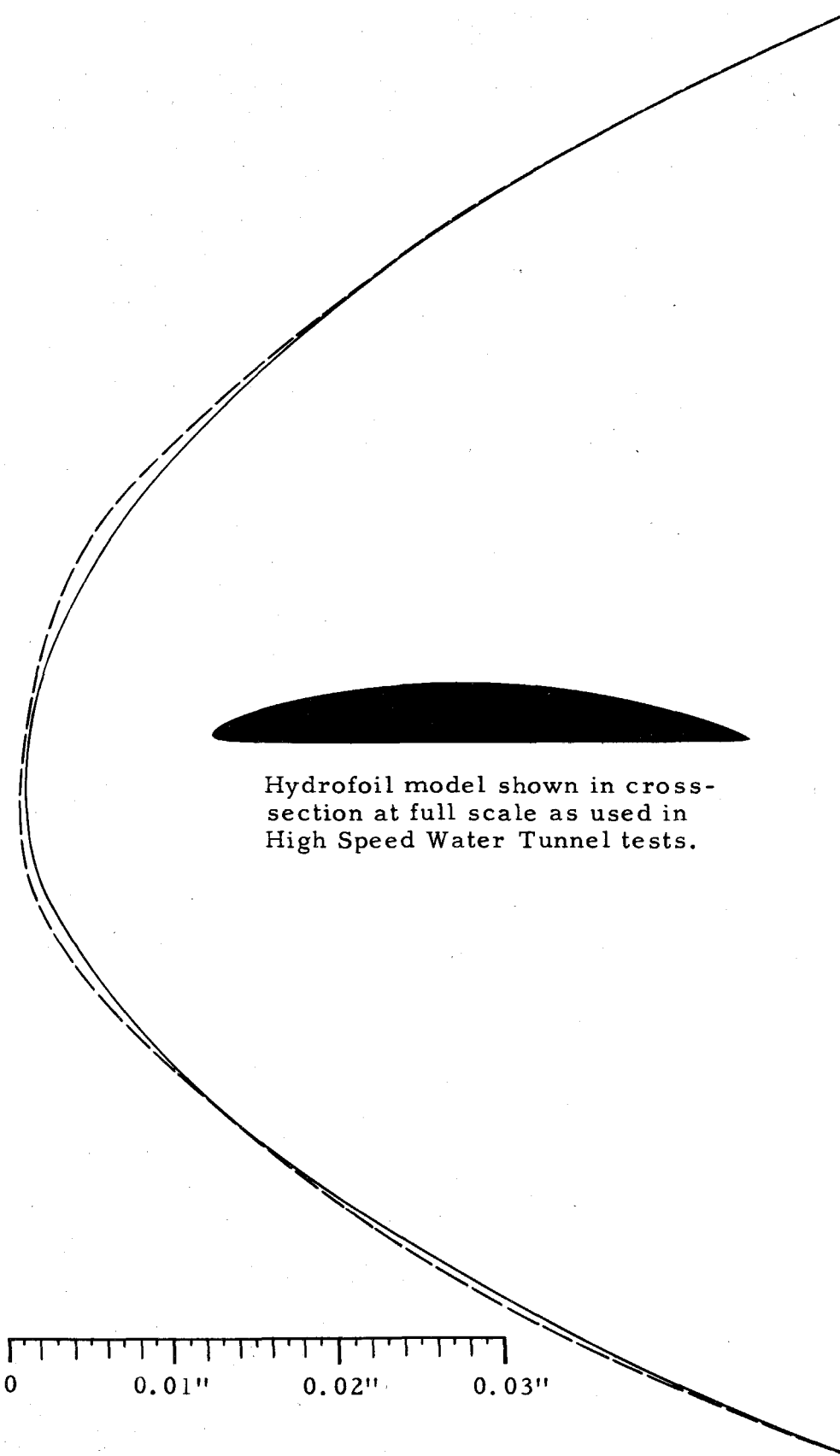


Fig. 34 - Contour of the leading edge of the Walchner profile 7 hydrofoil. The dashed line shows the profile before modification, the solid line shows the modified profile. Enlarged 100x

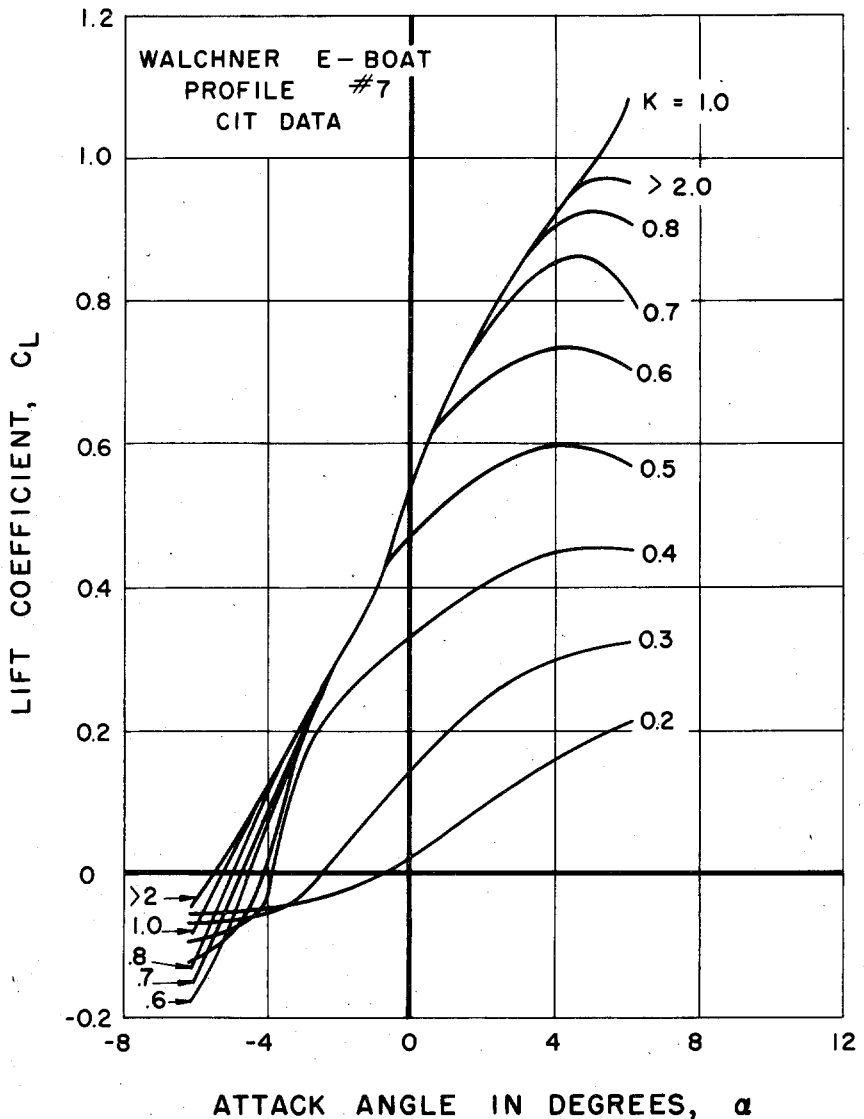


Fig. 35 - Lift coefficient as a function of angle of attack and cavitation number for the Walchner profile 7 hydrofoil. These curves are from the data of the present tests.

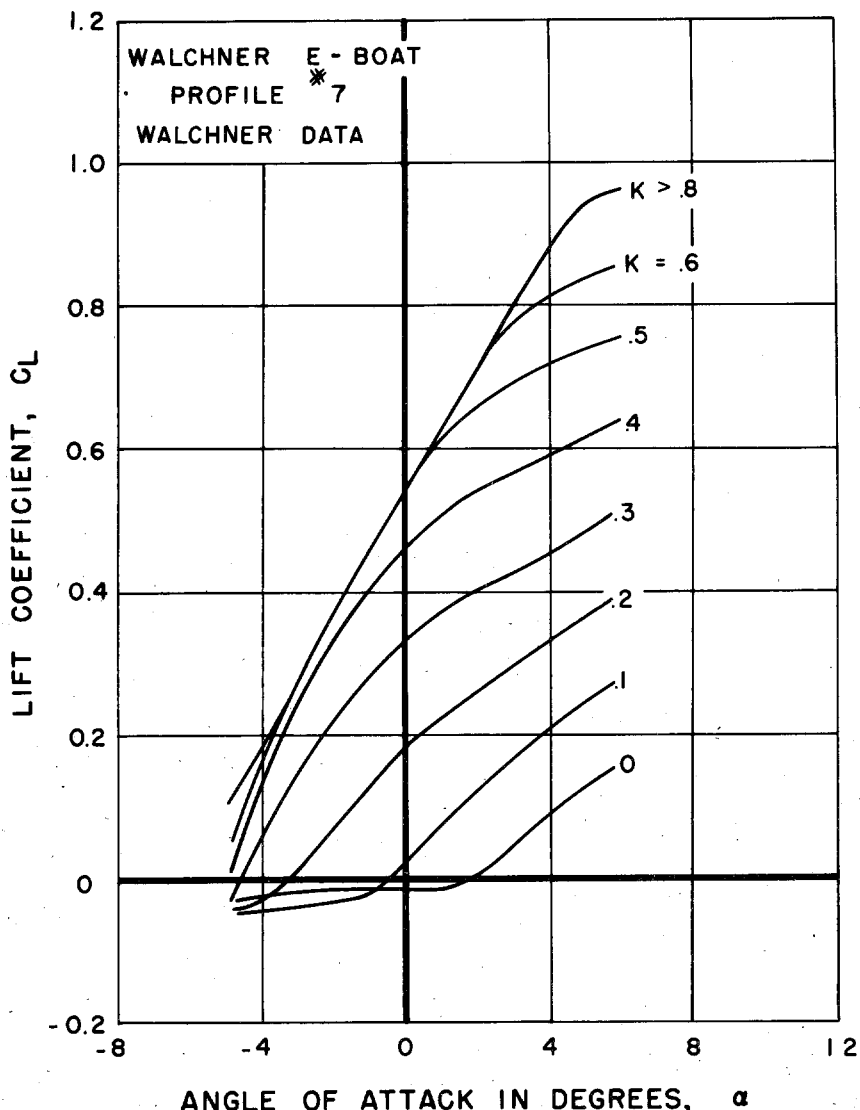


Fig. 36 - Lift coefficient as a function of angle of attack and cavitation number for Walchner profile 7 as reported by Walchner.

measured cavity pressure in calculating cavitation number. Walchner, however, indicates that vapor pressure was used to calculate cavitation number. Perhaps the results at zero cavitation number are extrapolations from the results at small cavitation numbers. If the present data is compared with that of Walchner for the same amount of cavitation, ignoring cavitation number differences, the results are in much better agreement.

The cavitation polar diagrams for the two sets of experiments are given in Figs. 37 and 38. The High Speed Water Tunnel data gives greater drag for fully wetted flow as was shown in Fig. 31 and like the curves of lift coefficient there is a difference in the results which amounts to a difference in cavitation number of approximately 0.10.

These differences in the results can be understood if the cavitation diagrams for the two series of experiments are compared. The cavitation diagram obtained in the CIT experiments is shown in Fig. 39 and that reported by Walchner in Fig. 40. The cavitation number for the inception of cavitation near the mid-chord point on the upper surface, denoted by $X \approx .5 c$ in the figures, is higher for the present experiments than reported by Walchner for all attack angles greater than -2 degrees. The difference in incipient cavitation numbers is 0.03 at zero degree, increasing to 0.10 at 4 degrees attack angle. In the present experiments the leading edge of the cavitation moves to the leading edge of the hydrofoil at an angle of attack of approximately 4.5 degrees but remained at the mid-chord position in Walchner's experiments up to attack angles of 6 degrees. Comparing the cavitation numbers at which the downstream end of the cavitation reaches to the trailing edge, we see again that there are considerable differences. At zero degree the cavitation number for collapse of the cavitation at the trailing edge is 0.07 greater in the CIT experiments than in the German tests. This difference increases to 0.17 at 6 degrees attack angle. Thus we see that on the upper surface, for the same cavitation number, the CIT hydrofoil was more fully cavitated than was Walchner's.

The same differences in the cavitation prevail on the lower surface for negative attack angles to -3 degrees; however, for large negative attack angles, the Walchner hydrofoil cavitated at higher cavitation numbers than did the CIT hydrofoil. The shaded band in Fig. 39 is in general narrower than that of Fig. 40, showing a more rapid increase in cavity length with decreasing

cavitation number for the CIT hydrofoil.

From this comparison we see that there was in general more cavitation on the CIT model at all cavitation numbers. Thus reduction in lift coefficient occurs at higher cavitation numbers for the CIT model and the loss in lift is greater for the same cavitation number.

The cavitation numbers in both series of experiments were based on vapor pressure so that the differences in cavitation may have resulted from differences in experimental technique or perhaps from small differences in the contour of the hydrofoils. If the cavitation numbers in the two series of tests were based on measured cavity pressure wherever possible, as discussed in the section on the NACA 4412 hydrofoil, perhaps the results would be in better agreement.

Figure 41 shows curves of pitching moment coefficient about the quarter chord point at constant cavitation number as functions of hydrofoil attack angle. The scale of pitching moment in this figure is greatly expanded over that for fully wetted flow, Fig. 30, therefore the kink or inflection near zero degree is more evident. The moment coefficient shows the same trend as with the NACA 4412 with the moment coefficient increasing toward zero as the cavitation number is reduced.

Curves of lift/drag ratio vs cavitation number at constant angle of attack are shown in Fig. 42. The dashed lines near the origin marked $X_1 = 1.0 c$ show the cavitation number at which the cavitation extends to the trailing edge of the hydrofoil. We see again that the greatest decrease in the lift/drag ratio occurs between cavitation inception and the point where the cavitation extends to the trailing edge.

The knee in the lift/drag ratio curves for Walchner profile 7 agrees more closely with the incipient cavitation number shown on the cavitation diagram, Fig. 39. From the experience with spurious cavitation on the stub spindle mounting of the NACA 4412 hydrofoil, it was decided to move the spindle attachment of the Walchner profile from its original position at the quarter chord point to a position nearer the trailing edge. By moving the attachment point as far downstream as strength limitations would permit, it was possible to get the stub spindle out of the low pressure region near the leading edge into the region of pressure recovery so that there was negligible

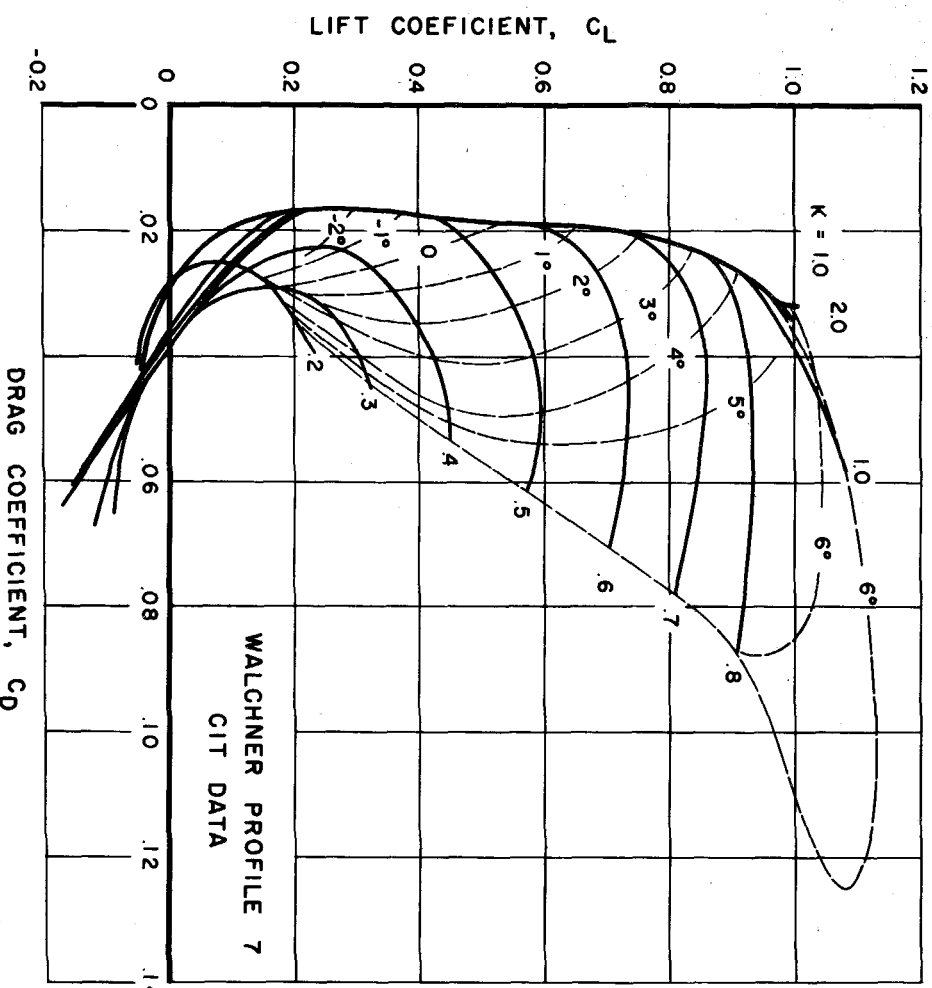


Fig. 37 - Polar diagram for cavitating and noncavitating flow for the Walchner profile 7 hydrofoil, CIT data.

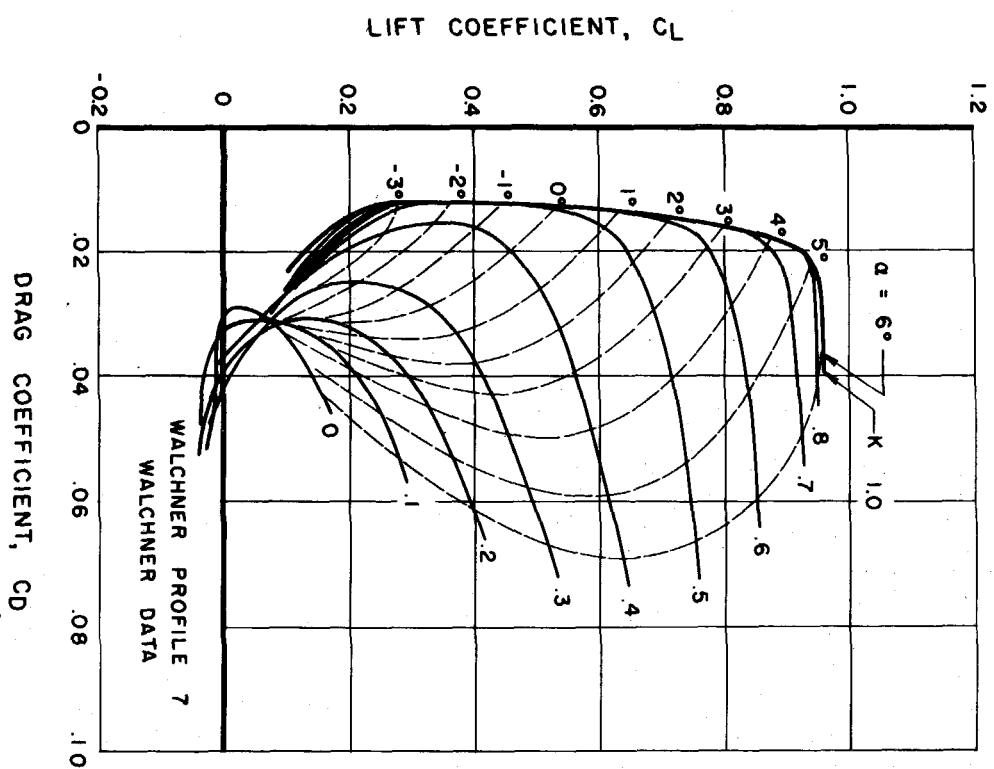


Fig. 38 - Polar diagram for cavitating and noncavitating flow for Walchner profile 7, Walchner's data.

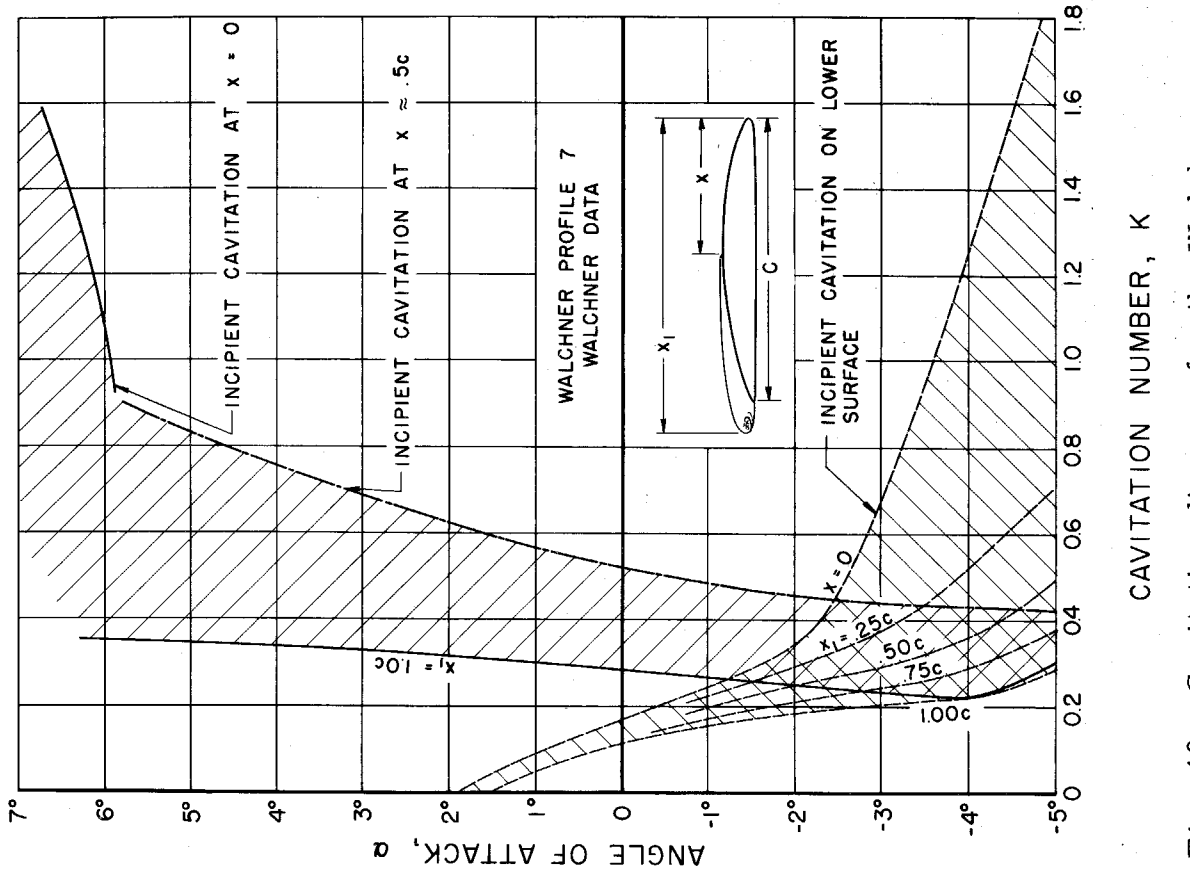


Fig. 39 - Cavitation diagram for the Walchner profile 7 hydrofoil, CIT data.

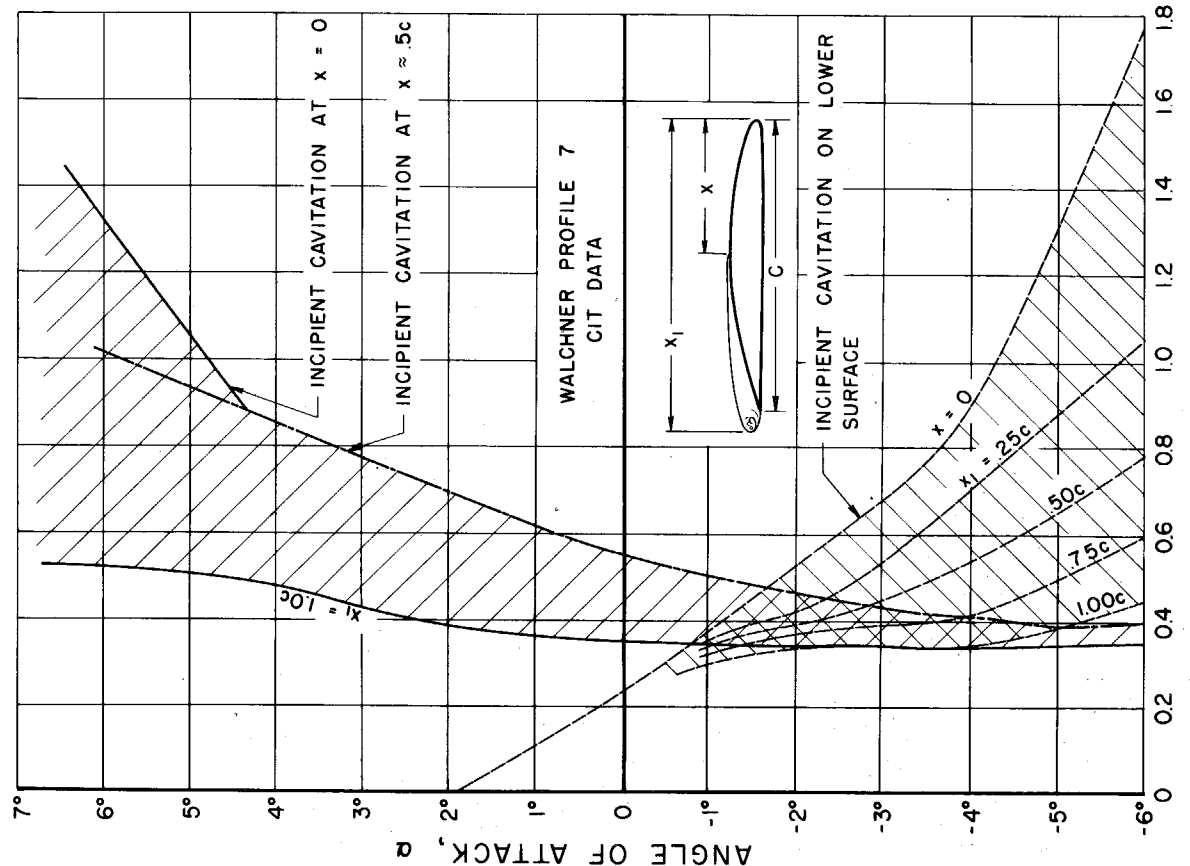


Fig. 40 - Cavitation diagram for the Walchner profile 7 hydrofoil, Walchner's data.

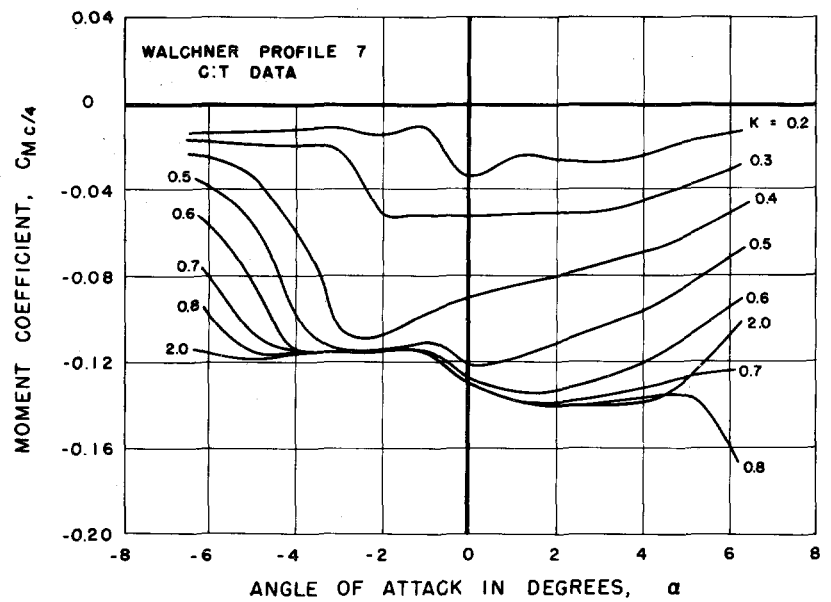


Fig. 41 - Moment coefficient about the quarter chord point as a function of angle of attack and cavitation number for the Walchner profile 7 hydrofoil.

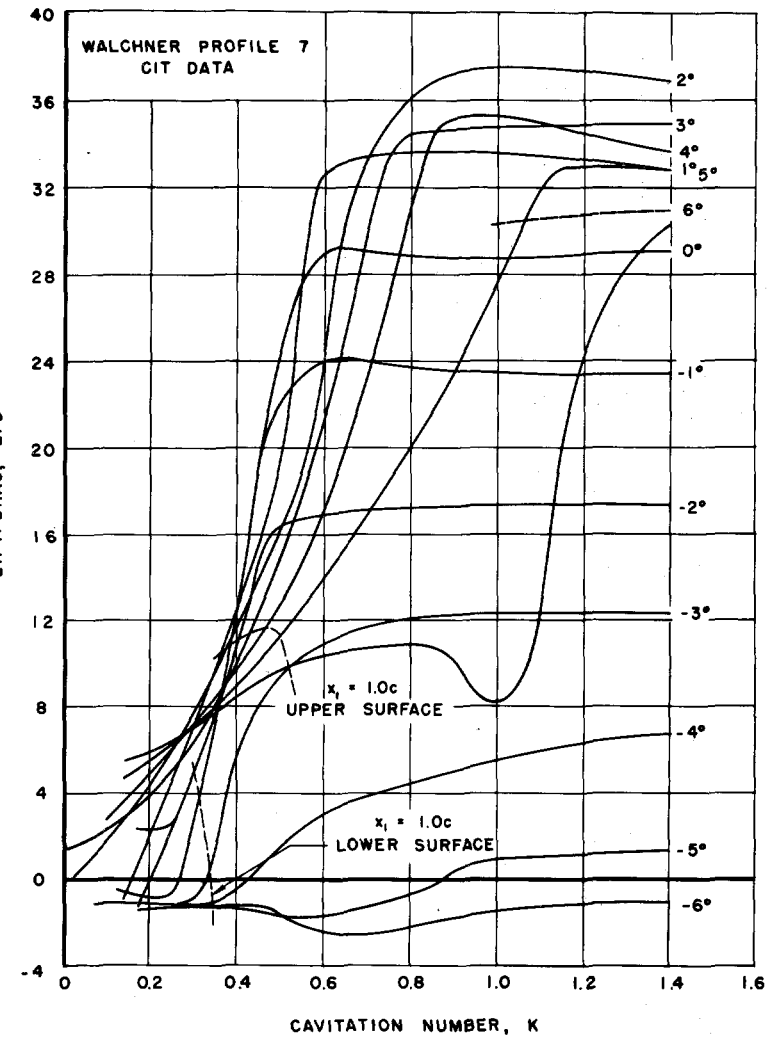


Fig. 42 - Lift/drag ratio as a function of cavitation number and angle of attack for the Walchner profile 7. The dashed lines at the lower left indicate the cavitation number at which the cavitation extends downstream to the trailing edge of hydrofoil.

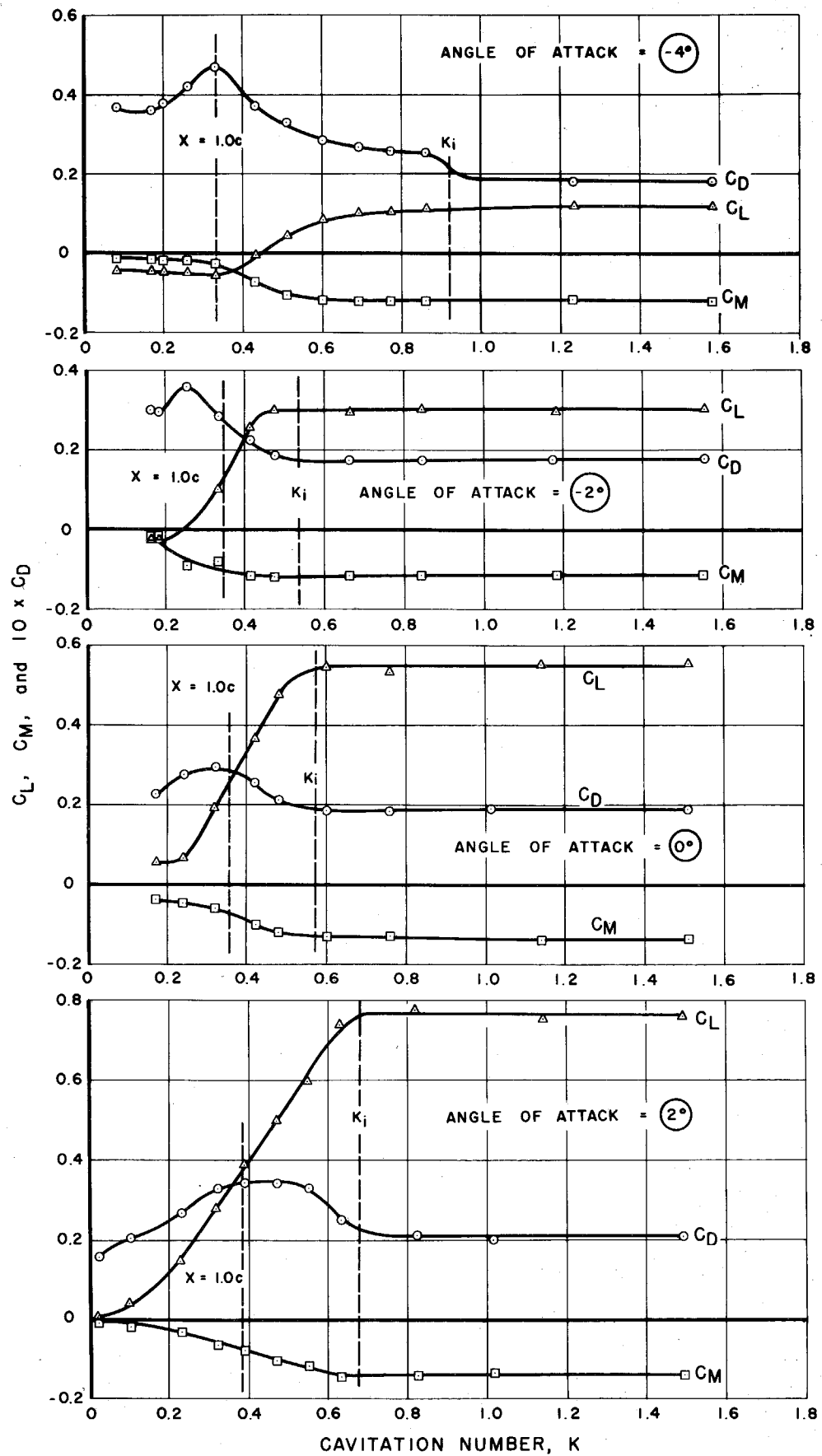


Fig. 43 (partial)

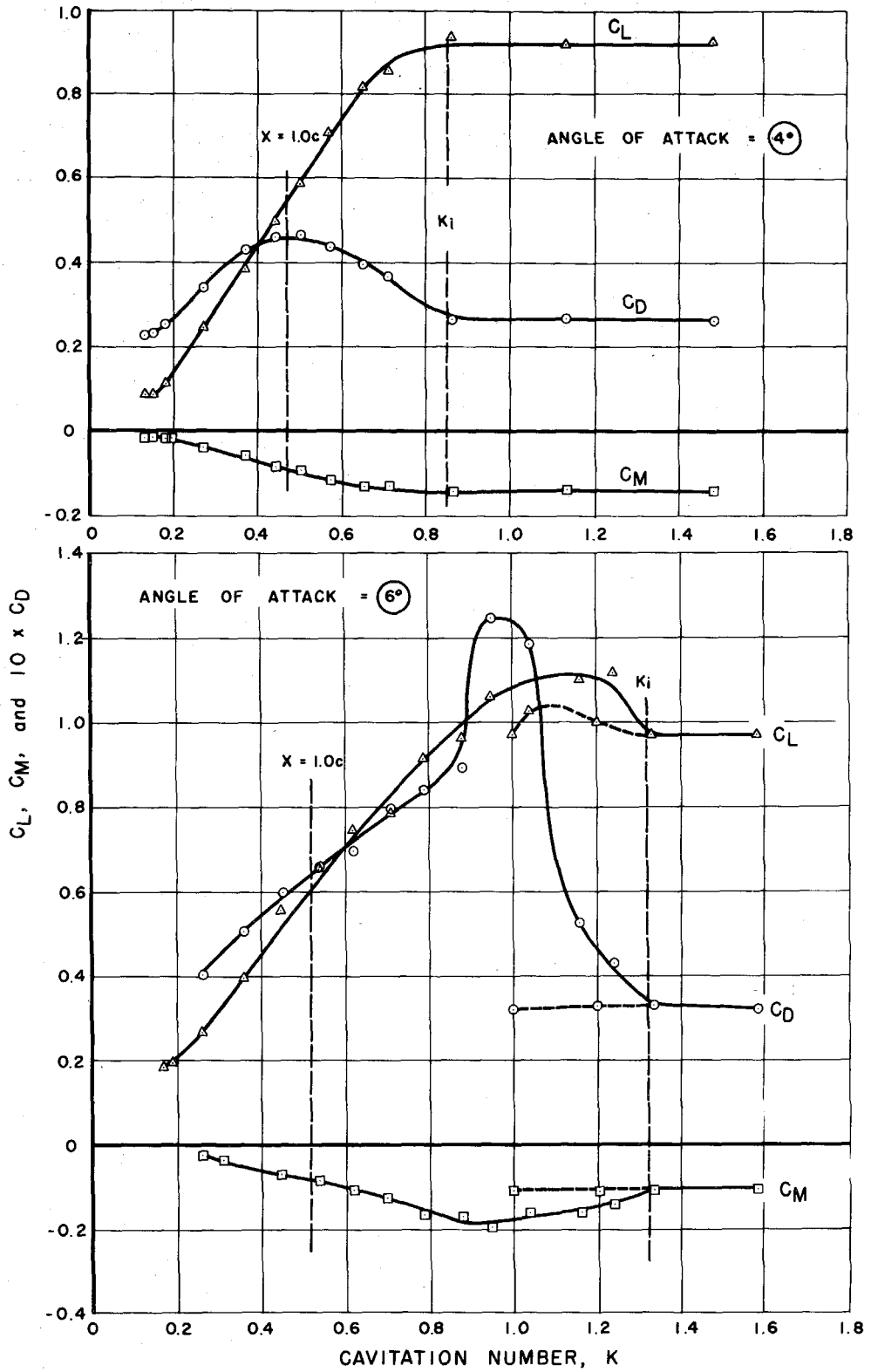


Fig. 43 - Lift, drag and pitching moment coefficients as functions of cavitation number for the Walchner profile 7 hydrofoil at angle of attack of -4, -2, 0, 2, 4, and 6 degrees. Each curve shows the results of one run. The dashed lines marked K_i show the cavitation number for incipient cavitation. The dashed lines noted as $x = 1.0c$ indicate the cavitation number at which the cavitation extended downstream to the trailing edge of the hydrofoil.

cavitation on the spindle. The problem of spurious spindle cavitation was finally solved by the use of the flush disk mount.

Lift, drag and pitching moment vs cavitation number for several attack angles are shown in Fig. 43. Each figure represents a different test run. The points on the curves are coefficients calculated from the measured data. These curves show the changes which occur in the force and moment coefficients as the cavitation number is varied at constant hydrofoil attack angle. Lines have been drawn in these figures to show the beginning of cavitation, K_1 , and the cavitation number at which the downstream end of the cavitation is at the trailing edge, $X_1 = 1.0$ c. In all the runs except at -2 and +6 degrees, Fig. 43, the drag coefficient reaches a maximum when the downstream end of the cavitation coincides with the trailing edge of the hydrofoil. At this point the hydrofoil has lost approximately half its lift. For lower cavitation number the cavity grows rapidly and the drag coefficient is reduced.

We see that the force coefficients for an attack angle of 6 degrees, Fig. 43, are double valued near incipient cavitation. This is due to the fact that the hydrofoil is near stall and the cavitation can attach itself either to the leading edge or to the mid-chord point on the hydrofoil. The dashed portion of the coefficient curves represents the conditions wherein cavitation inception at the leading edge is delayed. During the tests the cavitation sometimes alternated from being attached to the leading edge to being attached at the mid-chord point. This would produce sudden, violent fluctuations in the forces. The delayed cavitation gives a double valued curve of lift/drag ratio, Fig. 42. We note also at 6 degrees that there is an increase in lift coefficient with small amounts of cavitation beginning at the leading edge.

CONCLUSIONS

Some general conclusions may be drawn from the results of these tests.

1. The new High Speed Water Tunnel force balance provides an accurate means of obtaining the force characteristics of hydrofoils in noncavitating and

cavitating flow.

2. The results obtained in the tests of the NACA 4412 hydrofoil are in good agreement with those obtained on this profile in the NACA wind tunnel tests.

3. The results of the tests of Walchner profile 7 are in poor agreement with the results obtained by Walchner for cavitating flow. The differences in forces amount to a difference in cavitation number of approximately 0.1. The differences in cavitation number for the same flow geometry are confirmed by the cavitation diagrams. Therefore there seems to be some systematic difference in the cavitation numbers reported by Walchner and those reported here.

4. Large differences arise between the cavitation number based on vapor pressure and the cavitation number based on the measured cavity pressure. If the results obtained in different facilities are to be compared, they must be compared on the basis of the measured cavity pressure wherever possible.

5. Tests on the Walchner profile 7 show that extreme care must be taken to produce an accurate hydrofoil contour. The forces are particularly sensitive to the leading edge contour.

ACKNOWLEDGMENTS

The author wishes to express his appreciation to the many members of the laboratory staff who participated in this experimental investigation. He particularly wishes to thank Dr. B. R. Parkin for his help and advice throughout the investigation, Miss Z. M. Lindberg, and Messrs. R. L. Waid and S. B. Wheeler for their assistance in the test program, Miss Donna Snyder and Mr. E. R. Hoge for preparation of the illustrations and Mrs. Rose Grant for preparing the manuscript.

REFERENCES

1. Hotz, G. M. and McGraw, J. T., "The High Speed Water Tunnel Three-Component Force Balance", California Institute of Technology, Hydrodynamics Laboratory Report No. 47-2, January 1955.
2. Daily, J. W., "Force and Cavitation Characteristics of the NACA 4412 Hydrofoil", California Institute of Technology, HML No. ND-19, June 1944, subsequently published as: "Cavitation Characteristics and Infinite Aspect Ratio Characteristics of a Hydrofoil Section", Trans. ASME, Vol. 71, pp. 269-284, April 1949.
3. Walchner, O., "Bericht über die im Auftrag der Marinelichtung im Göttinger Kaiser-Wilhelm-Institut für Strömungsforschung durchgeführten Profilmessungen bei Kavitation", November 1934.
4. Knapp, R. T., Levy, J., O'Neill, J. P., Brown, F. B., "The Hydrodynamics Laboratory of the California Institute of Technology", Trans. ASME, Vol. 70, No. 5, pp. 437-457, July 1948.
5. Pankhurst and Holder, Wind Tunnel Technique, Pitman and Sons, 1952.
6. Loftin, L. K. and Smith, H. A., "Aerodynamic Characteristics of 15 NACA Airfoil Sections at Seven Reynolds Numbers from 0.7×10^6 to 9.0×10^6 ", NACA Technical Note 1945, October 1949.
7. Jacobs, E. N. and Sherman, A., "Airfoil Section Characteristics as Affected by Variations of the Reynolds Number", NACA Report No. 586, 1937.
8. Pinkerton, Robert M., "Calculated and Measured Pressure Distributions over the Midspan Section of the NACA 4412 Airfoil", NACA Report No. 563, 1936.
9. Carrow, D. D., "A Note on the Boundary Layer and Stalling Characteristics of Aerofoils", C. P. No. 174, Ministry of Supply, Aeronautical Research Council, October 1950.

APPENDIX A

WORKING SECTION FLOW CALIBRATION TESTS

Flow calibration experiments were made in order to determine the flow and pressure field in the two-dimensional channel. A five-tube total head rake was used for velocity head measurements. The rake was mounted in eleven positions in the working section. The locations of the total head rake during these runs are indicated in the sketch, Fig. 44. Figure 45 shows top and side views of the total head rake mounted at the balance spindle position, station 2D.

Five pressure taps were drilled in each of the vertical walls of the channel for static pressure measurement. The locations of these taps are included in Fig. 44. The static pressure taps and the total head tubes were connected to a multtube mercury manometer. The manometer readings were taken simultaneously during each run by photographing the entire manometer board using 35 mm microfilm cameras.

In addition to the total head rake, two single tube total head probes were used for a more detailed survey of the velocity profile at the balance spindle position.

The flow calibration runs were made at velocities of 10 to 50 fps for noncavitating flow. Tests were made at 40 fps with varying amounts of cavitation on the rake probes and body. No changes were observed in the flow pattern with cavitation.

The results of the rake calibration tests at 40 fps are shown in Fig. 46 and Table III. The velocity profile did not change over the velocity range tested. For simplicity, the results are plotted only for two rake stations, IB and 2D. Two sets of data were taken at each station at each velocity. The static pressure profile in the clear working section is shown in Fig. 47. Figure 48 shows the velocity profile at the spindle axis position as measured with the total head probes. Except for the boundary layer the flow was uniform throughout the portion of the channel which has been calibrated. From Fig. 48 it can be seen that the boundary layer thickness is approximately 0.22 in. at the balance spindle. Thus the total boundary layer flow is approximately 15% of the model span at the balance spindle axis.

APPENDIX A

TABLE I - ORDINATES OF NACA 4412 HYDROFOILS

Station % c	Ordinates % c		Station % c	Ordinates % c	
	upper	lower		upper	lower
0	0.62	0	30.0	9.76	-2.26
0.25	1.25	-0.60	40.0	9.80	-1.80
0.5	1.64	-0.88	50.0	9.19	-1.40
1.25	2.44	-1.43	60.0	8.14	-1.00
2.5	3.39	-1.95	70.0	6.69	-0.65
5.0	4.73	-2.49	80.0	4.89	-0.39
7.5	5.76	-2.74	85.0	3.83	-0.30
10.0	6.59	-2.86	90.0	2.71	-0.22
15.0	7.89	-2.88	95.0	1.47	-0.16
20.0	8.80	-2.74	98.0	0.68	-0.14
25.0	9.41	-2.50	100.0	0.13	-0.13
Leading edge radius, 1.58					
Slope of radius through end of chord, 4/20					

TABLE II - ORDINATES OF WALCHNER PROFILE 7

Station % c	Ordinates % c		Station % c	Ordinates % c	
	upper	lower		upper	lower
0	1.58	1.58	40	10.84	0
2.5	3.86	0.52	50	11.00	0
5.0	4.96	0.35	60	10.63	0
7.5	5.82	0.24	70	9.42	0
10.0	6.59	0.16	80	7.74	0
15.0	7.81	0.03	90	4.55	0
20.0	8.74	0	95	2.77	0
30.0	10.12	0	100	0.33	0.33
Leading edge radius, 0.74% c					

TABLE III - VELOCITY CALIBRATION IN TWO-DIMENSIONAL WORKING SECTION, VELOCITY = 40 FPS

Velocity at Each Total Head Probe

Working Section $\frac{C}{w}$ Velocity

Y = Distance of Probe from Wall Opposite Balance

w = Two-Dimensional Channel Width = 2.90 In.

Rake Station	$\frac{Y}{w} = .054$	$\frac{Y}{w} = .268$	$\frac{Y}{w} = .482$	$\frac{Y}{w} = .696$	$\frac{Y}{w} = .942$
1A	1.000	1.000	1.000	1.000	0.999
	1.000	1.000	1.000	1.000	0.999
1B	1.000	1.000	1.000	1.000	0.999
	0.999	1.000	1.000	1.000	1.000
1C	1.000	1.000	1.000	1.000	0.999
	0.999	1.000	1.000	1.000	1.000
1D	1.000	1.000	1.000	1.000	1.000
	1.000	1.000	1.000	1.000	1.000
2A	0.998	1.000	1.000	1.000	0.999
	0.998	1.000	1.000	1.000	0.999
2B	0.985	1.000	1.000	1.000	0.995
	0.985	1.000	1.000	0.999	0.994
2C	0.986	1.000	1.000	1.000	0.993
	0.986	1.000	1.000	1.000	0.991
2D	0.994	1.000	1.000	1.000	0.972
	0.995	1.000	1.000	1.000	0.975
2E	0.980	1.000	1.000	1.000	0.991
	0.985	1.000	1.000	1.000	0.992
2F	0.986	1.000	1.000	0.999	0.993
	0.987	1.000	1.000	1.000	0.991
2G	0.996	1.000	1.000	1.000	0.998
	0.996	1.000	1.000	1.000	0.997

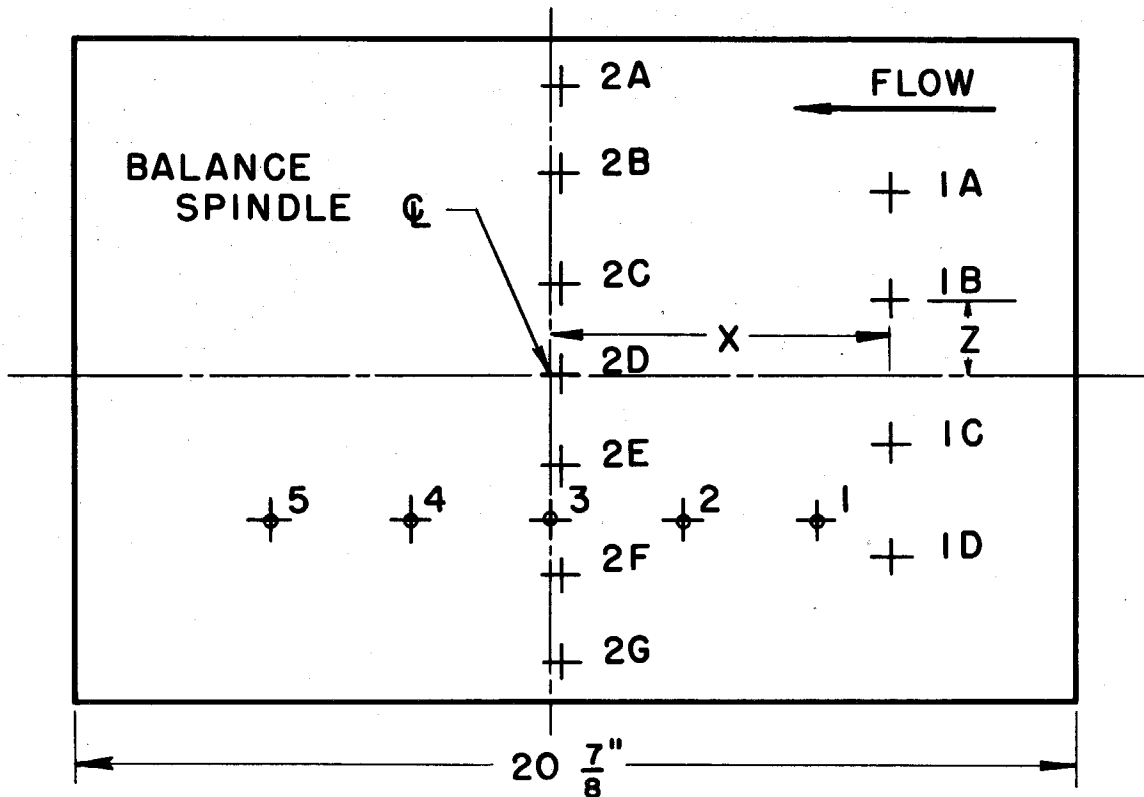


Fig. 44 - Sketch showing locations of static pressure taps in the two-dimensional channel walls and the stations at which the velocity surveys were made. The static pressure taps are noted 1 through 5. The velocity surveys were made at Stations 1A through 2G. The positions of these stations are given in the table below.

WORKING SECTION FLOW CALIBRATION

Total Head Rake Stations and Static Pressure Tap Locations in Two-Dimensional Working Section

Rake Station	x in.	z in.	Static Pressure Tap	x in.	z in.
1A	7.125	3.750	1	5.500	3
1B	7.125	1.500	2	2.750	3
1C	7.125	-1.500	3	0	3
1D	7.125	-3.750	4	-2.785	3
2A	1.625	6.000	5	-5.750	3
2B	1.625	4.188			
2C	1.625	1.785			
2D	1.625	0			
2E	1.625	-1.785			
2F	1.625	-4.188			
2G	1.625	-6.000			

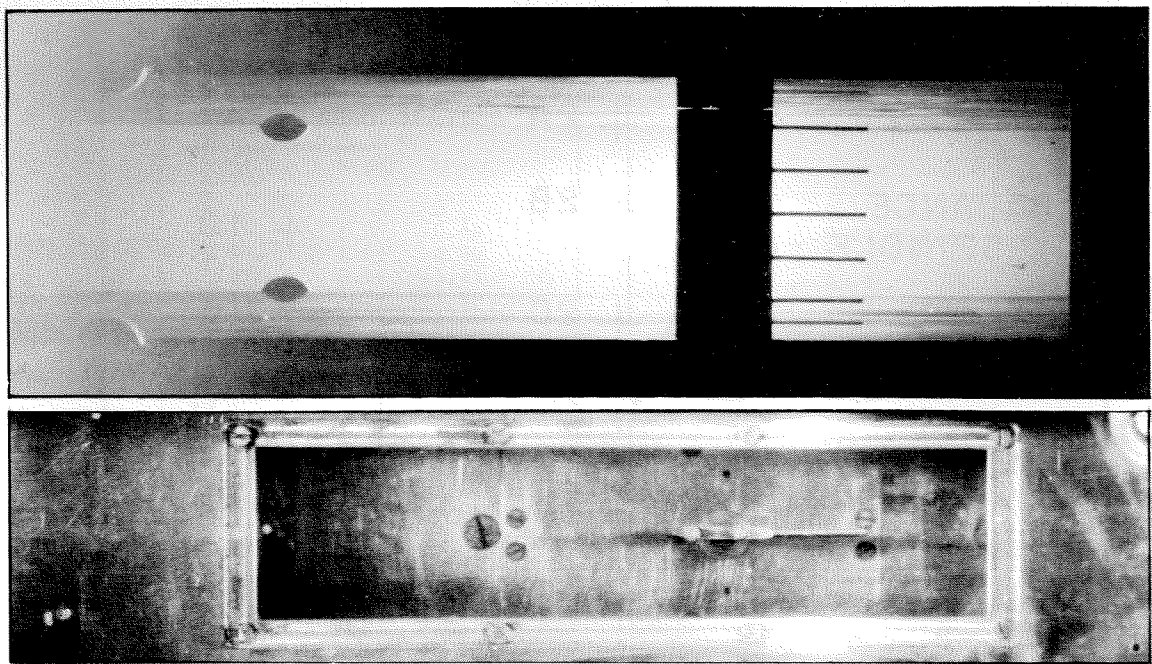


Fig. 45 - Top and side views of the total head calibration rake mounted at the balance spindle position, Station 2D, Fig. 44.

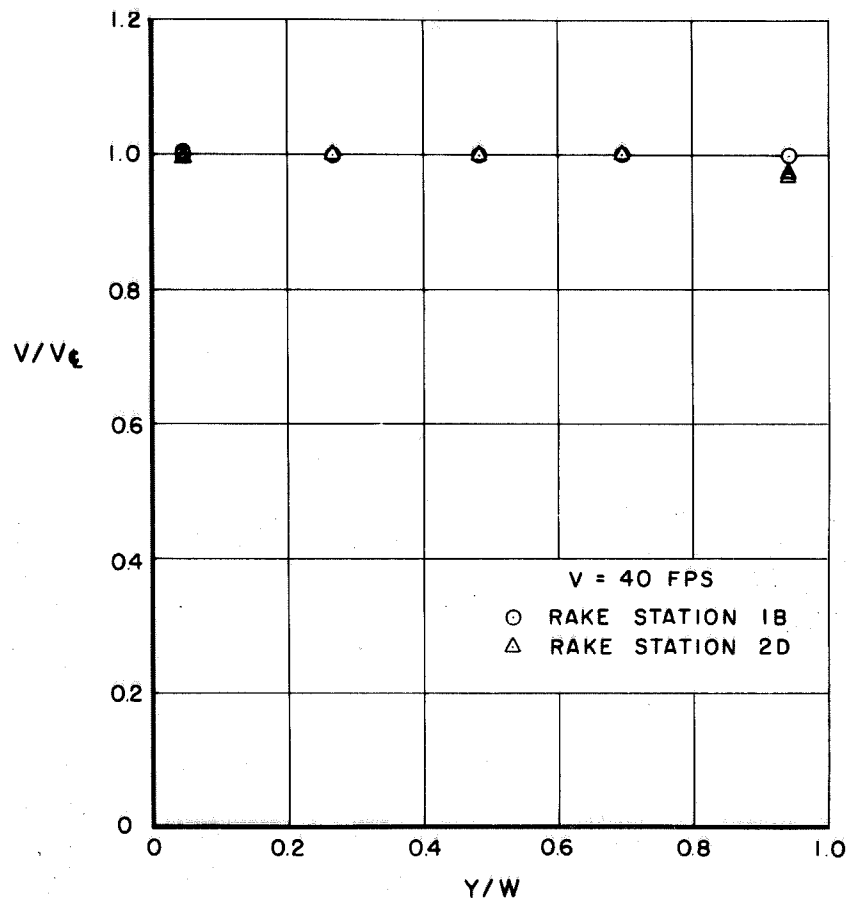
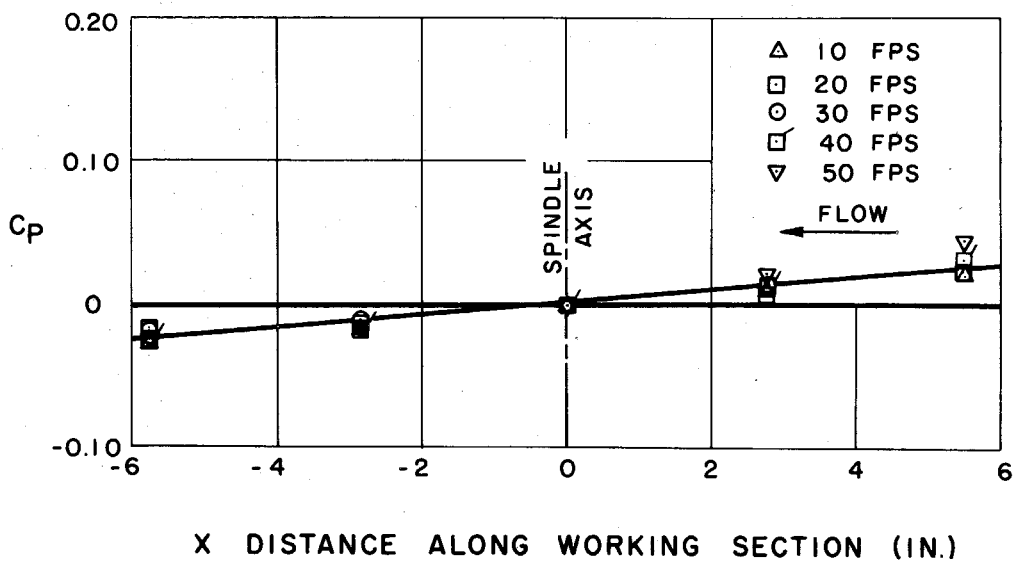


Fig. 46 - Velocity calibration from the total head rake measurements at Stations 1B and 2D, Fig. 44.



X DISTANCE ALONG WORKING SECTION (IN.)

Fig. 47- Static pressure calibration in the region near the spindle axis in the two-dimensional working section. The pressure coefficient, C_p , is based on the pressure at the spindle axis

$$\left(C_p = \frac{P - P_\infty}{\rho/2 V^2} \right)$$

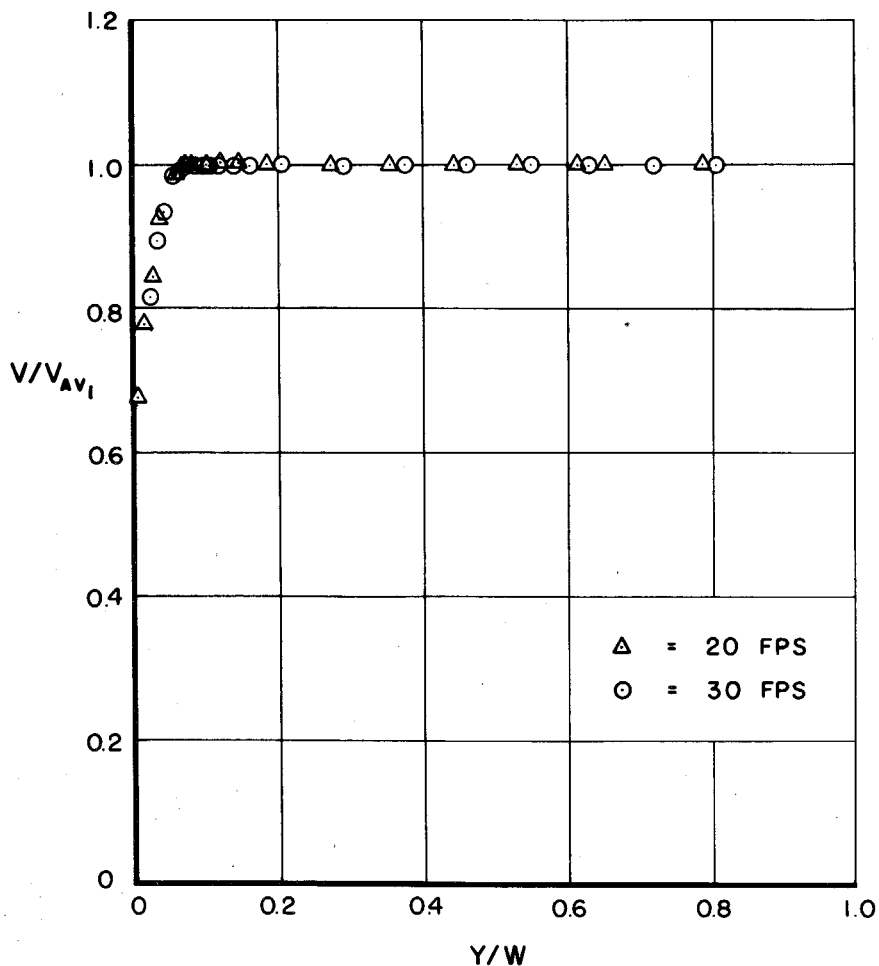


Fig. 48 - Velocity profile at the spindle axis, Station 2D, as measured with the total head probe.

APPENDIX B

HYDROFOIL END GAP EXPERIMENTS

In supporting the hydrofoils on the force balance in the two-dimensional working section, it was necessary to provide clearance gaps at each end of the hydrofoil span to prevent interference with the channel walls. These end gaps were adjusted to a width of approximately 0.002 in. during each run; however, even with this small gap there was visible flow through the clearance gap. Since flow from the pressure to the suction side of the hydrofoil will cause a reduction in lift, calibration runs were made to determine the effect of clearance gap width on the forces on the NACA 4412 hydrofoil.

The gap between the end of the hydrofoil and the lucite viewing window in the channel wall opposite the balance can be adjusted during a run by tightening or loosening two bolts in the wall support struts. These two bolts pass through the outer working section window. A brass tube containing the lines from the static pressure taps in the channel walls passes through a seal in the outside lucite window. A dial indicator fastened to the outside of the circular working section was used to measure the position of the end of the brass tube relative to the fixed working section walls.

Runs were made at a velocity of 30 fps at attack angles of 0 and 4 degrees. The end gap was varied from 0.001 to 0.032 in. for each run. The results are shown in Fig. 49. The lift coefficient was reduced by 8% and the drag coefficient was increased by 25% at an angle of attack of 4 degrees when the end gap was increased from 0.001 to 0.032 in. The lift was reduced by 13% and the drag increased by 11% at 1² degree angle of attack for the same change in end gap. The moment coefficient was not affected by changes in end gap in either run.

The end gap was adjusted visually during the force runs by sighting through the clearance gap toward a lighted background beneath the working section. As noted previously, the outboard gap was adjusted to approximately 0.002 in. during each run and probably never exceeded .006 during any of the force tests. The clearance gap on the balance side could not be

adjusted without removing the hydrofoil from the spindle. This gap was on the order of 0.004 in. though it varied with working section pressure from approximately 0.008 to 0.001 in.

In later tests the hydrofoil was mounted on the circular spindle disk thus eliminating completely the end gap on the balance side.

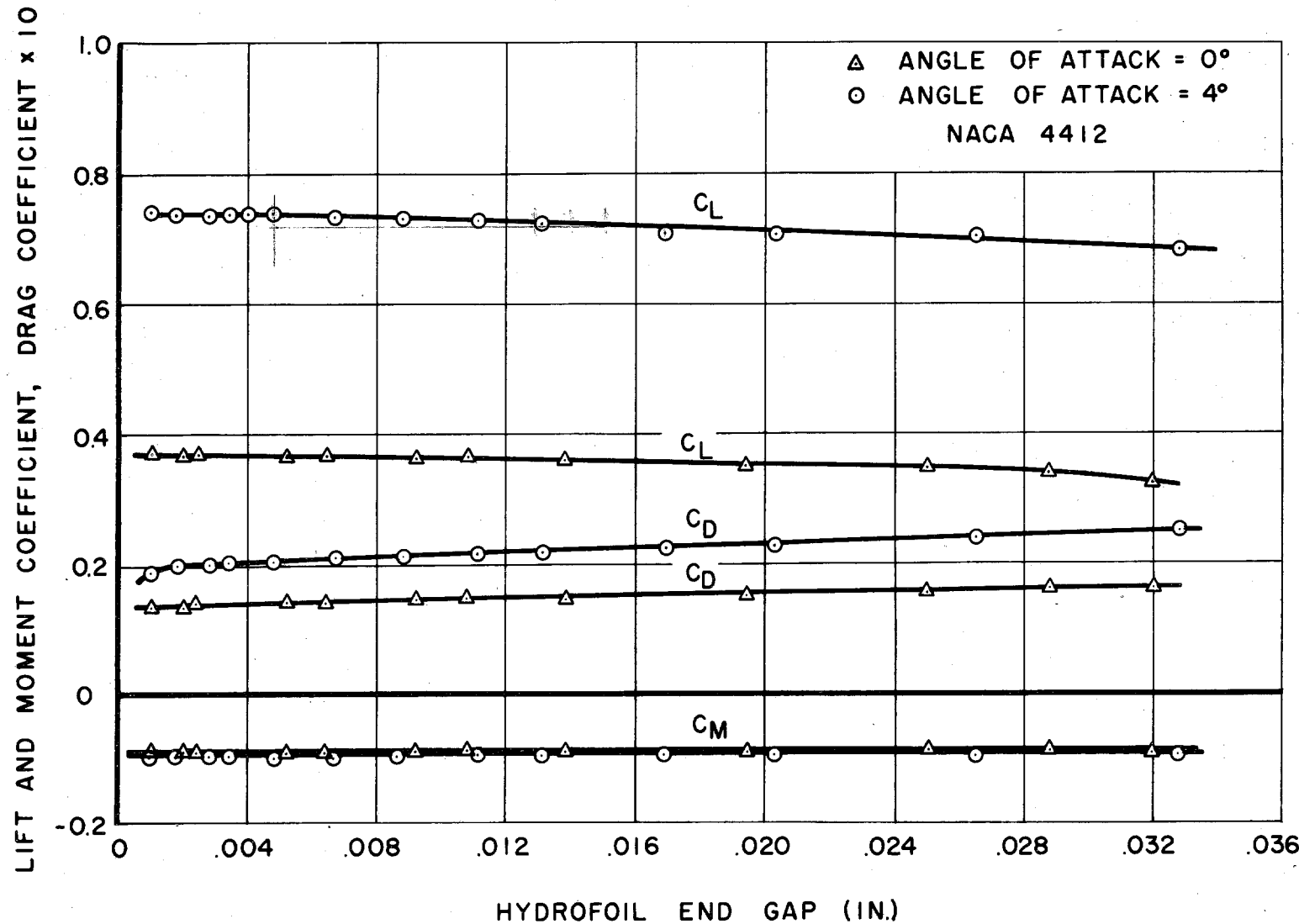


Fig. 49 - The effect of hydrofoil end gap on the lift, drag and pitching moment coefficients of the NACA 4412 hydrofoil in non-cavitating flow at angles of attack of 0 and 4 degrees. The drag coefficient is plotted to a scale 10 times that of the lift and moment coefficients.

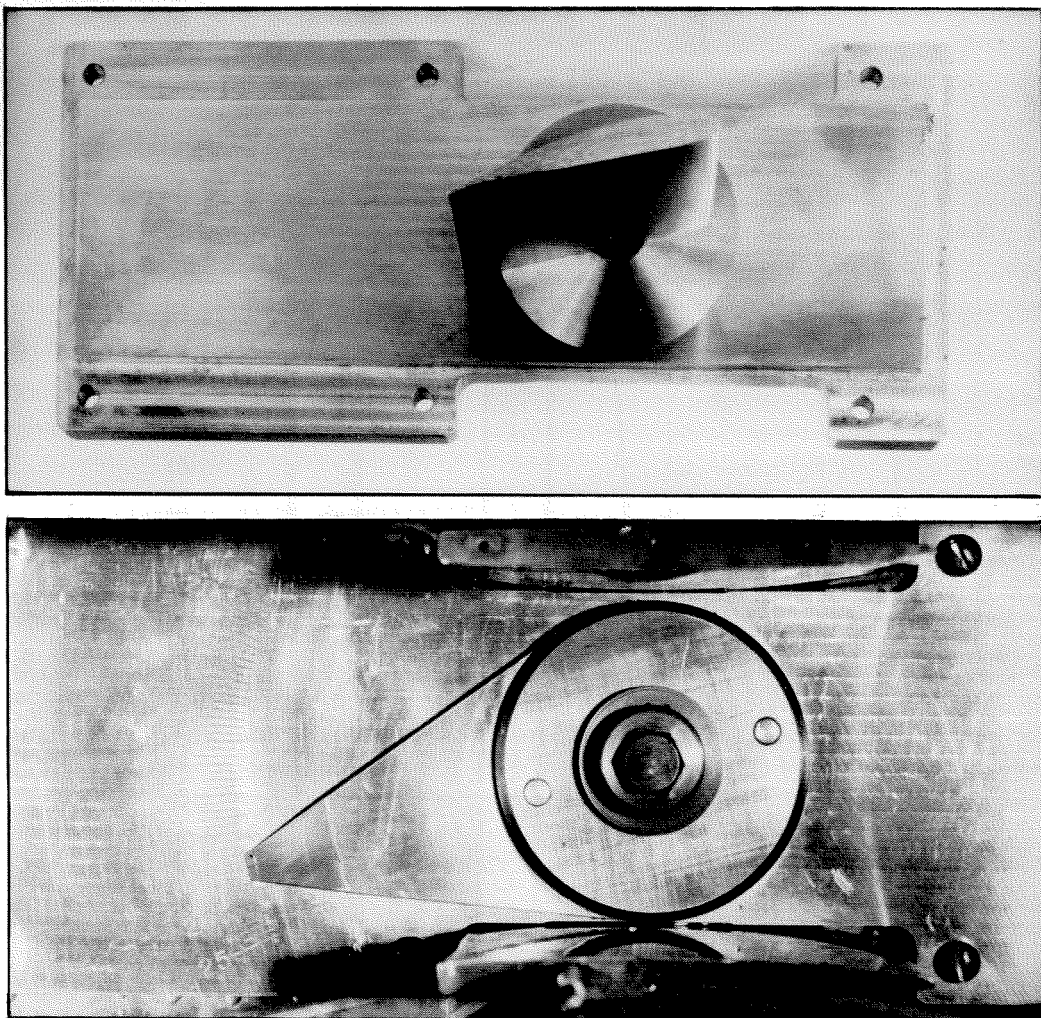


Fig. 50 - Two views of the hydrofoil mounting plate for calibrating the forces on the spindle disk. The NACA 4412 hydrofoil is attached to the plate in the upper photograph.

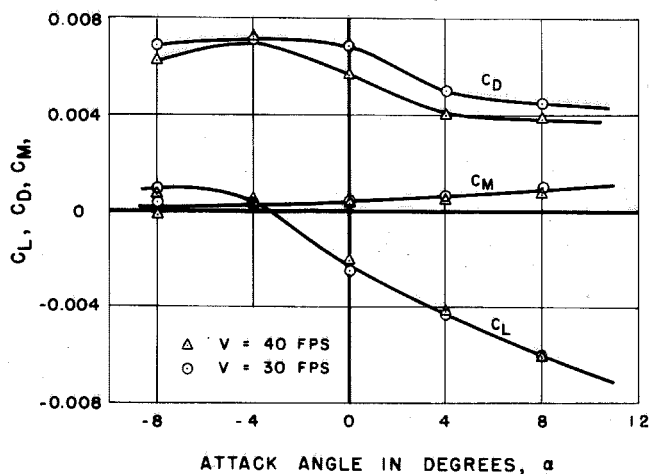


Fig. 51 - Lift, drag and pitching moment coefficients for the spindle disk as functions of angle of attack for the NACA 4412 hydrofoil in non-cavitating flow.

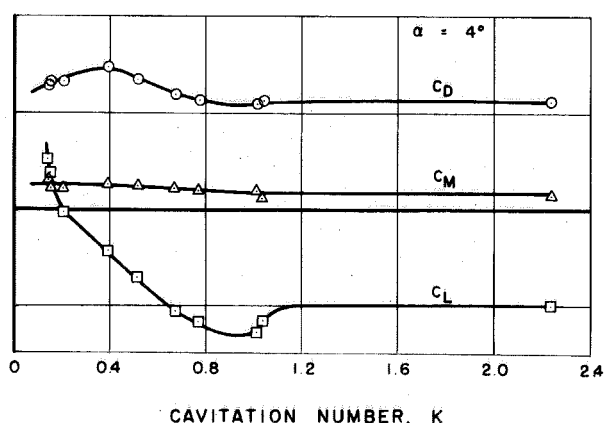


Fig. 52 - Lift, drag and pitching moment coefficients for the spindle disk as a function of cavitation number for the NACA 4412 hydrofoil at an angle of attack of 4 degrees and a velocity of 30 fps.

APPENDIX C

DATA CORRECTIONS

1. Spindle Disk Tare Forces

The present method for mounting the hydrofoils is to attach them to the 5-in. diameter spindle disk set flush in the channel wall as described in the section on apparatus and test procedure. With this setup the force balance measures the forces on the hydrofoil and the forces on the spindle disk. In order to determine the forces on the hydrofoil alone, it is necessary to measure the forces on the spindle disk separately and subtract them from the forces measured on the hydrofoil-disk combination. The forces on the disk alone are measured by mounting the hydrofoil from the opposite channel wall on a brass mounting plate which replaces the lucite viewing window. Two views of this mounting plate with the NACA 4412 hydrofoil attached are shown in Fig. 50. Mounting the hydrofoil on the wall opposite the force balance requires that the hydrofoil be upside down; however, this does not affect the force readings other than to change the directions of the forces and moments relative to the hydrofoil. The balance is designed to measure both positive and negative forces and moments. The hydrofoil is mounted with approximately 0.002 in. clearance between the end of the hydrofoil and the spindle disk. The force balance then measures the forces and moments on the spindle disk alone.

The angle of attack of the hydrofoil is changed by removing the outside working section window, loosening a bolt and resetting the attack angle. The pitching angle scale can be seen on the outside of the mounting plate in Fig. 50. Since the results of these calibration tests are corrections and are small relative to the total forces on the hydrofoil, the calibrations are not made at every attack angle at which the hydrofoil is tested. Instead the calibration tests are made at selected attack angles and the corrections interpolated where necessary between the data curves. All the conditions of fully wetted or cavitating flow which are obtained with the hydrofoil are repeated at each attack angle tested.

Figure 51 shows the spindle disk corrections for the NACA 4412 hydrofoil as functions of angle of attack for fully wetted flow. The lift and moment

corrections are small relative to the forces on the hydrofoil; however, the drag resulting from the viscous forces on the disk is a considerable part of the total drag of the hydrofoil-disk combination at low attack angles. Figure 52 shows the spindle disk corrections as functions of cavitation number at an angle of attack of 4 degrees. In these figures the corrections have been reduced to coefficient form based on the hydrofoil dimensions so they can be applied directly to the coefficients obtained with the hydrofoil-disk combination.

2. Tunnel Interference Corrections

If the results of water tunnel tests are to be directly applied to full-scale conditions, certain nondimensional parameters must be equal in both systems. The principal modeling parameter for fully wetted flow for deeply submerged hydrofoils is the Reynolds number. Even if the tunnel tests are made at prototype Reynolds number, the flow pattern around the model will generally differ from that of the full scale model in free fluid. The factors which produce these discrepancies arise in part from the distortion of the flow pattern due to the limited cross section of the tunnel. The interference effects are generally larger for a closed jet tunnel than for a free jet tunnel. Tunnel interference corrections have been calculated for the hydrofoils described in this report for fully wetted flow using the methods developed for two-dimensional wind tunnel airfoil experiments. The equations for these corrections were obtained from Ref. 5.

The precise nature of the effects of boundary constraint is complex and the problem is usually approached by dividing the interference into several independent components whose effects are assumed to be additive. The types of interference considered here include:

- (a) Solid blockage, involving a change of axial velocity past the hydrofoil, owing to its partially blocking the flow.
- (b) Wake blockage, a similar effect due to the reduction of velocity within the wake of the hydrofoil.
- (c) Lift effect, due to the constraint imposed on the curved streamlines by the tunnel walls. The effects of the flow curvature constraint may be regarded as a change of hydrofoil camber and incidence.

(d) Interference due to static-pressure gradient, which introduces spurious drag due to the horizontal buoyancy.

(e) Wall boundary layer interference, which introduces a departure from two-dimensional conditions at the walls.

These interference effects are considered separately below and some of the values of the corrections are given for the NACA 4412 hydrofoil.

(a) Solid blockage

If the working section has straight rigid walls, as is the case with the High Speed Water Tunnel, continuity of mass flow requires that the axial velocity in the vicinity of the model shall exceed the velocity farther upstream. Blockage does not influence the components of velocity normal to the free stream direction. It is convenient to express the blockage in terms of a factor ϵ_S where

$$V_F = V_T (1 + \epsilon_S)$$

where V_T is the tunnel speed and V_F is the corresponding free stream speed. The equation which was used for the solid blockage factor is

$$\epsilon_S = \frac{\pi}{6} (k_0 + k_1 \frac{t}{c}) \frac{A'}{h^2}$$

where

$$\left. \begin{array}{l} k_0 = 1.0 \\ k_1 = 1.2 \end{array} \right\} \text{empirical values from wind tunnel tests on airfoils.}$$

t = hydrofoil thickness

c = hydrofoil chord

A' = chordwise sectional area of hydrofoil

h = height of working section

The solid blockage is a constant for each profile and is 0.0022 for the NACA 4412 hydrofoil.

(b) Wake blockage

The velocity in the wake of a hydrofoil model is lower than in the surrounding stream. In order to satisfy conditions of continuity of mass flow in a closed working section, therefore, the velocity outside the wake must

exceed the velocity far upstream of the model, whereas in a free fluid these velocities are equal. Thus the axial velocity in a closed jet tunnel gradually increases past the model, (except for the reduced velocity inside the wake), and the velocity at the position of the hydrofoil is correspondingly greater than the tunnel speed. This effect is termed wake blockage. As in the case of solid blockage, it is convenient to express the wake blockage in terms of a factor ϵ_w defined by the equation

$$V_F = V_T (1 + \epsilon_w)$$

where V_T again denotes tunnel speed and V_F the free stream speed. The equation from Ref. 5 for wake blockage is

$$\epsilon_w = \frac{1}{4} \frac{c}{h} C_{DT}$$

where c and h are as defined above, C_{DT} is the measured hydrofoil drag coefficient. The wake blockage is a function of the drag coefficient, hence angle of attack. For the NACA 4412 hydrofoil

$$\epsilon_w = 0.0427 C_{DT} .$$

In practice the solid and wake blockage are combined into a single factor, $\epsilon = \epsilon_s + \epsilon_w$. This gives the velocity correction as before,

$$V_F = V_T (1 + \epsilon) .$$

The forces and moments which were measured in the tunnel were first reduced to coefficient form as defined in the section on data reduction. The drag coefficient for example is

$$C_{DT} = \frac{\text{Drag}}{\frac{\rho}{2} V_T^2 A}$$

where the subscript T denotes measured tunnel values. The force coefficient should be based on the dynamic head corresponding to the equivalent free stream speed, V_F . The measured tunnel force coefficient C_{DT} is related to the corrected free stream value, C_{DF} , by

$$C_{DF} = C_{DT} \left(\frac{V_T}{V_F} \right)^2 = C_{DT} \frac{1}{(1+\epsilon)^2}$$

$$= C_{DT} (1 - 2\epsilon) .$$

The corresponding lift and moment coefficient corrections are

$$C_{LF} = C_{LT} (1 - 2\epsilon)$$

$$C_{MF} = C_{MT} (1 - 2\epsilon) .$$

We see that the measured values of the force and moment coefficients are too large.

At zero degree attack angle the blockage factor, $\epsilon = \epsilon_S + \epsilon_\infty$ for the NACA 4412 hydrofoil is $\epsilon = 0.0022 + 0.0005 = 0.0027$. This gives a correction to the force coefficients of 0.54%.

(c) Lift effect

The constraint which the boundaries of the working section impose on the velocity field due to the vortex system of a lifting hydrofoil are termed "lift effect". Unlike solid blockage the lift effect would still occur if the dimensions of the model were so small compared with those of the tunnel that the hydrofoil could be treated as a lifting line. The conditions in a closed working section are the same as those in an unlimited stream whose curvature is such that there is no flow across the surfaces which correspond to the tunnel walls. The effect of this flow curvature may be regarded as a change of hydrofoil camber and incidence. The lift effect can be calculated as an effective increase of camber and increase in attack angle; however, since experiments are performed to determine the performance of a hydrofoil of a given camber at a given attack angle, the effective change in camber and incidence are converted to an equivalent change in lift, drag, and pitching moment. Omitting the details of the calculations given in Ref. 5, the lift effect corrections are:

$$C_{LF} - C_{LT} = -\frac{\pi^2}{48} \left(\frac{c}{h}\right)^2 C_{LT} - \frac{\pi}{96} \left(\frac{c}{h}\right)^2 (C_{LT} + 4C_{MT}) \frac{\partial C_{LT}}{\partial a}$$

$$C_{DF} - C_{DT} = \frac{\pi}{96} \left(\frac{c}{h}\right)^2 (C_{LT} + 4C_{MT}) \left(C_{LT} - \frac{\partial C_{DT}}{\partial a}\right)$$

$$C_{MF} - C_{MT} = \frac{\pi^2}{192} \left(\frac{c}{h}\right)^2 C_{LT} - \frac{\pi}{96} \left(\frac{c}{h}\right)^2 (C_{LT} + 4C_{MT}) \frac{\partial C_M}{\partial a},$$

where the subscript T denotes measured tunnel values and the subscript F denotes the corrected free stream values. For the hydrofoils tested, $\partial C_{MT}/\partial a$ may be taken as zero and the moment coefficient correction reduces to

$$C_{MF} - C_{MT} = \frac{\pi^2}{192} \left(\frac{c}{h}\right)^2 C_{LT}.$$

The values of the lift effect correction for the NACA 4412 hydrofoil at zero degree attack angle are:

$$C_{LF} - C_{LT} = -0.0094 C_{LT} - 0.0047 (C_{LT} + 4C_{MT}) \frac{\partial C_{LT}}{\partial a}$$

$$= -0.0040$$

$$C_{DF} - C_{DT} = 0.0015 (C_{LT} + 4C_{MT}) \left(C_{LT} - \frac{\partial C_{DT}}{\partial a}\right)$$

$$= 0.00001$$

$$C_{MF} - C_{MT} = 0.0023 C_{LT}$$

$$= 0.0009$$

For positive attack angles we see that the lift effect correction must be subtracted from the measured lift coefficient and added to the measured drag and moment coefficients. The lift effect correction is small at zero degree but increases with angle of attack.

(d) Interference due to static pressure gradient

As the boundary layers on the channel walls thicken, the axial velocity

of the main stream must increase steadily in order to preserve continuity of flow. This increase in velocity is accompanied by a steady decrease in pressure. The correction for static pressure gradient, or horizontal buoyancy, must be applied to the drag measured on the force balance. Besides the spurious drag arising from the horizontal buoyancy, a further correction has to be applied because the hydrofoil is effectively being tested in an accelerating flow. These effects depend only on the shape of the body and the value of the pressure gradient. The total drag correction per unit span is given in Ref. 5 as:

$$D_F - D_T = A'' \frac{dp}{dx}$$

where A'' is the equivalent chordwise sectional area of the hydrofoil

$$A'' = (k_0 + k_1 \frac{t}{c}) A'$$

where $k_0 = 1.0$ and $k_1 = 1.2$ as in (a) above, and A' is the chordwise sectional area of the hydrofoil, dp/dx is the static pressure gradient in the empty tunnel. Converting this correction to coefficient form, we get:

$$C_{DF} - C_{DT} = \frac{A''}{c} \frac{d}{dx} \frac{p}{\frac{\rho}{2} V^2}$$

where $d/dx (p/\frac{\rho}{2} V^2)$ is the gradient of the pressure coefficient and c is the hydrofoil chord.

We see from Fig. 47, Appendix A, that the pressure coefficient gradient is -0.0047 per in. Thus for the NACA 4412 hydrofoil the horizontal buoyancy correction is

$$C_{DF} - C_{DT} = -0.0013$$

(e) Wall boundary layer interference

In the case of a wing which completely spans a closed tunnel, a further interference usually arises because the boundary layers of the side walls cause transverse contamination of the laminar boundary layer of the airfoil. This effect is greatest when the transition point is well aft on the airfoil so

that there is a large region of laminar flow. The transverse contamination of the boundary layer spreads out in a wedge-like fashion downstream, however the angle at which it spreads seldom exceeds ten degrees. Due to the high turbulence level of the water tunnel and the Reynolds number range of these experiments, the region of laminar boundary layer flow on the hydrofoils is probably quite short.

At one time it was believed that the lift fell off rapidly within the boundary layers of the tunnel walls; however, more recent work cited in Ref. 5 shows that actually the lift is maintained within the wall boundary layers to a far greater extent than was formerly assumed, and for most practical purposes the effects of wall boundary layers are negligible. For these reasons no tunnel boundary layer corrections have been applied to the data.

In summarizing the tunnel interference corrections we see that four separate interference corrections have been applied to the data for fully wetted flow. The total interference corrections, together with the per cent corrections are shown in Fig. 53 for the NACA 4412 hydrofoil and in Fig. 54 for Walchner profile 7. In these figures the scale on the left is the per cent correction and the scale on the right is the force coefficient correction. The scale of the interference corrections has been made approximately the same as that of the figures showing the force coefficients in order to show the relative magnitude of the interference effects. As noted previously, the pitching moment coefficients were not corrected for tunnel interference effects because the correction is negligible when plotted to the scale of the moment coefficient curves.

No tunnel interference corrections have been applied to the force and moment coefficients for cavitating flow. The interference effects surely exist, however their magnitude with cavitation is not known.

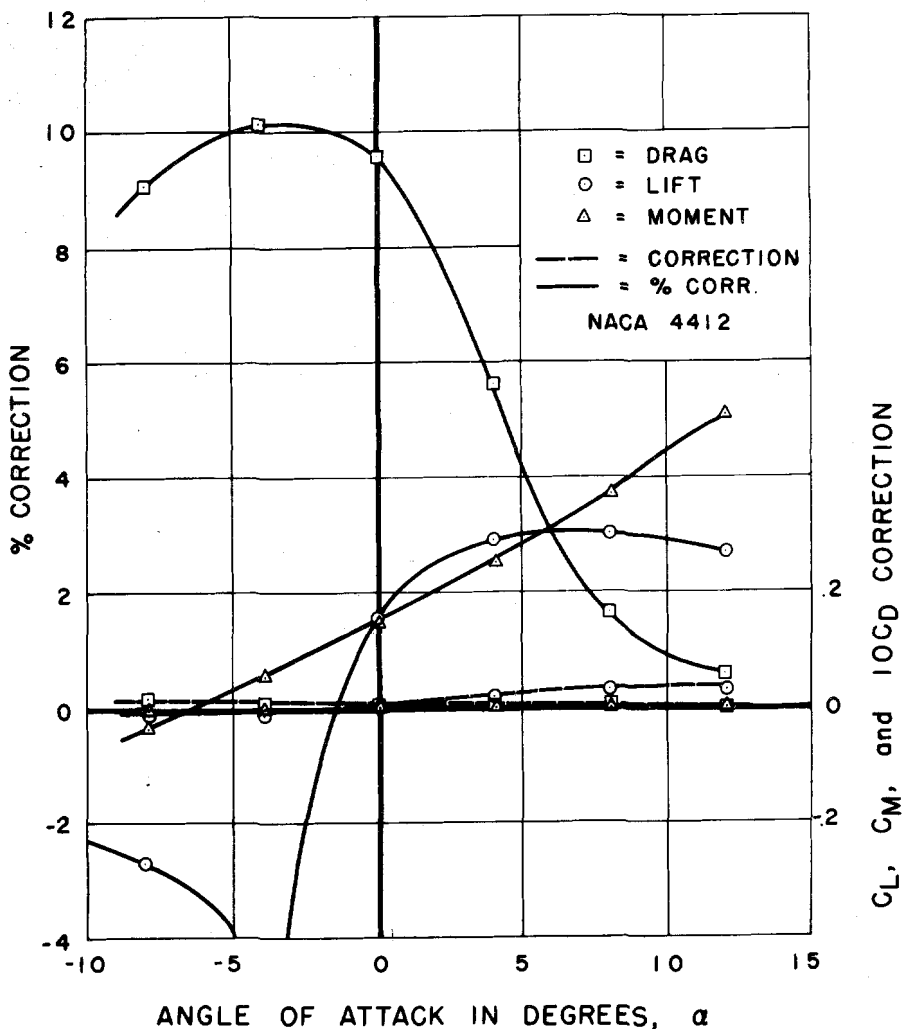


Fig. 53 - Tunnel interference corrections for the NACA 4412 hydrofoil in noncavitating flow. The drag coefficient correction has been plotted to a scale 10 times that of the lift and moment coefficient corrections.

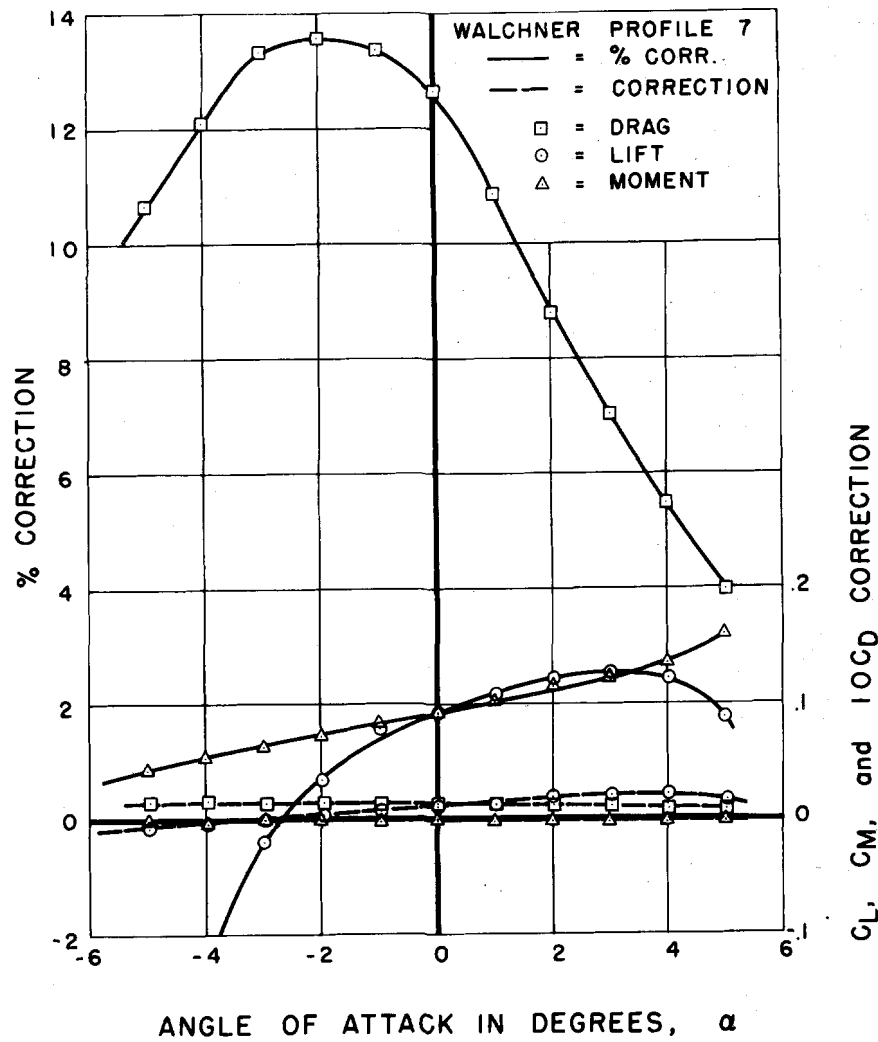


Fig. 54 - Tunnel interference corrections for the Walchner profile 7 hydrofoil in noncavitating flow. The drag coefficient correction has been plotted to a scale 10 times that of the lift and moment coefficient corrections.

APPENDIX D - DATA TABLES

TABLE IA - NACA 4412 Hydrofoil. Section Characteristics of the NACA 4412 Hydrofoil in Noncavitating Flow (data corrected for tunnel interference effects).

V = 21.1 fps Re = 550,000				V = 31.5 fps Re = 800,000				V = 41.9 fps (continued) Re = 1,090,000				
α	C_L	C_D	C_M	α	C_L	C_D	C_M	α	C_L	C_D	C_M	
0	.362	.0153	-0.090	0	.378	.0133	-0.090	-1	.304	.0082	-0.086	
0.5	.406	.0161	-0.090	1	.463	.0138	-0.093	0	.401	.0080	-0.087	
1.0	.445	.0169	-0.089	2	.553	.0134	-0.091	1	.497	.0081	-0.087	
1.5	.481	.0166	-0.088	3	.643	.0150	-0.090	2	.584	.0076	-0.085	
2.0	.538	.0173	-0.090	4	.736	.0168	-0.091	3	.684	.0088	-0.087	
2.5	.584	.0180	-0.090	5	.835	.0190	-0.092	4	.771	.0106	-0.085	
3.0	.639	.0195	-0.092	6	.909	.0221	-0.090	5	.855	.0127	-0.084	
3.5	.692	.0208	-0.093	7	.982	.0252	-0.086	6	.939	.0150	-0.082	
4.0	.737	.0215	-0.093	8	1.056	.0301	-0.084	7	1.022	.0184	-0.078	
4.5	.799	.0237	-0.095	9	1.134	.0343	-0.082	8	1.054	.0215	-0.071	
5.0	.861	.0244	-0.095	10	1.190	.0391	-0.079	9	1.135	.0257	-0.068	
6.0	.946	.0271	-0.094	11	1.231	.0475	-0.077	10	1.197	.0297	-0.066	
7.0	1.021	.0308	-0.091	12	1.300	.0503	-0.071	5	.873	.0135	-0.086	
8.0	1.098	.0368	-0.088	13	1.330	.0607	-0.073	0	.414	.0084	-0.089	
9.0	1.157	.0405	-0.083	14	1.372	.0744	-0.078					
10.0	1.216	.0468	-0.079	15	1.377	.0905	-0.081					
11.0	1.276	.0526	-0.076	16	1.368	.1074	-0.085					
12.0	1.321	.0584	-0.071	17	1.338	.1282	-0.089					
13.0	1.357	.0647	-0.069	18	1.289	.1550	-0.096					
14.0	1.372	.0774	-0.071	19	1.224	.1836	-0.102					
15.0	1.401	.0919	-0.073	20	1.199	.2639	-0.124					
16.0	1.397	.1076	-0.078	15	1.376	.0893	-0.079	0	.417	.0087	-0.088	
18.0	1.352	.1420	-0.088	10	1.214	.0373	-0.079	-5	-0.074	.0134	-0.087	
20.0	1.280	.1782	-0.094	5	.846	.0171	-0.094	-7	-0.270	.0155	-0.083	
V = 21.3 fps Re = 555,000				0	.381	.0119	-0.095	-6	-0.171	.0121	-0.083	
α	C_L	C_D	C_M	-1	.294	.0103	-0.094	-5	-0.071	.0108	-0.084	
	0	.358	.0164	-0.091	-2	.209	.0099	-0.093	-4	.024	.0100	-0.084
	-0.5	.333	.0155	-0.093	-3	.114	.0103	-0.093	-3	.121	.0094	-0.084
	-1.0	.278	.0149	-0.095	-4	.020	.0110	-0.093	-2	.213	.0083	-0.084
	-1.5	.233	.0133	-0.093	-5	-0.080	.0122	-0.092	-1	.311	.0074	-0.084
	-2.0	.194	.0123	-0.096	-6	-0.175	.0134	-0.088	0	.412	.0071	-0.087
	-2.5	.142	.0120	-0.094	-7	-0.271	.0147	-0.087	1	.505	.0071	-0.086
	-3.0	.107	.0115	-0.094	-8	-0.367	.0176	-0.087	2	.598	.0070	-0.085
	-3.5	.062	.0107	-0.093	-9	-0.469	.0211	-0.087	3	.698	.0077	-0.086
	-4.0	.019	.0130	-0.096	-5	-0.068	.0119	-0.090	4	.785	.0099	-0.084
	-4.5	-0.030	.0120	-0.091	0	.374	.0108	-0.091	5	.878	.0133	-0.083
	-5.0	-0.079	.0117	-0.092					0	.423	.0070	-0.088
	-6.0	-0.178	.0166	-0.093								
	-7.0	-0.273	.0167	-0.089								
	-8.0	-0.372	.0220	-0.088								
	-9.0	-0.476	.0260	-0.085								
	-10.0	-0.581	.0297	-0.080								
	-5.0	-0.082	.0134	-0.093								
	0	.354	.0188	-0.091								
V = 41.9 fps Re = 1,090,000				V = 41.9 fps Re = 1,090,000				V = 57.7 fps Re = 1,494,000				
α	C_L	C_D	C_M	α	C_L	C_D	C_M	α	C_L	C_D	C_M	
0	.409	.0086	-0.088	-5	-0.057	.0106	-0.087	0	.425	.0096	-0.090	
-5	-0.419	.0356	-0.087	-9	-0.363	.0179	-0.085	-4	.018	.0107	-0.089	
-8	-0.250	.0146	-0.085	-7	-0.164	.0125	-0.085	-3	.117	.0117	-0.088	
-7	-0.060	.0110	-0.086	-6	.028	.0107	-0.086	-2	.220	.0112	-0.091	
-6	.121	.0099	-0.086	-5	.215	.0091	-0.087	-1	.319	.0102	-0.090	
-5	-0.121	.0099	-0.086	-4	-0.215	.0091	-0.087	0	.421	.0097	-0.091	
-4	-0.121	.0099	-0.086	-3	-0.215	.0091	-0.087	1	.523	.0096	-0.091	
-3	-0.121	.0099	-0.086	-2	-0.215	.0091	-0.087	2	.624	.0107	-0.090	

TABLE IB - NACA 4412 Hydrofoil. Incipient Cavitation Characteristics of the NACA 4412 Hydrofoil (cavitation number based on vapor pressure).

$\alpha = -6^\circ$ Pressure(bottom) Side		$\alpha = -5^\circ$ Pressure(bottom) Side		$\alpha = -4^\circ$ Pressure(bottom) Side	
Cavitation Began	Cavitation Disappeared	Cavitation Began	Cavitation Disappeared	Cavitation Began	Cavitation Disappeared
V	K	V	K	V	K
27.36	1.673	27.40	2.094	27.12	1.267
27.20	2.730	27.39	2.915	27.28	1.254
21.01	1.343	21.60	1.842	20.92	1.269
21.10	1.608	21.50	1.740	20.96	1.279
31.95	1.748			31.95	1.262
31.91	2.680	32.12	1.866	32.03	1.293
32.1	1.866	38.42	1.287	38.42	1.347
38.65	1.726	38.42	1.246	38.58	1.436
38.40	1.740	38.58	2.286	42.55	1.349
42.98	1.863	38.78	2.278	42.60	1.401
42.61	1.830	42.50	2.359	51.12	1.572
50.40	1.770	42.92	2.275	50.01	1.648
51.80	2.046	49.90	2.257	56.45	1.724
				57.01	1.585
				55.63	1.752
				56.34	1.133
				62.73	1.149
				62.11	1.237

APPENDIX D - DATA TABLES

TABLE 1B - NACA 4412 Hydrofoil. Incipient Cavitation Characteristics of the NACA 4412 Hydrofoil (cavitation number based on vapor pressure).

APPENDIX D - DATA TABLES

TABLE IB - NACA 4412 Hydrofoil, Incipient Cavitation Characteristics of the NACA 4412 Hydrofoil (cavitation number based on vapor pressure).

Suction (top) Side				Suction (top) Side				Suction (top) Side			
Cavitation Began		Cavitation Disappeared		Cavitation Began		Cavitation Disappeared		Cavitation Began		Cavitation Disappeared	
V	K	V	K	V	K	V	K	V	K	V	K
20.88	.791	28.33	.630	21.32	.980	21.37	.938	21.65	1.889	21.71	3.052
28.49	.680			21.36	.912	21.55	.953	21.52	1.941	21.70	2.423
33.23	.685	33.22	.676	28.22	.993	28.22	1.072	28.09	2.429	28.06	2.623
33.29	.675	33.08	.661	32.99	1.022	32.91	1.103	28.06	2.361	28.03	2.771
39.79	.599	39.96	.736	33.11	1.079	33.07	1.054	32.83	2.510	33.00	2.645
39.90	.666	39.87	.704	39.83	1.170	40.03	1.361	32.88	2.523	32.95	2.659
43.64	.730	43.41	.737	39.99	1.172	39.96	1.357	39.46	2.766	39.43	2.843
43.74	.769	43.56	.727	43.75	1.397	43.49	1.523	39.47	2.835	39.50	2.852
48.09	.838	48.32	.803	43.48	1.366	43.50	1.384	43.37	2.901	43.25	2.862
48.17	.804	47.92	.756	48.20	1.306	48.40	1.643	42.92	2.921	43.12	2.926
51.81	.688	51.14	.817	48.04	1.199	48.20	1.548				
51.22	.812	51.23	.823	51.31	1.577						
56.41	.840	56.42	.868	52.50	1.510	52.32	1.621				
56.43	.864	56.68	.867								
63.21	.776	62.70	.845								
64.21	.880	63.28	.845								
$\alpha = 4^\circ$				$\alpha = 7^\circ$				$\alpha = 11^\circ$			
Suction (top) Side				Suction (top) Side				Suction (top) Side			
Cavitation Began		Cavitation Disappeared		Cavitation Began		Cavitation Disappeared		Cavitation Began		Cavitation Disappeared	
V	K	V	K	V	K	V	K	V	K	V	K
20.88	.733	20.88	.837	21.16	1.138	21.62	1.257	21.50	2.222	21.81	3.023
28.11	.661	28.05	.726	21.38	1.089	21.70	1.166	21.47	2.458	21.69	2.846
28.15	.717	28.22	.748	28.04	1.358	28.09	1.488	27.83	2.887	27.92	2.883
33.23	.773	33.26	.766	28.36	1.102	28.30	1.516	27.90	2.716	27.95	2.868
33.26	.736	33.14	.731	33.00	1.457	33.18	1.525	32.83	2.958	32.86	2.950
40.05	.699	40.05	.849	33.21	1.419	32.95	1.546	32.91	2.973	32.83	3.062
40.15	.792	40.09	.838	39.86	1.569	39.79	1.589	39.44	3.199	39.41	3.158
43.61	.857	43.42	.872	39.79	1.535	39.85	1.595	43.23	3.245	43.18	3.229
43.61	.839	43.38	.921	43.41	1.749	43.51	1.875				
48.02	.846	47.93	.906	43.42	1.768	43.56	1.907				
48.04	.930	48.09	.900	48.17	1.807	48.17	1.886				
51.50	.814	50.72	.930	48.06	1.804						
51.81	.951	51.40	.976								
56.80	.861	55.94	1.033								
56.09	.953	55.71	.991								
$\alpha = 5^\circ$				$\alpha = 8^\circ$				$\alpha = 12^\circ$			
Suction (top) Side				Suction (top) Side				Suction (top) Side			
Cavitation Began		Cavitation Disappeared		Cavitation Began		Cavitation Disappeared		Cavitation Began		Cavitation Disappeared	
V	K	V	K	V	K	V	K	V	K	V	K
21.33	.853			21.44	1.651	21.71	1.623	21.41	2.086	21.82	3.438
20.56	.856	21.47	.824	21.47	1.608	21.63	1.618	21.50	2.594	27.74	3.177
28.16	.838	28.37	.893	28.09	1.721	28.23	1.814	27.56	3.077	27.81	3.197
28.21	.749	28.28	.884	28.15	1.552	28.19	1.888	27.74	3.162	32.84	3.232
33.44	.875	33.44	.884	33.05	1.752	33.03	1.876	32.86	3.226	32.63	3.355
33.03	.835	33.09	.870	33.04	1.815	32.89	1.833	32.63	3.216	39.42	3.754
39.93	.820	39.68	.911	39.34	1.875	39.50	2.091	39.43	3.464	39.43	3.967
39.92	.917	39.83	.898	39.57	1.961	39.55	2.036	42.96	3.780	42.90	3.874
43.47	1.005	43.67	1.147	43.35	2.053	43.17	2.198				
43.71	1.041	43.52	1.116	43.41	2.143	43.33	2.235				
48.20	1.013	47.90	1.075	48.30	2.238	47.95	2.366				
48.33	1.013	47.90	1.084	48.10	2.233	48.24	2.391				
$\alpha = 9^\circ$				$\alpha = 13^\circ$				Suction (top) Side			
Suction (top) Side				Suction (top) Side				Suction (top) Side			
Cavitation Began		Cavitation Disappeared		Cavitation Began		Cavitation Disappeared		Cavitation Began		Cavitation Disappeared	
V	K	V	K	V	K	V	K	V	K	V	K
21.45	1.637	21.77	2.100	21.54	2.451			21.59	2.850	21.71	3.758
21.37	1.434	21.86	2.030	27.54	3.272	27.73	4.222	21.60	1.928	21.80	2.065
27.95	2.001	28.18	2.291	27.74	3.377	27.60	3.840	28.06	1.986	28.22	2.285
32.99	2.145	32.95	2.266	32.53	3.522	32.42	4.154	32.51	3.738	32.15	3.918
39.46	2.527	39.41	2.440	38.97	4.573	38.86	4.800	32.99	2.086	32.75	2.161
39.55	2.298	39.43	2.460					39.46	2.527	39.41	2.440
43.12	2.504	43.35	2.576					43.12	2.504	43.35	2.576
43.36	2.534	43.34	2.557					43.36	2.534	43.34	2.557
47.97	2.604	48.14	2.741					47.97	2.604	48.14	2.741
48.26	2.671	48.20	2.732					48.26	2.671	48.20	2.732

APPENDIX D - DATA TABLES

TABLE IB - NACA 4412 Hydrofoil. Incipient Cavitation Characteristics of the NACA 4412 Hydrofoil (cavitation number based on vapor pressure).

TABLE IC - NACA 4412 Hydrofoil. Force Characteristics of the NACA 4412 Hydrofoil in Cavitating Flow (data not corrected for tunnel interference effects; cavitation number based on vapor pressure).

APPENDIX D - DATA TABLES

**TABLE IC - NACA 4412 Hydrofoil. Force Characteristics of the NACA 4412
Hydrofoil in Cavitating Flow (data not corrected for tunnel interference effects; cavitation number based on vapor pressure).**

V = 30 fps $\alpha = 1^\circ$ (cont'd)				V = 30 fps $\alpha = 4^\circ$				V = 30 fps $\alpha = 5^\circ$			
K	C _L	C _D	C _M	K	C _L	C _D	C _M	K	C _L	C _D	C _M
2.665		.0159	-0.083	5.033	.788	.0179	-0.096	5.191	.861	.0220	-0.091
.249		.0333	-0.061	4.251	.777	.0180	-0.095	3.632	.871	.0217	-0.092
.180	.177	.0293	-0.026	3.452	.775	.0176	-0.095	2.026	.875	.0214	-0.094
.153	.192	.0289	-0.030	2.751	.785	.0177	-0.096	1.156	.874	.0215	-0.094
.145	.212	.0284	-0.034	1.934	.786	.0182	-0.098	.902	.874	.0245	-0.095
.510	.279	.0165	-0.076	1.135	.773	.0179	-0.096	.757	.813	.0444	-0.110
2.102	.458	.0157	-0.088	.850	.772	.0208	-0.098	.688	.748	.0550	-0.115
5.157	.463	.0147	-0.090	.717	.740	.0240	-0.098	.544	.563	.0600	-0.097
				.687	.721	.0373	-0.110	.465	.447	.0584	-0.079
				3.460	.784	.0183		.323	.244	.0467	-0.046
				5.039	.796	.0192	-0.094	.223	.088	.0341	-0.024
				4.247	.781	.0191	-0.093	.892	.857	.0259	-0.094
				3.510	.777	.0184	-0.093	5.187	.868	.0222	-0.092
V = 30 fps $\alpha = 2^\circ$				V = 30 fps $\alpha = 5^\circ$				V = 30 fps $\alpha = 6^\circ$			
K	C _L	C _D	C _M	K	C _L	C _D	C _M	K	C _L	C _D	C _M
5.232	.565	.0173	-0.092	1.960	.790	.0192	-0.095	5.035	.970	.0236	-0.087
3.611	.557	.0172	-0.090	1.136	.778	.0177	-0.094	3.482	.965	.0234	-0.092
2.071	.553	.0181	-0.091	.842	.759	.0206	-0.093	1.957	.962	.0240	-0.093
1.544	.547	.0172	-0.090	.736	.756	.0241	-0.096	1.158	.963	.0245	-0.093
1.161	.552	.0183	-0.091	.705	.734	.0294	-0.104	.917	.939	.0369	-0.104
.795	.538	.0185	-0.090	.661	.708	.0410	-0.109	.853	.912	.0504	-0.113
.638	.544	.0198	-0.094	.583	.596	.0505	-0.106	.785	.868	.0596	-0.119
.540	.510	.0313	-0.105	.505	.503	.0514	-0.093	.665	.733	.0688	-0.112
.475	.439	.0359	-0.099	.407	.366	.0490	-0.072	.549	.596	.0689	-0.096
.442	.400	.0372	-0.094	.345	.256	.0453	-0.055	.431	.409	.0602	-0.067
.400	.325	.0384	-0.083	.260	.126	.0383	-0.035	.353	.308	.0534	-0.051
.344	.224	.0384	-0.066	.207	.053	.0319	-0.086	1.967	.968	.0259	-0.093
.300	.152	.0351	-0.057	.991	.762	.0217	-0.092	5.054	.958	.0241	-0.092
				2.931	.782	.0206	-0.094	.179	.096	.0328	-0.021
.206	-0.007	.0299	-0.005	5.994	.781	.0186					
.173	-0.008	.0306	-0.004								
.153	-0.006	.0285	-0.004								
.146	-0.006	.0280	-0.005								
.496	.459	.0328	-0.062								
2.018	.562	.0174	-0.092								
5.075	.552	.0168	-0.090								
V = 30 fps $\alpha = 3^\circ$				V = 35 fps $\alpha = 4^\circ$				V = 30 fps $\alpha = 7^\circ$			
K	C _L	C _D	C _M	K	C _L	C _D	C _M	K	C _L	C _D	C _M
3.740	.783	.0172	-0.094	3.740	.783	.0172	-0.094	5.060	1.036	.0274	-0.088
2.569	.775	.0175	-0.094	2.569	.775	.0184	-0.095	3.515	1.036	.0252	-0.079
1.950	.782	.0184	-0.095	1.950	.782	.0196	-0.096	1.985	1.042	.0275	-0.091
1.325	.785	.0196	-0.096	1.325	.785	.0194	-0.095	1.592	1.040	.0274	-0.092
.990	.782	.0194	-0.095	.990	.782	.0194	-0.095	1.432	1.053	.0303	-0.093
.745	.769	.0214	-0.096	.745	.769	.0214	-0.096	1.315	1.038	.0359	-0.094
.733	.759	.0314	-0.108	.733	.759	.0314	-0.108	1.240	1.024	.0433	-0.097
.713	.748	.0424	-0.115	.713	.748	.0424	-0.115	1.164	1.007	.0569	-0.104
.669	.719	.0442	-0.118	.669	.719	.0442	-0.118	1.004	.987	.0788	-0.129
.643	.687	.0459	-0.117	.643	.687	.0459	-0.117	.817	.862	.0910	-0.130
.611	.647	.0484	-0.114	.611	.647	.0484	-0.114	.703	.746	.0910	-0.118
.587	.607	.0502	-0.109	.587	.607	.0502	-0.109	.608	.638	.0481	-0.104
.555	.569	.0507	-0.104	.555	.569	.0507	-0.104	.525	.553	.0763	-0.088
.530	.524	.0518	-0.099	.530	.524	.0518	-0.099	.452	.464	.0686	-0.072
.482	.474	.0510	-0.091	.482	.474	.0510	-0.091	.402	.408	.0634	-0.062
.412	.303	.0489	-0.065	.412	.303	.0489	-0.065	.346	.315	.0549	-0.046
.345	.268	.0454	-0.057	.345	.268	.0454	-0.057	1.137	1.012	.0510	-0.102
.201	.067	.0324	-0.028	.201	.067	.0324	-0.028	1.693	1.031	.0291	-0.089
.560	.574	.0514	-0.105	.560	.574	.0514	-0.105	.5193	1.047	.0279	-0.090
1.930	.769	.0197	-0.094	1.930	.769	.0197	-0.094				
3.783	.771	.0186	-0.093	3.783	.771	.0186	-0.093				
V = 25 fps $\alpha = 4^\circ$				V = 40 fps $\alpha = 4^\circ$				V = 30 fps $\alpha = 8^\circ$			
K	C _L	C _D	C _M	K	C _L	C _D	C _M	K	C _L	C _D	C _M
7.578	.773	.0227	-0.095	1.996	.813	.0133	-0.091	5.182	1.102	.0308	-0.084
5.236	.767	.0221	-0.095	1.547	.807	.0130	-0.091	3.574	1.118	.0315	-0.086
3.428	.769	.0225	-0.096	1.044	.809	.0131	-0.091	2.009	1.107	.0308	-0.086
2.645	.758	.0227	-0.094	.816	.809	.0232	-0.100	1.684	1.131	.0371	-0.090
2.106	.756	.0218	-0.094	.725	.780	.0376		1.633	1.136	.0401	-0.091
1.600	.763	.0219	-0.095	.697	.735	.0458	-0.121	1.565	1.101	.0450	-0.085
1.310	.764	.0224	-0.095	.618	.660	.0509	-0.115	1.506	1.116	.0499	-0.094
1.094	.753	.0222	-0.094	.530	.552	.0523	-0.102	1.331	1.092	.0731	-0.106
.823	.750	.0263	-0.095	.488	.476	.0523	-0.093	1.244	1.083	.0849	-0.122
.690	.722	.0279	-0.097	.427	.421	.0498	-0.084	1.114	1.045	.1041	-0.137
.598	.640	.0441	-0.105	.384	.319	.0422	-0.082	.971	.966	.1135	-0.141
.472	.455	.0501	-0.087	.323	.253	.0438	-0.056	.836	.872	.1092	-0.131
.349	.238	.0419	-0.051	.247	.165	.0394	-0.042	.675	.713	.1037	-0.114
.220	-0.040	.0298	-0.013	.220	.099	.0350	-0.032	.510	.519	.0869	-0.081
1.066	.764	.0232	-0.094	.184	-0.039	.0308	-0.023	.358	.326	.0659	-0.047
3.424	.768	.0244	-0.093	.139	-0.012	.0253	-0.006	.276	.245	.0562	-0.035
7.441	.752	.0228	-0.094	.123	-0.014	.0248	-0.003	.218	.187	.0481	-0.028
				.592	.626	.0501	-0.112	.968	.978	.1165	-0.146
				1.616	.816	.0140	-0.094	1.744	1.111	.0356	-0.093
				1.996	.803	.0128	-0.090	5.231	1.105	.0322	-0.085

APPENDIX D - DATA TABLES

TABLE IC - NACA 4412 Hydrofoil. Force Characteristics of the NACA 4412 Hydrofoil in Cavitating Flow (data not corrected for tunnel interference effects; cavitation number based on vapor pressure).

V = 30 fps $\alpha = 10^\circ$				V = 30 fps $\alpha = 12^\circ$				V = 30 fps $\alpha = 14^\circ$ (cont'd)			
K	C _L	C _D	C _M	K	C _L	C _D	C _M	K	C _L	C _D	C _M
5.161	1.246	.0414	-0.077	5.216	1.352	.0537	-0.073	1.781	1.421	.2545	-0.160
3.575	1.244	.0404	-0.080	3.564	1.329	.0513	-0.071	1.378	1.258	.2720	-0.181
2.515	1.244	.0427	-0.081	3.096	1.373	.0591	-0.076	.973	.928	.2386	-0.145
2.413	1.271	.0444	-0.082	2.936	1.416	.0670	-0.081	.706	.714	.1958	-0.107
2.271	1.279	.0483	-0.083	2.793	1.421	.0724	-0.085	.561	.530	.1567	-0.074
2.149	1.295	.0553	-0.086	2.623	1.424	.0820	-0.086	.354	.329	.1267	-0.045
1.939	1.278	.0708	-0.091	2.466	1.404	.0928	-0.089	2.074	1.428	.1985	-0.125
1.778	1.249	.0842	-0.098	2.328	1.383	.0963	-0.086	5.437	1.421	.7280	-0.072
1.610	1.236	.1074	-0.113	2.144	1.382	.1179	-0.093				
1.479	1.232	.1309	-0.135	1.959	1.382	.1382	-0.088				
1.287	1.164	.1504	-0.150	1.708	1.377	.1877	-0.083				
1.136	1.081	.1616	-0.156	1.514	1.323	.2092	-0.084				
.952	.936	.1626	-0.149	1.334	1.223	.2152	-0.078				
.791	.805	.1505	-0.130	1.149	1.093	.2139	-0.056				
.630	.659	.1268	-0.101	.902	.881	.2000	-0.141				
.489	.484	.1030	-0.069	.746	.747	.1745	-0.118				
.380	.379	.0857	-0.052	.534	.543	.1572	-0.082				
.303	.302	.0733	-0.040	.396	.396	.1080	-0.057				
.256	.256	.0673	-0.033	.300	.323	.0925	-0.044				
1.179	1.101	.1585	-0.155	1.348	1.233	.2179	-0.178				
2.324	1.295	.0483	-0.085	2.490	1.417	.0878	-0.088				
5.168	1.244	.0402	-0.077	5.181	1.341	.0535	-0.070				
V = 30 fps $\alpha = 14^\circ$				V = 30 fps $\alpha = 16^\circ$							
K	C _L	C _D	C _M	K	C _L	C _D	C _M	K	C _L	C _D	C _M
5.523	1.415	.1089	-0.082	5.111	1.384	.1117	-0.084				
4.552	1.555	.1216	-0.074	4.189	1.529	.1331	-0.075				
3.772	1.531	.1519	-0.079	3.306	1.512	.1716	-0.083				
3.046	1.507	.1900	-0.090	2.777	1.489	.2073	-0.098				
2.482	1.451	.2281	-0.110	2.177	1.415	.2555	-0.128				
1.861	1.416	.2916	-0.158	1.527	1.302	.3054	-0.177				
1.194	1.079	.3049	-0.170	.974	.921	.2778	-0.143				
.581	.630	.1977	-0.090	.455	.506	.1684	-0.069				
.390	.455	.1572	-0.060	1.600	1.294	.2885	-0.061				
3.345	1.393	.1692	-0.064	5.609	1.428	.1077	-0.080				

TABLE ID - NACA 4412 Hydrofoil. Cavity Pressure Data for the NACA 4412 Hydrofoil.

$\alpha = 4^\circ, T_\omega = 76.1^\circ\text{F}, P_v = .444 \text{ psia}$					$\alpha = 8^\circ, T_\omega = 77.0^\circ\text{F}, P_v = .458 \text{ psia}$					$\alpha = 12^\circ, T_\omega = 77.2^\circ\text{F}, P_v = .460 \text{ psia}$				
V	P _o	P _k	K _v	K _k	V	P _o	P _k	K _v	K _k	V	P _o	P _k	K _v	K _k
fps	psia	psia			fps	psia	psia			fps	psia	psia		
45.68	8.127	2.306	.548	.415	31.32	6.214	1.684	.874	.703	29.62	2.165	.581	.289	.269
45.70	7.540	1.931	.506	.400	31.14	5.991	1.584	.849	.676	28.35	2.036	.552	.292	.275
45.92	6.819	1.578	.450	.370	31.06	5.727	1.385	.814	.671	27.12	1.872	.563	.286	.265
45.50	6.455	1.185	.433	.380	30.97	5.469	1.256	.778	.623					
45.68	5.780	1.056	.381	.337	31.14	5.111	1.115	.714	.613					
45.92	5.058	.863	.326	.296	31.14	4.818	1.091	.669	.572					
45.62	4.642	.710	.300	.281	30.79	4.659	1.009	.659	.573					
45.50	4.108	.645	.264	.250	30.97	4.295	0.956	.596	.518					
45.66	3.433	.604	.213	.202	31.06	3.967	.951	.542	.466					
46.10	2.611	.610	.152	.140	30.97	3.415	.775	.459	.410					
45.32	2.465	.587	.146	.136	30.97	2.828	.645	.368	.339					
44.47	2.353	.581	.144	.133	31.06	2.206	.604	.270	.248					
43.55	2.277	.593	.144	.132	30.70	1.760	.604	.205	.182					
42.66	2.159	.593	.141	.128	29.43	1.649	.599	.204	.180					
41.72	2.066	.587	.139	.127	28.11	1.532	.587	.203	.179					
40.67	2.024	.587	.142	.129	26.82	1.391	.587	.193	.166					
39.75	1.895	.587	.137	.123										
38.64	1.848	.587	.140	.126										
37.78	1.672	.587	.128	.113										
36.61	1.625	.581	.131	.116										
34.23	1.508	.569	.135	.119										
$\alpha = 4^\circ, T_\omega = 77.4^\circ\text{F}, P_v = .464 \text{ psia.}$					$\alpha = 12^\circ, T_\omega = 77.2^\circ\text{F}, P_v = .460 \text{ psia}$					$\alpha = 16^\circ, T_\omega = 77.3^\circ\text{F}, P_v = .462 \text{ psia}$				
V	P _o	P _k	K _v	K _k	V	P _o	P _k	K _v	K _k	V	P _o	P _k	K _v	K _k
fps	psia	psia			fps	psia	psia			fps	psia	psia		
31.14	3.932	1.461	.532	.379	30.70	11.736	5.252	1.780	1.024	30.35	11.871	5.803	1.844	.980
31.16	3.632	1.162	.485	.378	31.14	10.979	3.603	1.614	1.132	30.35	10.697	4.254	1.654	1.041
31.16	3.339	1.068	.440	.348	31.23	10.422	3.280	1.517	1.103	30.79	9.354	2.734	1.396	1.039
31.05	3.098	0.939	.407	.333	31.23	9.770	2.852	1.421	1.056	30.70	8.215	2.247	1.224	.942
31.42	2.652	.863	.330	.270	31.23	9.183	2.371	1.331	1.040	30.97	6.936	1.754	1.005	.804
31.14	2.470	.663	.308	.277	31.23	8.597	2.159	1.242	0.982	30.61	5.897	1.256	.864	.738
30.95	2.247	.663	.278	.247	31.23	8.010	2.030	1.152	.912	30.97	4.589	.921	.641	.569
31.16	1.872	.634	.216	.190	31.32	7.388	1.948	1.051	.826	31.14	3.351	.616	.443	.419
31.23	1.555	.599	.166	.146	30.97	6.936	1.772	1.005	.802	29.62	2.752	.569	.388	.370
30.84	1.414	.581	.149	.131	30.88	6.384	1.596	.925	.747	27.02	2.494	.557	.319	.311
30.46	1.262	.581	.128	.109	30.88	5.796	1.379	.833	.690	26.99	1.332	.540	.177	.162
29.86	1.197	.575	.123	.105	30.88	5.211	1.191	.741	.627					
29.13	1.174	.575	.124	.105	31.14	4.524	1.086	.623	.527					
					31.32	3.867	0.886	.517	.452					
					31.32	3.280	.780	.428	.379					
					31.06	2.793	.628	.360	.335					
					30.52	2.412	.593	.312	.291					

APPENDIX D - DATA TABLES

TABLE II A - Walchner Profile 7 Hydrofoil, Section Characteristics of the Walchner Profile 7 Hydrofoil in Noncavitating Flow (data corrected for tunnel interference effects).

V = 19.9 fps, Re = 533,000 (before leading edge modification)				V = 30 fps, Re = 896,000 (before leading edge modification)				V = 20.2 fps, Re = 575,000 (after leading edge modification)			
a	C _L	C _D	C _M	a	C _L	C _D	C _M	a	C _L	C _D	C _M
-7	-0.144	.0593	-0.099	0	.507	.0160	-0.122	0	.540	.0128	-0.125
-6	-0.057	.0409	-0.106	1	.637	.0174	-0.132	-7	-0.067	.0396	-0.115
-5	.029	.0279	-0.111	2	.712	.0185	-0.130	-6	.002	.0293	-0.115
-4	.110	.0168	-0.112	3	.794	.0203	-0.128	-5	.087	.0158	-0.116
-3	.190	.0139	-0.111	4	.910	.0227	-0.132	-4	.173	.0159	-0.118
-2	.266	.0131	-0.106	5	.946	.0250	-0.120	-3	.261	.0145	-0.116
-1	.340	.0126	-0.106	6	.942	.0292	-0.104	-2	.340	.0129	-0.116
0	.511	.0138	-0.127	7	.999	.0333	-0.099	-1	.434	.0119	-0.120
1	.586	.0151	-0.125	6	.938	.0293	-0.103	0	.560	.0124	-0.128
2	.677	.0176	-0.128	5	.943	.0256	-0.122	-1	.635	.0137	-0.125
3	.743	.0190	-0.124	4	.906	.0233	-0.134	2	.719	.0165	-0.127
4	.828	.0223	-0.126	3	.819	.0209	-0.135	3	.815	.0187	-0.128
5	.920	.0264	-0.129	2	.740	.0191	-0.138	4	.859	.0213	-0.121
6	.947	.0274	-0.116	1	.641	.0175	-0.136	5	.925	.0232	-0.118
7	.926	.0318	-0.093	0	.519	.0156	-0.127	6	.923	.0263	-0.099
0	.510	.0143	-0.133	-1	.378	.0150	-0.112	7	.955	.0308	-0.090
				-2	.297	.0145	-0.113	0	.566	.0125	-0.129
V = 25 fps, Re = 720,000 (before leading edge modification)				-2	.297	.0149	-0.113				
				-3	.215	.0147	-0.113				
				-4	.124	.0152	-0.112				
				-5	.047	.0162	-0.113				
				-6	-.034	.0377	-0.113				
0	.504	.0171	-0.122	-7	-.018	.0544	-0.107				
1	.621	.0188	-0.128	-7	-.019	.0546	-0.105				
2	.689	.0206	-0.122	-6	-.039	.0386	-0.111				
3	.776	.0215	-0.128	-5	-.033	.0150	-0.109				
4	.882	.0239	-0.130	-4	.120	.0142	-0.109				
5	.942	.0271	-0.131	-3	.206	.0141	-0.110				
6	.939	.0314	-0.107	-2	.291	.0138	-0.109				
7	.974	.0355	-0.101	-1	.375	.1036	-0.108				
6	.941	.0308	-0.108	0	.525	.0148	-0.125	-3	.250	.0116	-0.117
5	.963	.0279	-0.130	1	.640	.0169	-0.134	-2	.332	.0112	-0.117
4	.892	.0257	-0.126	2	.741	.0181	-0.137	-1	.402	.0102	-0.114
3	.803	.0211	-0.132	3	.835	.0194	-0.140	0	.545	.0108	-0.125
2	.714	.0196	-0.134	4	.906	.0219	-0.134	1	.636	.0117	-0.129
1	.625	.0175	-0.133	5	.941	.0251	-0.126	2	.711	.0128	-0.126
0	.514	.0163	-0.128	6	.941	.0310	-0.106	3	.808	.0148	-0.128
-1	.365	.0144	-0.110					4	.878	.0159	-0.122
-2	.284	.0148	-0.111					5	.895	.0186	-0.098
-3	.199	.0148	-0.111					6	.890	.0217	-0.093
-4	.120	.0160	-0.111					7	.933	.0251	-0.086
-5	.043	.0241	-0.113					4	.879	.0163	-0.125
-6	-.037	.0380	-0.111					0	.566	.0110	-0.132
-7	.0131	.0555	-0.102								
-7	-.0129	.0549	-0.104								
-6	-.047	.0390	-0.108								
-5	.033	.0245	-0.107								
-4	.112	.0145	-0.108								
-3	.194	.0139	-0.107								
-2	.278	.0136	-0.105								
-1	.360	.0139	-0.106								
0	.501	.0155	-0.121	1	.668	.0170	-0.142				
1	.621	.0172	-0.132	2	.748	.0186	-0.139				
2	.697	.0189	-0.128	3	.826	.0213	-0.135				
3	.791	-.0209	-0.134	4	.910	.0250	-0.137				
4	.878	.0232	-0.134	5	.939	.0280	-0.121				
5	.950	.0269	-0.131	6	.944	.0327	-0.106				
6	.937	.0319	-0.110	0	.554	.0163	-0.138				

V = 35 fps, Re = 1,050,000
(before leading edge modification)

a	C _L	C _D	C _M
-6	-.032	.0375	-0.122
-5	.043	.0212	-0.114
-4	.128	.0150	-0.119
-3	.221	.0145	-0.118
-2	.310	.0139	-0.118
-1	.386	.0138	-0.115
0	.551	.0157	-0.133
1	.668	.0170	-0.142
2	.748	.0186	-0.139
3	.826	.0213	-0.135
4	.910	.0250	-0.137
5	.939	.0280	-0.121
6	.944	.0327	-0.106

TABLE II B - Walchner Profile 7 Hydrofoil, Force Characteristics of the Walchner Profile 7 Hydrofoil in Cavitating Flow (data not corrected for tunnel interference effects; cavitation number based on vapor pressure).

V = 30 fps a = -6°				V = 30 fps a = -6° (cont'd)				V = 30 fps a = -5° (cont'd)			
K	C _L	C _D	C _M	K	C _L	C _D	C _M	K	C _L	C _D	C _M
5.404	-.041	.0408	-0.117	.211	-.058	.0459	-0.014	1.183	.035	.0312	-0.118
3.657	-.043	.0413	-0.116	2.106	-.046	.0385	-0.118	.988	.029	.0326	-0.120
2.112	-.043	.0419	-0.118	5.252	-.044	.0408	-0.116	.918	.024	.0342	-0.119
1.654	-.038	.0392	-0.115					.705	-.012	.0388	-0.109
1.378	-.046	.0413	-0.115					.525	-0.084	.0494	-0.062
1.196	-.052	.0447	-0.116					.414	-0.055	.0537	-0.037
1.019	-.073	.0475	-0.114					.353	-0.066	.0539	-0.023
.880	-.096	.0516	-0.104					.249	-0.054	.0462	-0.014
.712	-.142	.0591	-0.080					.212	-0.050	.0429	-0.012
.614	-.164	.0649	-0.049					.189	-0.048	.0410	-0.013
.531	-.122	.0641	-0.041	5.120	.043	.0209	-0.117	2.038	.036	.0237	-0.117
.433	-.075	.0650	-0.034	3.628	.040	.0230	-0.116	5.203	.041	.0232	-0.130
.339	-.075	.0590	-0.020	2.042	.038	.0223	-0.118				
.262	-.065	.0505	-0.014	1.520	.041	.0270	-0.118				
.214	-.058	.0453	-0.012	1.349	.039	.0288	-0.119				

APPENDIX D - DATA TABLES

TABLE IIB - Walchner Profile 7 Hydrofoil. Force Characteristics of the Walchner Profile 7 Hydrofoil in Cavitating Flow (data not corrected for tunnel interference effects; Cavitation number based on vapor pressure).

V = 30 fps $\alpha = -4^\circ$				V = 30 fps $\alpha = 0^\circ$				V = 30 fps $\alpha = 4^\circ$			
K	C _L	C _D	C _M	K	C _L	C _D	C _M	K	C _L	C _D	C _M
5.458	.129	.0179	-0.119	5.075	.554	.0184	-0.131	5.039	.915	.0273	-0.138
3.687	.123	.0179	-0.114	5.075	.548	.0175	-0.126	3.491	.916	.0269	-0.139
2.121	.120	.0180	-0.115	3.508	.542	.0184	-0.130	2.004	.924	.0263	-0.138
1.581	.121	.0181	-0.117	2.007	.543	.0191	-0.128	1.481	.924	.0262	-0.141
1.226	.120	.0182	-0.115	1.512	.558	.0191	-0.134	1.125	.920	.0265	-0.139
.856	.113	.0256	-0.116	1.140	.554	.0193	-0.135	.872	.935	.0267	-0.143
.774	.108	.0260	-0.116	.762	.534	.0186	-0.129	.711	.855	.0369	-0.131
.690	.102	.0271	-0.116	.602	.543	.0186	-0.129	.650	.814	.0396	-0.130
.601	.085	.0286	-0.115	.484	.476	.0214	-0.119	.572	.705	.0439	-0.115
.512	.047	.0321	-0.100	.484	.476	.0216	-0.121	.499	.587	.0467	-0.093
.426	-0.002	.0374	-0.069	.424	.363	.0258	-0.102	.441	.498	.0461	-0.082
.334	-0.052	.0471	-0.023	.322	.190	.0297	-0.058	.368	.382	.0431	-0.056
.256	-0.046	.0424	-0.016	.238	.067	.0278	-0.043	.270	.244	.0340	-0.038
.201	-0.042	.0380	-0.012	.168	.059	.0229	-0.040	.176	.110	.0251	-0.015
.080	-0.041	.0371	-0.012	2.028	.547	.0198	-0.131	.152	.087	.0232	-0.013
.167	-0.040	.0363	-0.012	5.078	.538	.0189	-0.126	.134	.087	.0230	-0.014
2.544	.120	.0177	-0.116					1.993	.922	.0267	-0.134
5.085	.126	.0170	-0.120					5.075	.913	.0263	-0.134
V = 30 fps $\alpha = -3^\circ$				V = 30 fps $\alpha = 1^\circ$				V = 30 fps $\alpha = 5^\circ$			
K	C _L	C _D	C _M	K	C _L	C _D	C _M	K	C _L	C _D	C _M
5.038	.210	.0166	-0.112	4.984	.636	.0191	-0.129	5.026	.968	.0282	-0.126
3.504	.211	.0176	-0.114	3.502	.658	.0201	-0.136	3.459	.974	.0291	-0.130
2.020	.211	.0175	-0.115	1.980	.655	.0201	-0.135	1.988	.972	.0306	-0.129
1.503	.210	.0178	-0.115	1.448	.664	.0196	-0.138	1.449	.982	.0306	-0.131
1.098	.212	.0173	-0.115	1.101	.666	.0199	-0.140	1.119	.990	.0303	-0.133
.763	.209	.0171	-0.114	.749	.657	.0196	-0.137	.971	.989	.0383	-0.140
.609	.208	.0199	-0.116	.472	.463	.0286	-0.105	.918	.975	.0426	-0.143
.525	.203	.0207	-0.116	.402	.383	.0296	-0.087	.740	.896	.0462	-0.131
.445	.184	.0230	-0.114	.340	.282	.0304	-0.070	.662	.831	.0514	-0.128
.368	.092	.0284	-0.089	.253	.109	.0284	-0.035	.575	.716	.0546	-0.101
.328	-0.007	.0380	-0.038	.166	-0.003	.0216	-0.009	.503	.616	.0543	-0.083
.256	-0.043	.0386	-0.012	.128	-0.011	.0214	-0.005	.442	.524	.0536	-0.073
.192	-0.035	.0338	-0.012	2.017	.687	.0202	-0.143	.367	.399	.0483	-0.053
2.570	.219	.0179	-0.117	4.890	.668	.0186	-0.136	.270	.249	.0382	-0.030
.185	-0.034	.0331	-0.012					.192	.162	.0299	-0.016
.156	-0.034	.0328	-0.011					.157	.137	.0278	-0.015
2.004	.215	.0173	-0.113					.151	.137	.0277	-0.017
5.018	.219	.0161	-0.103					2.007	.974	.0308	-0.013
V = 30 fps $\alpha = -2^\circ$				V = 30 fps $\alpha = 2^\circ$				V = 30 fps $\alpha = 6^\circ$			
K	C _L	C _D	C _M	K	C _L	C _D	C _M	K	C _L	C _D	C _M
5.194	.301	.0170	-0.116	5.240	.767	.0199	-0.136	5.237	.978	.0311	-0.106
3.688	.297	.0166	-0.114	3.616	.765	.0214	-0.137	3.643	.970	.0318	-0.106
2.098	.301	.0177	-0.116	2.046	.767	.0204	-0.139	2.119	.963	.0317	-0.104
1.549	.299	.0175	-0.115	1.487	.758	.0210	-0.142	1.576	.970	.0322	-0.107
1.180	.294	.0177	-0.113	1.143	.753	.0201	-0.137	1.197	1.004	.0327	-0.111
.838	.300	.0172	-0.116	.817	.777	.0213	-0.141	.995	.971	.0321	-0.107
.656	.294	.0173	-0.114	.639	.735	.0250	-0.140	1.040	1.029	.1186	-0.159
.469	.297	.0185	-0.117	.547	.597	.0332	-0.117	.955	1.052	.1244	-0.195
.406	.247	.0225	-0.113	.465	.498	.0347	-0.100	.876	.963	.0894	-0.171
.333	.100	.0285	-0.080	.392	.384	.0348	-0.076	.794	.913	.0840	-0.165
.248	.137	.0357	-0.088	.095	.037	.0208	-0.013	.706	.788	.0795	-0.128
.180	-0.026	.0295	-0.011	.021	.002	.0161	-0.006	.621	.743	.0695	-0.108
.160	-0.025	.0299	-0.015	.418	.413	.0319	-0.086	.537	.655	.0660	-0.087
5.260	.316	.0171	-0.121	2.133	.785	.0222	-0.144	.453	.555	.0597	-0.071
				5.124	.759	.0207	-0.138	.360	.394	.0508	-0.038
V = 30 fps $\alpha = -1^\circ$				V = 30 fps $\alpha = 3^\circ$				V = 30 fps $\alpha = 6^\circ$			
K	C _L	C _D	C _M	K	C _L	C _D	C _M	K	C _L	C _D	C _M
5.086	.390	.0169	-0.114	5.081	.851	.0228	-0.143	1.160	1.140	.0523	-0.162
3.538	.389	.0164	-0.114	3.549	.843	.0226	-0.138	1.239	1.120	.0428	-0.140
1.983	.381	.0163	-0.112	1.994	.848	.0237	-0.145	1.328	.968	.0330	-0.103
1.484	.383	.0158	-0.113	1.470	.838	.0238	-0.138	2.105	.967	.0317	-0.104
1.120	.390	.0166	-0.116	1.117	.845	.0243	-0.142	5.229	.955	.0306	-0.102
.780	.384	.0163	-0.114	.774	.832	.0243	-0.139				
.602	.386	.0159	-0.114	.600	.729	.0337	-0.130				
.471	.368	.0178	-0.111	.537	.631	.0387	-0.108				
.404	.288	.0223	-0.096	.474	.552	.0400	-0.100				
2.583	.388	.0173	-0.113	.415	.460	.0416	-0.082				
.338	.165	.0272	-0.072	.337	.357	.0384	-0.063				
.248	-0.028	.0310	-0.010	.250	.227	.0324	-0.044				
.171	-0.016	.0268	-0.008	.155	.067	.0224	-0.001				
2.613	.393	.0173	-0.115	2.553	.844	.0251	-0.140				
.146	-0.014	.0264	-0.010	.038	.030	.0184	-0.011				
2.082	.382	.0172	-0.112	2.067	.858	.0254	-0.142				
5.216	.378	.0163	-0.109	5.094	.831	.0252	-0.140				

**DISTRIBUTION LIST FOR TECHNICAL REPORTS ISSUED UNDER
CONTRACT NONR-220(12)**

<u>Item</u>	<u>Address</u>	<u>No. Copies</u>
1	Commanding Officer and Director, David Taylor Model Basin, Washington 7, D.C., Attn: Code 580	54
2	Chief of Naval Research, Office of Naval Research, Department of the Navy, Washington 25, D.C., Attn: Mechanics Branch (Code 438)	6
3	Commanding Officer, Branch Office, Office of Naval Research, 495 Summer St., Boston 10, Mass.	1
4	Commanding Officer, Branch Office, Office of Naval Research, 346 Broadway, New York 13, N. Y.	1
5	Commanding Officer, Branch Office, Office of Naval Research, The John Crerar Library Bldg., 10th Floor, 86 E. Randolph St., Chicago 1, Ill.	1
6	Commanding Officer, Branch Office, Office of Naval Research, 1000 Geary St., San Francisco 9, Calif.	1
7	Commanding Officer, Branch Office, Office of Naval Research, 1030 E. Green Street, Pasadena 1, Calif.	2
8	Asst. Naval Attaché for Research, Office of Naval Research, American Embassy, London, England, Navy 100, F. P. O. New York, N.Y.	2
9	Director, Naval Research Laboratory, Office of Naval Research, Washington 25, D.C. Attn: Librarian	9
10	Bureau of Aeronautics, Dept. of the Navy, Washington 25, D.C., Attn: Aero and Hydro Branch (Code AD3)	2
11	Bureau of Ordnance, Dept. of the Navy, Washington 25, D.C., Attn: Code Re9 Code Re6 Code Re3	1 1 1
12	Commander, U.S. Naval Ordnance Laboratory, U.S. Navy Bureau of Ordnance, White Oak, Silver Spring 19, Maryland	2
13	Underwater Ordnance Dept., Naval Ordnance Test Station, 3202 E. Foothill Blvd., Pasadena, Calif. Attn: Pasadena Annex Library (Code P 5507)	3
14	Chief, Bureau of Ships, Dept. of the Navy, Washington 25, D.C. Attn: Technical Library (Code 312) for additional distribution to:	10

Distribution List (continued)

<u>Item</u>	<u>Address</u>	<u>No. Copies</u>
	(Bureau of Ships distribution) Research and Development (Code 300) Ship Design (Code 410) Preliminary Design (Code 420) Hull Design (Code 440) Hull Scientific (Code 442) Propeller Design (Code 554)	
15	Mr. R. H. Kent, Ballistic Research Laboratories, Dept. of the Army, Aberdeen Proving Ground, Maryland	1
16	Director of Research, National Advisory Committee for Aeronautics, 1512 H Street, N.W., Washington 25, D.C.	1
17	Director, Langley Aeronautical Lab., National Advisory Committee for Aeronautics, Langley Field, Virginia	1
18	Commander, Naval Ordnance Test Station, Inyokern, China Lake, Calif., Attn: Library (Code 5507)	1
19	Dr. K.S.M. Davidson, Experimental Towing Tank, Stevens Institute of Technology, Hoboken, N.J.	1
20	Dr. J.H. McMillen, National Science Foundation, 1520 H Street, N.W., Washington 25, D.C.	1
21	Dr. A. Miller, Bureau of Ordnance (Code Re3d) Navy Dept. Washington 25, D.C.	1
22	Dr. H. Rouse, Iowa Institute of Hydraulic Research, State University of Iowa, Iowa City, Iowa	1
23	Dr. R.G. Folsom, Director, Engineering Research Institute, University of Michigan, East Engineering Bldg. Ann Arbor, Michigan	1
24	Dr. V.L. Streeter, Engineering Dept., University of Michigan, Ann Arbor, Michigan	1
25	Dr. G.F. Wislicenus, Pennsylvania State University, Ordnance Research Laboratory, University Park, Pa.	1
26	Dr. A.T. Ippen, Dept. of Civil and Sanitary Engineering, Massachusetts Institute of Technology, Cambridge 39, Mass.	1
27	Dr. L.G. Straub, St. Anthony Falls Hydraulic Laboratory, University of Minnesota, Minneapolis 14, Minn.	1
28	Prof. K.E. Schoenherr, University of Notre Dame, College of Engineering, Notre Dame, Indiana	1
29	Director, Ordnance Research Laboratory, Pennsylvania State University, University Park, Pa.	1

Distribution List (continued)

<u>Item</u>	<u>Address</u>	<u>No. Copies</u>
30	Society of Naval Architects and Marine Engineers 74 Trinity Place, New York 6, N.Y.	1
31	Prof. J. K. Vennard, Stanford University, Dept. of Civil Engineering, Stanford, California	1
32	Prof. J. L. Hooper, Worcester Polytechnic Institute, Alden Hydraulic Laboratory, Worcester 6, Mass.	1
33	Prof. J. M. Robertson, Dept. of Theoretical and Applied Mechanics, University of Illinois, Urbana, Ill.	1
34	Dr. A. B. Kinzel, President, Union Carbide and Carbon Research Lab., Inc., 30 E. 42nd St., New York, N.Y.	1
35	Goodyear Aircraft Corp., Akron 15, Ohio, Attn: Security Officer	1
36	Prof. H. R. Henry, Hydraulics Laboratory, Michigan State College, East Lansing, Michigan	1
37	British Joint Services Mission, Navy Staff, Via: David Taylor Model Basin, Code 580, Navy Department, Washington 7, D.C.	9
38	Commander, Submarine Development Group TWO, Box 70, U.S. Naval Submarine Base, New London, Conn.	1
39	Commanding Officer and Director, U.S. Navy Engineering Experiment Station, Annapolis, Maryland	1
40	Library of Congress, Washington 25, D.C., Attn: ASTIA	1
41	Dr. P. R. Garabedian, Stanford University, Applied Mathematics and Statistics Laboratory, Stanford, California	1
42	Armed Services Technical Information Agency, Knott Building, Dayton, Ohio	5
43	Mr. J. G. Baker, Baker Manufacturing Company, Evansville, Wisconsin	1
44	Mr. T. M. Buerman, Gibbs and Cox, Inc., 21 West St., New York 6, New York	1
45	Dynamic Developments, Inc., St. Mark's Lane, Islip, Long Island, New York, Attn: Mr. W. P. Carl, Jr.	1
46	Hydrodynamics Research Laboratory, Consolidated-Vultee Aircraft Corporation, San Diego 12, California	1

Distribution List (continued)

<u>Item</u>	<u>Address</u>	<u>No. Copies</u>
47	Mr. R. K. Johnston, Miami Shipbuilding Corporation, 615 S. W. Second Avenue, Miami 36, Florida	1
48	Mr. J. D. Pierson, The Glenn L. Martin Company, Baltimore 3, Maryland	1
49	Mr. W. R. Ryan, Edo Corporation, College Point 56, Long Island, New York	1
50	Dr. Robert C. Seamans, Radio Corporation of America, Waltham, Massachusetts	1
51	Dr. A. G. Strandhagen, Department of Engineering Mechanics, University of Notre Dame, Notre Dame, Ind.	1
52	Dr. H. W. E. Lerbs, Hamburgische Schiffbau-Versuchsanstalt Hamburg 33, Bramfelderstrasse 164	1
53	Commander, Air Research and Development Command, P.O. Box 1395, Baltimore, Maryland. Attn: RDTDED	1
54	Avco Manufacturing Corp., Advanced Development Div., 2385 Revere Beach Parkway, Everett 49, Mass. Attn: Technical Librarian	1
55	Dr. L. Landweber, Iowa Inst. of Hydraulic Research, State University of Iowa, Iowa City, Ia.	1